UNIVERSITE DE NEUCHATEL

Institut de Microtechnique
Rue A.-L. Breguet 2, CH-2000 Neuchâtel
Switzerland

Microcrystalline Silicon Thin Films Deposited by VHF Plasmas for Solar Cell Applications

Thesis

submitted to the Faculty of Science for the Degree of Doctor of Philosophy

by

Roger Sylvain Flückiger

Die Deutsche Bibliothek - CIP-Einheitsaufnahme

Flückiger, Roger Sylvain:
Microcrystalline silicon thin films deposited by VHF plasmas for solar cell applications / Roger Sylvain Flückiger. - 1. Aufl. - Konstanz : Hartung-Gorre, 1995
Zugl.: Neuchâtel, Univ., Diss., 1995
ISBN 3-89191-965-4

Erste Auflage 1995

HARTUNG - GORRE VERLAG
KONSTANZ

ISBN 3-89191-965-4

IMPRIMATUR POUR LA THÈSE

Microcrystalline Silicon Thin Films Deposited by VHF Plasmas for Solar Cell Applications

de M. Roger Flückiger

UNIVERSITÉ DE NEUCHÂTEL

FACULTÉ DES SCIENCES

La Faculté des sciences de l'Université de Neuchâtel sur le rapport des membres du jury,

MM. A. Shah, R. Dändliker , J.M. Moret , G.Willeke (Constance) et F. Demichelis (Turin)

autorise l'impression de la présente thèse.

Neuchâtel, le 25 septembre 1995

Le doyen:

H.-H. Nägeli

"*Whence it is that nature does nothing in vain; and whence arises all that order and beauty which we see in the world* "

Isaac Newton 1642 - 1727

To my wife and son

MICROCRYSTALLINE SILICON THIN FILMS DEPOSITED BY VHF PLASMAS FOR SOLAR CELL APPLICATIONS

SUMMARY

The Very High Frequency - Glow Discharge (VHF-GD) deposition method, is used, at an excitation frequency of 70 MHz for the preparation of microcrystalline silicon (μc-Si:H). As source gas, silane (SiH_4) strongly diluted with hydrogen (H_2) was used. Extensive investigations on the influence of the deposition parameters (temperature, power, pressure, gas phase dilutions and boron doping ratio) have been carried out, in connection with the deposition of undoped, "truly intrinsic" (compensated midgap material) and boron-doped μc-Si:H films. The electrical, optical and structural properties of these specimens as well as the features of their initial growth regime are compared with the deposition parameters: this is done methodically with a view to identify the optimal preparation conditions for the requested solar cell applications as photovoltaic active material, window layers and tunnel junctions.

Starting with a temperature series of undoped (or rather, "not intentionally doped") μc-Si:H films, a wide range of film properties could be obtained, corresponding to film structures ranging from almost amorphous to fully microcrystalline. The usual <n>-type character of films deposited by glow discharge is identified here by the very low measured values of the dark conductivity activation energy. Comparing this series with a series deposited in an ultra high vacuum chamber at the standard industrial plasma excitation frequency of 13.56 MHz, leads to the conclusion that an excitation frequency of 70 MHz offers major advantages from the point of view of film properties and of film deposition.

The strong <n>-type character of the "undoped" films is probably due to contamination by oxygen which acts as "unintended" dopant; this <n>-type character was compensated by boron microdoping, i.e. by low-level doping, adding diborane to the silane, in the volume part per million (vppm) range. The compensated film which has its Fermi level near midgap, was revealed to exhibit the lowest dark conductivity, the highest dark conductivity activation energy and (surprisingly !) a stability (of its photoconductivity value), during intensive light-soaking experiments; on the other hand "undoped", <n>-type samples show no such stability: this makes the compensated film to be potentially a very interesting candidate, for a new stable photovoltaically active material within solar cell devices.

By carefully optimising the boron doping, very thin <p>-type μc-Si:H and even <p>-type μc-SiC:H films of thicknesses lower than 150 Å could be deposited; these very thin films have contrary to similar films produced at 13.56 MHz quite reasonable electrical and optical properties. They were even shown to be potentially better than the standard <p>-type a-Si:H or <p>-type a-SiC:H films used so far for window layer applications. Finally, the effectiveness of the VHF-GD technique with an excitation frequency of 70 MHz with respect to favourable microcrystalline growth conditions is further emphasised by our discovery of <p>-type Si epitaxial growth onto c-Si substrates at the low deposition temperature of 170 °C. With all these promising results, μc-Si:H deposited by our 70 MHz VHF-GD technique becomes a very interesting candidate for various device applications such as solar cells, thin-film transistors (TFT's) for flat panel displays and possibly as an electrode material for the gate of FET's in microelectronics.

TABLE OF CONTENTS

1 INTRODUCTION

I was just two years old when the history of microcrystalline silicon (μc-Si:H) started. It was in 1968, Veprek and Marecek [Veprek 1968] were the first to deposit a microcrystalline silicon semiconductor layer, using the chemical vapour transport in a hydrogen plasma at temperatures of about 600 °C. Several years later, in 1979, a Japanese group [Usui 1979] showed that doped μc-Si:H can be deposited from a high input power level inductive silane glow discharge (GD), already widely used for the preparation of amorphous silicon (a-Si:H) films. From that time, many research groups have carried out extensive investigations on the preparation and characterisation of μc-Si:H as a new thin film semiconductor material.

When in 1975 Spear and LeComber [Spear 1975] achieved a successful doping of the hydrogenated amorphous silicon material at low temperatures (~ 200 °C) using the plasma enhanced chemical vapour deposition (PECVD), a-Si:H together with hydrogenated microcrystalline silicon attracted even more attention as candidates for low cost solar cell fabrication [Carlson 1977]. The high conductivity and high transparency obtained for μc-Si:H material have motivated many research groups to substitute it for doped amorphous layers (which have conductivities lower by 3 to 4 orders of magnitude [Willeke 1992 and Luft 1993]) in p-i-n solar cells [e.g. Yang 1994]. This new material (μc-Si:H) found quickly various other promising applications in opto-electronic devices as the already mentioned solar cells, flat panel displays and large area microelectronics [Kanicki 1991] and in electronic devices like in thin film transistors (TFTs) [He 1993, Hsu 1994 and Parsons 1994]. One of the main new trends in microcrystalline applied research during these few last years is the grain size manipulation. There are two opposite fields of work depending on the expected final crystallite size; for small crystallite sizes (< 100 Å), the Japanese group of Oda [Oda 1995], for example, developed the so-called "digital CVD" technique in order to deposit silicon "quantum dots" (very small crystallites of sizes ≤ 40 Å). In contrary, Finger et al. [Finger 1994] are dealing with large grain size (> 300 Å) microcrystalline silicon deposited by the very high frequency-glow discharge (VHF-GD) technique. Finally, electroluminescence and photoluminescence from nanocrystalline silicon (nc-Si) - with crystallite sizes ≤ 40 Å - are nowadays also extensively studied by many research groups [e.g. Veprek 1995].

Very generally, microcrystalline material can be described as small grained polycrystalline specimens. They lie on the borderline between the amorphous and polycrystalline phases. These microcrystalline semiconductors are composed of small crystallites with an average grain size δ of about 50 - 300 Å embedded in an amorphous matrix (see Fig. 1.1). They are therefore often described as diphasic material. The average grain size is usually determined by X-ray or electron diffraction methods. The crystalline volume fraction X_C represents the relative crystalline phase amount contained in the film and is usually determined from Raman spectroscopy experiments. For high crystallinity films, X_C can take values from 70 to almost 100 % and the remaining volume fraction is essentially related to zones of high density of states called grain boundaries (gb's). These defect rich regions, where hydrogen passivates some defects, act as trap centers for charge carriers. These mixed phases make it difficult to model the electrical and optical properties of microcrystalline films.

Compared to a-Si:H, μc-Si:H has a lower optical absorption in the visible range of the sun light spectrum, higher electrical conductivity and carrier mobility, and a higher doping efficiency [Luft 1993]. The hydrogen content of μc-Si:H films depends on the deposition parameters and can be as low as 5 % for highly crystalline material with $X_C > 90$ %. In general, the optical properties of microcrystalline films are mostly determined by the amorphous phase (and/or grain boundaries), while the electrical properties are mostly determined by the crystalline phase

[Hattori 1987]. The work by the Dundee group [LeComber 1983] has shown that the electronic properties of μc-Si:H deposited by glow discharge can, despite its relatively small average grain size of about 60 - 80 Å, be interpreted in terms of the well-established models for polycrystalline silicon [e.g. Seto 1975]. The high conductivity reached in μc-Si:H is attributed to the four fold doping within the crystallites as found in crystalline silicon and to the high free carrier concentration in the conduction or valence bands, as compared to in a-Si:H [Spear 1981 and Willeke 1992]. Besides, the long range order (100 - 250 Å) in the crystallites also improves the mobility of the carriers. In poor μc-Si:H (with X_C below the percolation threshold value of about 20 %) the transport is dominated by the amorphous phase [Komuro 1984]. While the properties of μc-Si:H thick films (> 500 Å) are not too sensitive to the deposition methods, in contrast, the initial nucleation and film growth influence strongly the properties of thin films (< 500 Å) [Carlson 1988].

The pioneer work on microcrystalline silicon using the chemical transport method [e.g. Veprek 1968] suggests that stable nuclei for microcrystalline growth are likely to be formed under plasma conditions whereby a "chemical equilibrium" is approached at the plasma solid interface [Iqbal 1980]. Nowadays, most a-Si:H and μc-Si:H films are deposited using the silane glow discharge techniques. In these techniques, the chemical equilibrium for microcrystalline growth is approached by using appreciably higher radio frequency (rf) power levels (than for the deposition of amorphous material) and a gas phase dilution of silane in hydrogen. The observed deposition rate is slowed down in spite of the enhanced rf power indicating that the system is fairly close to a "dynamic equilibrium". The increased etching process at the film surface (which removes weak or strained Si-Si bonds) by using higher power densities (typically 200 - 300 mW/cm^2) and high hydrogen dilutions (> 95 %) for the deposition of microcrystalline films with the standard 13.56 MHz PECVD technique has similar effects on the film growth as increasing the substrate temperature but without the disadvantage of enhancing the impurity contamination of the material. The high gas phase dilution of silane in hydrogen and the high discharge power enrich the plasma with atomic hydrogen and the interface between the plasma and the film growth surface approaches "partial chemical equilibrium" (PCE) [Veprek 1988]. Under these conditions a balance is reached between the deposition of silicon atoms and radicals and the erosion of weak and disordered bonds, promoting, thus, microcrystalline growth. The effect of the atomic hydrogen on the preferential elimination of the weak and disordered bonds by a chemical etching mechanism [Tsai 1988 and Heintze 1993] seems to play a predominant role. Matsuda and Goto [Matsuda 1990] proposed that the high substrate temperature (T ≥ 200 °C) provides the necessary energy to enhance the surface mobility of the oncoming reactive species and for the desorption of the surplus of hydrogen. Finally, the group of Shimizu [Shimizu 1989] suggested that atomic hydrogen performs a "chemical annealing" of the silicon network by energetic relaxation and restructuration.

Apart from the already mentioned PECVD technique several other more complex methods have been used so far, to fabricate microcrystalline silicon layers such as electron-cyclotron resonance (ECR) PECVD, photo CVD, plasma magnetron CVD, remote PECVD, hydrogen-radical-enhanced CVD and so on [e.g. Luft 1993 and references therein].

The standard capacitively coupled 13.56 MHz industrial frequency PECVD technique is the commonly used method for thin film deposition. Only few groups reported the use of other plasma excitation frequencies (e.g. 27.12 MHz [Kausche 1989], 40.68 MHz [Spear 1981], 110 MHz [Chatham 1989], 144 MHz [Oda 1988], and 250 MHz [Zedlitz 1992]).

Since 1987, the very high frequency (VHF) plasma excitation of 70 MHz - introduced the first time by our group - has been used for the PECVD deposition in our laboratory of both a-Si:H and μc-Si:H films. This frequency was found to be optimal from our investigations on the influence of the discharge frequency on the deposition rate and film properties of a-Si:H, carried out in the

range of 25 to 150 MHz [Curtins 1987, 1987a and 1987b]. For the development of a-Si:H based solar cells, we have carried out extensive research on the preparation and optimisation of μc-Si:H, using the plasma excitation frequency of 70 MHz. The influence of the hydrogen dilution, discharge power and doping concentration on the properties of microcrystalline silicon films has been investigated in detail in a previous thesis work [Prasad 1991].

In the following, we focus on the research and further optimisation of microcrystalline silicon thin films for applications in solar cell devices. Microcrystalline Si and SiC films are used in our solar cells as window layers, tunnel junctions and as active photovoltaic layers. In the quest for higher sunlight conversion efficiencies of a-Si:H based solar cells, a number of approaches appear promising: 1) the use of multiple junction devices, 2) the use of highly conductive and transparent <p>- and <n>-type layers and 3) the reduction of interface recombination losses. Microcrystalline silicon with its weaker absorption in the visible range of the sun light spectrum and higher conduction (than a-Si:H) is useful in all these approaches [Luft 1993]. "Truly intrinsic" (midgap material) μc-Si:H films show the potential as newly developed photovoltaic stable material in a complete microcrystalline silicon solar cell [Wang 1990 and Meier 1994a]. Furthermore, the increased infrared response of this new cell together with its improved stability to light-soaking experiments lead to its incorporation as a bottom cell in standard a-Si:H tandem cells.

1.1 The 70 MHz PECVD technique

The past decade has seen an important growth of amorphous and microcrystalline silicon technologies. By simply tuning a few of the deposition parameters from a-Si:H thin film growth conditions, μc-Si:H could often be deposited. PECVD is amongst all techniques the most popular and widely used. While 13.56 MHz is the commonly used authorised industrial plasma excitation frequency, our group investigated the frequency range from 25 to 150 MHz for a conventional capacitively-coupled diode reactor with an adapted matching network [Curtins 1987 and 1987a]. Whereas the opto-electronic properties of the a-Si:H investigated films were comparable with those of films deposited at 13.56 MHz [Curtins 1987b], we observed for our reactor geometry and the selected set of process parameters an increase of the deposition rate when increasing frequency. This increase in the deposition rate seems to be linked with a higher power transfer efficiency into the bulk of the plasma, a higher decomposition of silane and an increase in surface reactivity of the film precursors - due to an increased ion flux - at higher frequencies [Howling 1992, Kroll 1994 and Heintze 1993a]. The high deposition rate obtained at 70 MHz was considered to be of advantage to reduce production cost of a-Si:H based solar cells by achieving a higher throughput. In view of the investigation of such a possibility, this frequency has been used in our laboratory for both a-Si:H and μc-Si:H depositions.

The tendency of the high deposition rate as well as the effects of the 70 MHz plasma excitation frequency on the growth and properties of μc-Si:H films were treated in a previous thesis work [Prasad 1991]. Compared to the conventional 13.56 MHz plasma process, the very high frequency technique at 70 MHz shows several advantages for the growth of microcrystalline silicon films as e.g. a higher deposition rate and larger grain sizes [Prasad 1991 and Finger 1994]. Results from plasma diagnostics [Howling 1992 and Heintze 1993a] and impedance analysis [Kroll 1994] suggest that a higher density and less energetic ion flux and a higher atomic hydrogen and radicals flux to the growth surface lead to favourable growth of μc-Si:H under VHF conditions. More detailed plasma studies and impedance analyses are treated elsewhere [Kroll 1994a and Keppner 1995].

1.2 Description of the work

After this general introduction on microcrystalline silicon material, let us focus on the body of this thesis work. It consists in the optimisation of μc-Si:H thin films deposited by VHF-GD at 70 MHz for solar cell applications. The layout of the present work is developed hereafter.

Chapter 2 describes the deposition system and the deposition process used for the preparation of the different specimens. Some detailed system characterisation, such as the calibration of the plasma power, of the deposition substrate temperature and of the gas fluxes, are also presented in detail. A complete and precise deposition system characterisation is absolutely essential for the study of the effects of the deposition parameters on the film properties. Chapter 3 is the main chapter of this thesis work; the results concerning the individual effects of the deposition parameters on the electrical, optical and structural properties of undoped, compensated ("truly intrinsic" midgap material) and boron doped films are discussed. All films deposited were tentatively developed and optimised for specific solar cell applications. Furthermore, the advantages of the 70 MHz by comparison with the standard industrial 13.56 MHz plasma excitation frequency are pointed out with respect to the film deposition and the film properties. Chapter 4 briefly mentions the realised applications (in our laboratory) of the developed μc-Si:H thin films to all kinds of solar cells. References to extended work are joined for additional information. Chapter 5 summarises some important conclusions and suggestions for possible future work. Finally, chapter 6 gives details on the cleaning procedures and on the various techniques used for the electrical, optical and structural characterisation of the specimens. Some details on the kind of information expected from these techniques and its interpretation are also briefly given. The references mentioned throughout this manuscript are listed in chapter 7.

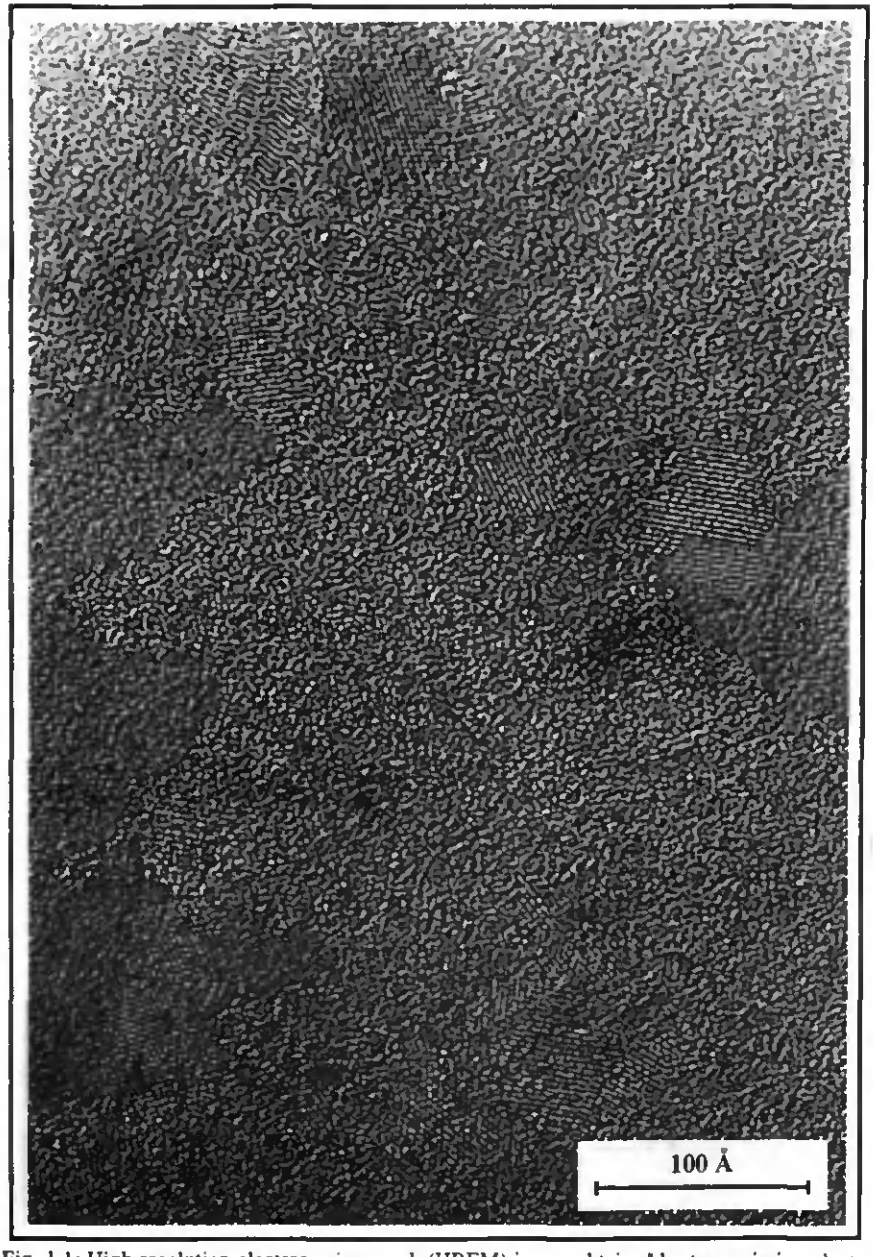

Fig. 1.1: High resolution electron micrograph (HREM) image obtained by transmission electron microscopy (TEM) of a <p> μc-Si:H very thin film (d = 255 Å) deposited by the VHF-GD at the plasma excitation frequency of 70 MHz, clearly showing a large amount of randomly growing spherically-shaped crystalline particles with different orientations and with sizes between 50 and 80 Å.

2 VHF-GD DEPOSITION SYSTEM AND PROCESS

This chapter is divided into two parts. In the first one, the 70 MHz PECVD deposition system and process are described. The second part presents some detailed system characterisation.

2.1 Deposition system and process descriptions

2.1.1 Deposition system

Fig. 2.1.1 illustrates schematically the capacitively-coupled VHF-GD system used for the deposition of the films and solar cells. The reactor consists of a stainless steel vacuum chamber (with cubic dimensions of 25x25x25 cm^3 corresponding to a volume of about 15 litres) containing two stainless steel electrodes. Both electrodes are 13 cm in diameter and are separated by 15 mm (inter-electrode distance). The upper one - that is grounded and holds the substrate on which the film is deposited - can be heated using an integrated coaxial heating coil and is temperature controlled from room temperature (RT) up to about 400 °C. The lower electrode - that is not temperature controlled - is coupled to the high frequency source and an amplifier by means of a standing-wave-ratio (SWR) power meter and an intermediate impedance matching π or LC filter via a 50 Ω coaxial line. The SWR power meter measures the forwarded as well as the reflected power. The matching box adapts the reactor's impedance to the amplifier output impedance, so as to minimise the reflected high frequency (HF) power.

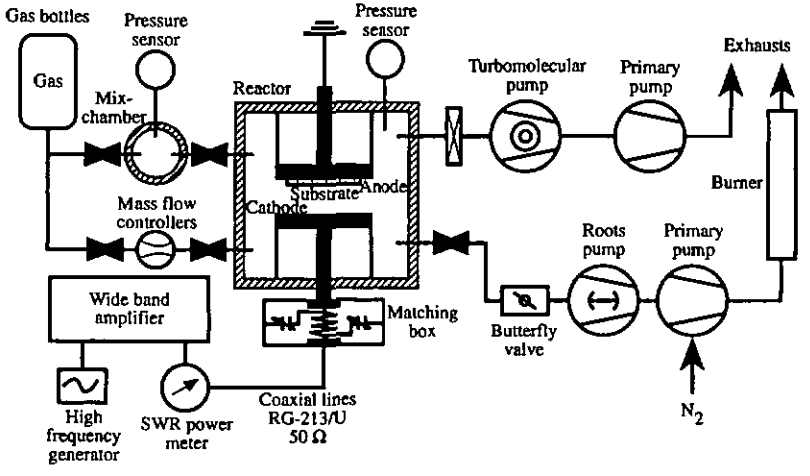

Fig. 2.1.1: VHF-GD deposition system schematics (taken from [Prasad 91 and Kroll 94a] and transformed), with all its major components.

A mixing chamber (abbreviated "mix-chamber") made of stainless steel with a volume of about 1.5 litre was added to the main chamber for the compensation experiments which require doping in the volume part per million (vppm) range.

Mass flow controllers and control electronics enable a constant and controlled gas feed into the reactor. During deposition, the pressure is controlled and regulated by the use of a capacitive manometer, a butterfly valve and control electronics. The gases are constantly pumped out of the reactor by a pumping stand comprising a Roots blower and a primary pump. Before reaching air, the extracted gases are diluted in nitrogen and decomposed in a burner at temperatures of about 700 °C.

Prior to deposition, the two chambers (main and mix-chamber) are heated at about 80 °C for outgassing purposes (elimination of impurities, especially of water vapour), under high vacuum, with the help of a turbomolecular backed by a primary pump. A standard overnight (~ 12 hours) base pressure of about 2×10^{-6} mbar and an outgassing rate of about 2×10^{-5} mbar l/s are typically reached (the latter is estimated from the pressure rise in the main chamber with all its valves closed for a given time interval).

The gases used for the process were nitrogen (N_2), argon (Ar), hydrogen (H_2), silane (SiH_4) and methane (CH_4). For doping experiments, phosphine (PH_3) and diborane (B_2H_6) gases diluted to 500 and 1000 ppm (parts per million), respectively, in hydrogen, are employed. Very low doping levels in the vppm range for "microdoping" were achieved through extra dopant gas dilution in hydrogen in the mix-chamber (that was specially developed for this purpose).

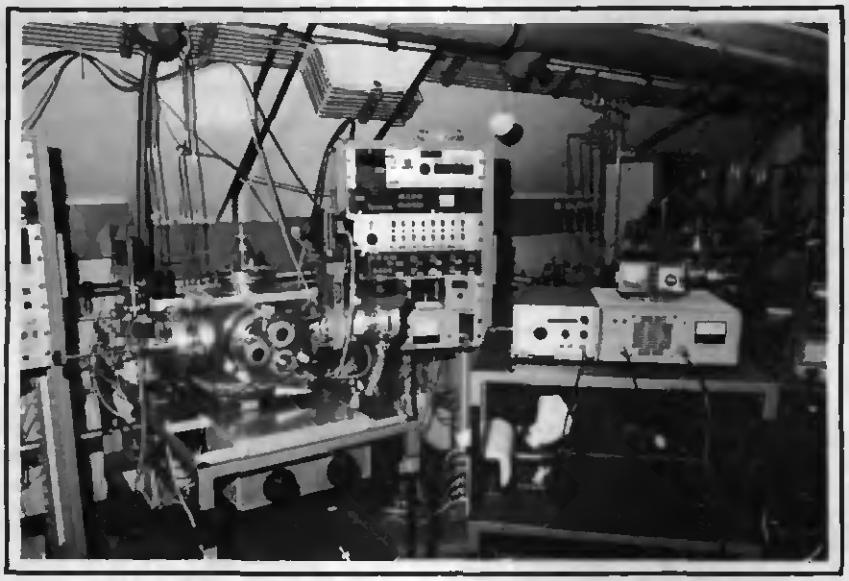

Fig. 2.1.2: Front view picture of the deposition system used in this work, as already represented schematically in Fig. 2.1.1.

2.1.2 Deposition process

A typical, complete deposition process is described in detail hereafter: The substrate is first loaded - after unloading of the last deposition sample - onto the grounded electrode, using a stainless steel chemically cleaned holder. If needed, in order to minimise film dopant contamination from the chamber walls and from the electrode surfaces, a dummy layer was previously deposited. A chemically cleaned stainless steel plate (see annexe (6.1) for chemical cleaning procedure of stainless steel surfaces) is placed on the powered electrode. The system is then pumped down overnight (or at least for 4 to 5 hours) and the chamber walls are heated. The substrate temperature value is set for overnight pumping in the case of a film deposition. If a cell is planned to be deposited onto a transparent conductive oxide (TCO) coated glass, the substrate temperature is only set some minutes prior to deposition since the TCO-coated glass does not support high temperatures for hours under vacuum.

Early next morning, the base pressure and the outgassing rate are recorded to allow for a control of the reactor vacuum state. The heating of the chamber walls during deposition is stopped to prevent too high an outgassing rate which would possibly lead to additional film contamination. In case of a deposition that involves the mix-chamber, the gas phase mixture is carefully prepared and the mix-chamber filled to a pressure of about 0.8 mbar.

For film depositions, three individual steps - as listed in Table 2.1.1 - are performed in order to prepare the chamber surfaces and substrate for deposition. These steps are avoided in case of cell depositions since the TCO substrates used are reputed as not being able to support well Ar nor H_2 plasma treatments.

	Step # 1	Step # 2	Step # 3
Plasma (on / off)	On	Off	On
Input power (W)	50	-	20
Gas / flux (sccm)	Ar / 100	H_2 / 100	H_2 / 100
Duration (min.)	10	20	5
Pressure (mbar)	0.4	Of deposition	Of deposition
Goal / effect	"Strong" Ar ion bombardment for surface cleaning	H_2 flushing for further cleaning of the chamber walls and electrode surfaces whilst stabilising the temperature conditions for the deposition	"Soft" H_2 plasma for a final surface cleaning of the substrate before deposition of the film. Thought to produce a surface H_2 coverage ot the substrate surface

Table 2.1.1: Empirical substrate and chamber preparation steps prior to film deposition.

After step # 1, the system is pumped down to the base pressure of about $5x10^{-6}$ mbar in order to extract all the heavy gas phase species created from the high power Ar plasma. All these preparation steps, experimental parameters and explanations that are purely empirical and not strictly based on detailed experiments, where taken from an earlier work [Prasad 1991] and subjected to some minor modifications.

Then, the gas flows are set and allowed to stabilise for a couple of minutes, the deposition plasma is ignited manually with the help of a conventional flame igniter and the input power is carefully adjusted using the matching network in order to minimise the reflected power. After the estimated deposition time required to obtain the expected film thickness, the plasma is switched off and the gas flow rates are carefully and systematically calibrated by measuring the rise in the chamber pressure over a measured time with the chamber valves closed. The calibration factors obtained are used to constantly readjust the set points of the mass flow controllers. This calibration procedure is absolutely essential for knowing the exact gas phase fluxes prevalent during deposition. After switching off the gas flows, the chamber is pumped down to base pressure and the substrate cooled down to about RT by a constant cooling-down rate from 48 up to 90 °C/h, before unloading the chamber. Finally, the deposited films are cut up into different pieces, for various characterisation operations, and the cells are contacted.

2.1.3 Deposition parameters

Different series of microcrystalline films (undoped, compensated, <p>-doped and carbide <p>-doped) were deposited over a wide range of deposition parameters. This was done to obtain optimisation of film properties in view of solar cell applications. In the next Table (2.1.2), the main experimental parameters used in this work and their scan ranges are listed.

In the next chapter, each film series is treated in detail, the different characterisation methods used are described and the corresponding deposition parameters are given.

Deposition parameters	Symbols	Scan ranges	Units
Substrate temperature	T_{dep}	40 - 400	°C
Input discharge power	P	3 - 50	W
Input power density*		23 - 377	mW/cm^2
Working pressure	p	0.2 - 1	mbar
Silane dilution**	SiH_4/tot	1 - 5	%
Doping ratio**	$Dop/(SiH_4+CH_4)$	0 - 1	%
Methane ratio**	$CH_4/(SiH_4+CH_4)$	0 - 67	%
Electrode spacing (with substrate)		15	mm
Electrode diameter		13	cm
Electrode area		133	cm^2
Discharge excitation frequency		70	MHz

* neglecting matching network losses

** gas phase fluxes

Table 2.1.2: Deposition parameters used in this work and their scan ranges.

2.1.4 Substrates

For most of the electrical, optical and structural film studies, 0.83 mm thick 8.3x8.3 cm^2 alkali free glass substrates (DC 7059) were used. Infrared transmission measurements, elastic recoil detection analyses (ERDA) and epitaxial growth studies were performed on films deposited onto 5 to 7 Ωcm resistive polished <p>-type Czochralski (CZ) Si wafer pieces with <100> orientation. Transmission electron microscopy (TEM) planar view analyses are carried out on films grown

onto commercial thin copper grids and NaCl (water soluble) substrates. All the substrates mentioned here are fixed on a glass substrate with the help of a few thin metal rods.

For electron spin resonance (ESR) characterisation, 2 - 3 µm thick films are deposited on aluminum foils which are etched away by HCL after deposition, yielding typically 30 mg powder material. The cells are grown on glass coated with two different kinds of transparent conductive oxides (TCO), i.e. with either SnO_2 or ZnO. Some of the substrates had to be cleaned, cut and dried prior to deposition following our standard process described in the annexe (6.1). Table 2.1.3 summarises the different substrates used and their corresponding film characterisation.

Substrates	Characterisation and analyses
DC 7059	Thickness evaluation using a step profilometer, standard electrical measurement, photothermal deflection spectroscopy (PDS), UV/visible transmission and reflection spectroscopy, spectroscopic ellipsometry (SE), X-ray diffraction (XRD), Raman spectroscopy, and secondary ion mass spectroscopy (SIMS)
c-Si wafer	Infrared (IR) transmission spectroscopy, cross-section TEM, and ERDA
Copper grid	Planar view TEM
NaCl chip	Planar view TEM
Al foil	ESR
SnO_2 and ZnO coated glasses	Solar cell transparent conductive oxide substrates for standard cell characterisation

Table 2.1.3: Complete list of substrates used, together with the corresponding film characterisation and analysis methods employed.

It is important to keep in mind here that within a same film deposition run, different substrates are often simultaneously used, as required for the different film characterisation methods, leading possibly to a variation of film growth depending on the nature of the substrates.

2.2 Deposition system characterisation operation

2.2.1 Power calibration

For reactor optimisation and with goal of enabling a valid comparison between experimental data from different systems, the true power that is dissipated in a radio frequency discharge is a crucial parameter, which, however, is by no means easily accessible. In this work, as usually done, the discharge input power is measured with a standard SWR power meter in the 50 Ω line before the matching network; this means that the effective plasma power P_{pl} is generally not known. For a fixed plasma excitation frequency and under certain specific plasma conditions, however, the effective plasma power can be assumed to be proportional to the input power.

At the end of the period of this thesis, we had to transform the deposition system used for this work in order to make it compatible again, with the newer vacuum and deposition technologies introduced in our laboratory. This was then the last moment to characterise the effective plasma power of the system used, before executing these modifications. These measurements of effective

plasma power will be of great help for future optimisations of the films and devices that will be deposited in the new system.

The effective plasma power was in this operation roughly estimated by a "subtractive method" [Godyak 1990 and Howling 1991]. The input power without plasma P_{vac} is subtracted from the total input power (with plasma) P_{tot} to give the effective plasma power P_{pl}, with the constraint that both P_{vac} and P_{tot} are measured for the same electrode voltage. This condition is fulfilled by slightly adjusting the amplifier power output and re-tuning the matching system. The voltage probe must be positioned as close as possible to the plasma, so it was fixed behind the plasma-exposed surface of the rf electrode. In that case, the reactor circuit losses can be assumed to be in parallel with the plasma power dissipation (a necessary assumption to guarantee the correctness of the "subtractive method").

Fig. 2.2.1 shows the electrode square peak-to-peak voltage and total input power measurements for our reactor configuration and for a standard hydrogen plasma (70 MHz, 100 sccm H_2 at 0.4 mbar, cold electrodes and chamber walls). As expected for a linear circuit, $(V_{pp})^2$ in vacuum is proportional to the total input power. The data with plasma show, in contrast to this, a deviation from a straight line, for low input powers. For the ideal case of a linear dependency, as observed for input powers higher than 6 W, the plasma conductance is taken to be approximately independent of power. The data with plasma show a positive intercept with the vacuum line at about 2 W, and about $1x10^3$ V^2; this point is interpreted to represent a "minimum sustaining voltage" or, rather, a minimum sustaining plasma power for the glow discharge. This value corresponds well to the lowest practically observed input power for which the plasma can still burn. The deviation from the linear curve for low powers close to the extinction limit of the plasma corresponds to the case for which the fraction of power dissipated in the rf circuit becomes large compared to the very low values of actual plasma power. The observed rapid variation of the plasma power with input power could lead to reproducibility problems for depositions made at low input power.

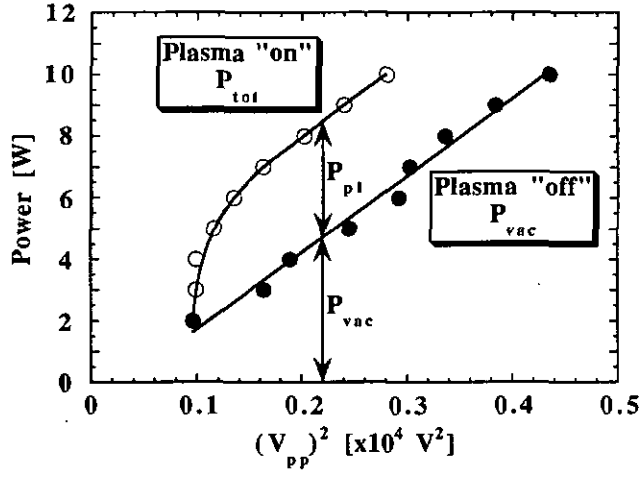

Fig. 2.2.1: Electrode square peak-to-peak voltage and input power measurements according to the "subtractive method".

In the high power regime (input power ≥ 8 W) it seems from Fig. 2.2.1 that the effective plasma power stays almost constant when increasing the input power, indicating that the additional power furnished to the system is lost somewhere in the network between the amplifier and the plasma. The author strongly suspects the match-box with its old capacitances (they are not vacuum capacitances !) to be responsible for the observed losses at high input powers.

Note: all power values mentioned in this work refer to the total input power and not to the actual plasma power if not otherwise specified.

2.2.2 Deposition substrate temperature and gas flux calibrations

2.2.2.1 Deposition substrate temperature calibration

The deposition substrate temperature T_{dep} is regulated by a temperature controller using a coaxial heating coil and a PT-100 temperature sensor positioned inside the grounded electrode. A temperature difference occurs between the heating block and the substrate due to low thermal conductivity, radiation and convection and thermal inertia of the electrode base plate. This difference in temperature depends on deposition conditions such as chamber wall temperature, chamber pressure and plasma power.

A calibration of the deposition substrate temperature of the system used for this work was already carried out and described in a previous work [Prasad 1991] using another PT-100 mounted on the substrate surface during trial runs in the absence of plasma. It was shown there that the effective substrate temperature is always lower under vacuum conditions than the electrode temperature, and that moreover this temperature difference decreases with increasing pressure. A hydrogen plasma of 20 W was further shown to increase the substrate temperature by about 20 °C, reducing thereby the offset between the effective substrate temperature and the set point of the temperature controller. As most of our deposited films were grown using only relatively low input power levels (< 10 W), the modifications of the substrate temperature due to the plasma and to the ion bombardment at the substrate were neglected.

All film temperatures mentioned in this work - if not specified - are calibrated deposition temperatures (T_{dep}), using the calibration curves (Fig. 2.3, p. 8) from Prasad's work [Prasad 1991].

2.2.2.2 Gas flux calibration

We observed experimentally that with time some gas fluxes - especially the silane gas flux - show non-negligible drifts leading to non-constant gas flux calibration factors. If one does not know the exact gas fluxes used for deposition, this could lead to erroneous film deposition parameters and improper interpretation of film characterisation experiments. By using the gas flux calibration method explained hereafter, it is possible to constantly adjust the calibration factor of the mass flow controllers leading thus to accurate gas flux values.

The simple gas flux calibration method used is based on the measurement of a constant rate increase in chamber pressure over a known elapsed time with all chamber valves closed [Kroll 1994a]. The gas fluxes expressed in the "sccm" unit (standard cubic centimetre per minute) have been shown [Kroll 1994a] to be proportional to the ratio of the pressure rise [mbar] and the elapsed time [s]. The constant proportionality coefficient which is also called "calibration factor" is in its turn proportional to the chamber volume and was estimated for our chamber configuration and typical deposition conditions to be 891 litres. This factor was used to calibrate the gas fluxes and adjust the mass flow controllers calibration factors after each deposition as just described.

2.3 Conclusions

In this chapter, a detailed description of our 70 MHz PECVD system and process is given. The necessary system characterisation techniques are also presented, allowing a clear knowledge and understanding of the subsequent technological work constituted by film and solar cell depositions. Since the system used for deposition was already built and exploited since many years, and belongs to a series of three identical "home-made" reactors in our laboratory, the author did not spend more time on what was already done by others but rather took over all this in the form of as "routine" work and standard "know-how".

The effective plasma power or true power was roughly estimated by a "subtractive method" and showed to be of great importance for film optimisations and studies. A minimum sustaining plasma power of about 2 W was obtained, corresponding well to the lowest practically observed input power for which the plasma can still burn. Moreover, for low input power close to the extinction limit of the plasma, a rapid variation of the effective plasma power with total input power was shown; this could possibly lead to reproducibility problems for depositions made at low input power.

Besides the power calibration, the calibrations of the deposition substrate temperature and of the gas fluxes are revealed to be essential for the knowledge of the accurate values of the deposition substrate temperature and of the gas fluxes used for deposition of the specimens.

All the efforts of the author were put into film deposition, characterisation and optimisation for solar cell applications; the detailed results are treated in the next chapter.

3 MICROCRYSTALLINE SILICON FILM SERIES STUDIES

Microcrystalline silicon material with its generally high conductivity, low absorption and enhanced stability with respect to light-soaking has shown the potential for multiple use in silicon-based solar cells [Luft 1993 and Meier 1994a]. We present here detailed studies of full series on undoped (i.e. slightly <n>-type), "compensated" and boron-doped μc-Si:H film series and their respective optimisation for solar cell applications. Several series of phosphorus-doped microcrystalline films were already extensively studied and presented in a previous work [Prasad 1991].

3.1 Undoped films

The present intensive efforts going on in many laboratories with the goal of developing more stable thin film solar cell materials, motivated us to study undoped μc-Si:H layers as a possible alternative to amorphous layers in thin film silicon solar cells. The deposition temperature and plasma excitation frequency effects on the film properties of undoped microcrystalline silicon are investigated here. The effects of the other main deposition parameters on the growth and properties of undoped μc-Si:H were already presented in a previous work [Prasad 1991].

3.1.1 Temperature series

Results of a systematic study of the variation of the deposition temperature from 40 to 400 °C are presented for undoped μc-Si:H material, showing the influence of temperature variation on the electrical, optical and structural properties of these films. The upper deposition substrate temperature limit of 400 °C is determined by the "non-bakable" nature of the viton o-rings (upper temperature limit of 200 °C) used in the present configuration of our deposition system.

3.1.1.1 Experimental

The temperature series of undoped μc-Si:H material was deposited at a dilution level of 3 % silane in hydrogen and a total gas flow of about 100 sccm. The power measured at the power meter was 3 W and the deposition temperature T_{dep} was varied in the range of 40 to 400 °C. The gas pressure was kept at 0.4 mbar. For a standard deposition temperature of 200 °C this specific set of parameters has been shown to lead to films of high crystallinity with a volume fraction X_c of almost 90 % [Prasad 1991]. The film thicknesses deposited were in the range of 0.2 to 0.6 μm and the corresponding deposition rates (that slightly decrease with increasing T_{dep}) were between 0.3 and 0.7 Å/s. The detailed experimental description of the different characterisation methods treated in the next part (3.1.1.2) can be found in [Flückiger 1992].

3.1.1.2 Results and discussion

The **room temperature dark conductivity** σ_d and the **dark conductivity activation energy** E_σ - determined from the low temperature region (from RT up to about 80 °C) of the Arrhenius plot of σ_d - are plotted in Fig. 3.1.1.1, as a function of T_{dep}. As shown in Fig. 3.1.1.1, the value of σ_d is always well above the corresponding value for standard undoped a-Si:H material ($\approx 1x10^{-10}$ S/cm) and increases drastically (five orders of magnitude) with T_{dep}. In parallel, E_σ decreases from about 0.4 to 0.1 eV. A similar tendency is observed for the illuminated (60 mW/cm^2)/dark current ratio (= 1 + photo/dark) that falls from a value of 10 at 40 °C to 1 for higher values of T_{dep}.

The ratio of illuminated to dark current gives structural information in the sense that values tending towards unity correlate well with a structural evolution towards more crystalline material. The structural changes that are at the origin of these results will be discussed later. The very low activation energy values measured - even much lower than the half gap of c-Si of 0.55 eV- are at present not fully understood and may be related to an unintentional contamination (oxygen ?) or to undetected doping (P or B) of our nominally undoped material, both of which would shift the Fermi level E_F away from midgap. SIMS and IR transmission spectroscopy analyses shown later on will give more details on possible contamination. According to the literature [Wang 1991] certain structural effects such as a high density of states in the grain boundaries that may cause a Fermi level pinning could possibly also contribute to explain the low values of E_σ that are generally measured for microcrystalline silicon.

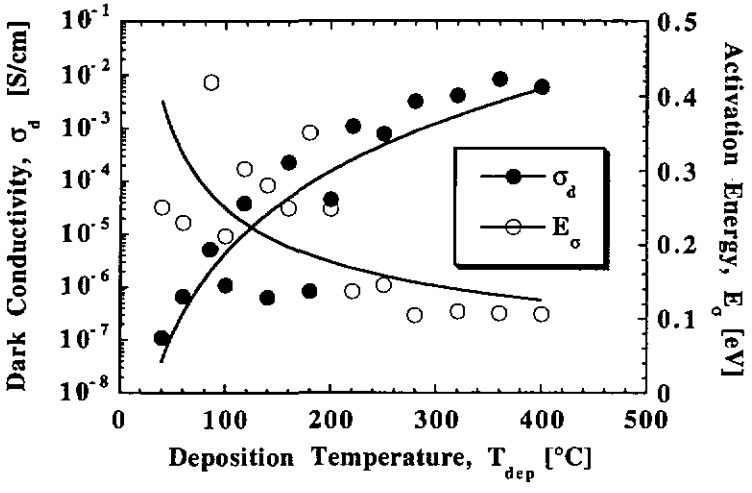

Fig. 3.1.1.1: Room temperature (RT) dark conductivity and dark conductivity activation energy as a function of deposition temperature.

In general, our undoped samples have a clear <n>-type character as can be inferred from thermopower experiment. This <n>-type character of our microcrystalline material is in fact common for most undoped amorphous and microcrystalline films deposited by glow discharge (GD). Finally, the scattering in the data observed in all electrical characterisation techniques of the films deposited in the temperature range from 100 to 200 °C has so far found no satisfactory

explanation. Inaccuracy or measurement errors can certainly be excluded from being the direct and only cause.

By **IR transmission spectroscopy measurements** one obtains information about silicon-hydrogen and silicon-oxygen chemical bondings [Brodsky 1977, Demichelis 1993 and Curtins 1986]. The relative changes in the IR absorption peaks of the as-deposited material with increasing T_{dep} were analysed. The tendency for all peaks (630 cm^{-1}, 900 cm^{-1}, 2000 cm^{-1} and 2080 cm^{-1}), except for the 1100 cm^{-1} peak, is a slight monotonous decrease with temperature, indicating a reduction of bonded hydrogen content C_H in the material. An exception is the 1100 cm^{-1} peak that increases drastically for increased film T_{dep} from 40 up to 220 °C and then remains almost constant.

For a more in-depth investigation of the 1100 cm^{-1} peak, which is related to bonded oxygen (Si-O groups) [Curtins 1986], we measured the samples some time later again, after a long exposure to air during about two months. This time-dependent analysis shows an increase of bonded oxygen only for the material deposited at temperatures lower than 220 °C. For material deposited at higher temperatures, the oxygen peak remains quite unaffected by further air exposure. Our low temperature deposited material seems to be quite porous - as will be inferred from the structural analyses - and that could be an explanation for the oxygen penetration behaviour mentioned above.

SIMS measurements performed on three representative samples of the series confirm the IR transmission spectroscopy results. The concentrations of hydrogen, of the main contaminants (O, C and N) and of the dopants (P and B) are plotted in Fig. 3.1.1.2 as a function of deposition temperature. (A residual amount of dopants is present in the deposition chamber and unintentionally dopes our films, even when we want to deposit a series of "nominally" undoped layers).

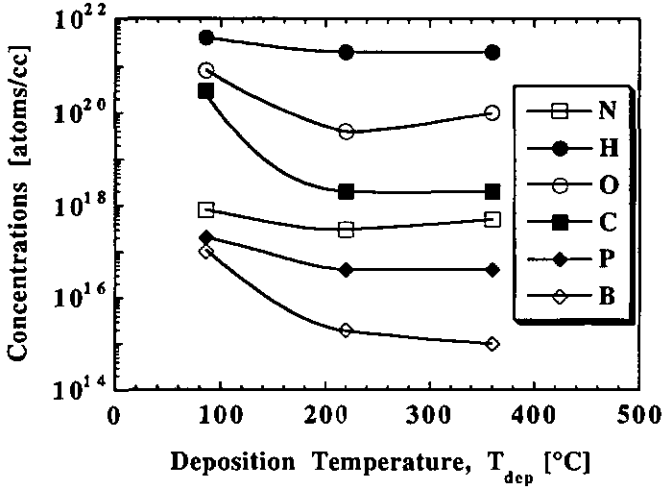

Fig. 3.1.1.2: Concentrations of hydrogen, the main contaminants (O, C and N) and (unwanted) dopants (P and B) in the films as a function of deposition temperature.

The silicon atom concentration (not plotted) increases slightly from $3x10^{22}$ to $4x10^{22}$ (atoms/cc) and then stays constant with increasing T_{dep}. The hydrogen concentration C_H slightly decreases from $4x10^{21}$ to $2x10^{21}$ (atoms/cc) and the oxygen content decreases from $8x10^{20}$ to $1x10^{20}$ (atoms/cc) with a minimum of $4x10^{19}$ (atoms/cc) for the material deposited at 220 °C. Except for carbon, the other elements (N, P and B) show concentration values in the films lower than $1x10^{18}$ (atoms/cc). All the above mentioned main contaminant (O, C and N) concentration values for our microcrystalline material are higher (by more than one order of magnitude) than those obtained for conventional device-quality rf GD (13.56 MHz) a-Si:H [Nakata 1993].

From the values of the SIMS impurity concentrations as shown in Fig. 3.1.1.2, it seems to us most likely that the oxygen element (0.1 - 2.3 % concentration in the material) together with possible structural effects should be responsible for the strong <n>-type character and very low dark conductivity activation energy values observed in our "nominally undoped" μc-Si:H.

More accurate values concerning the hydrogen content C_H of the samples were obtained by **ERDA measurements**. The results are shown in Fig. 3.1.1.3 and confirm the above mentioned IR transmission spectroscopy and SIMS analyses. C_H decreases when increasing T_{dep} from 40 to 200 °C and tends to a saturation value of about 5 at. %. For comparison, C_H measured by ERDA on a-Si:H samples deposited in the same temperature range are around a factor two higher [Finger 1990].

Again, the decrease of C_H in the material confirms the structural evolution towards more crystalline silicon layers. For low T_{dep}, the interface (layer-substrate) C_H value (the interface is estimated from this experiment to be about 1000 Å thick) is much bigger than the bulk one and the difference vanishes for higher temperatures (see Fig. 3.1.1.3). The hydrogen accumulation at the interface for low T_{dep} could be related to porous and/or amorphous interface material that seems to vanish for high deposition temperatures.

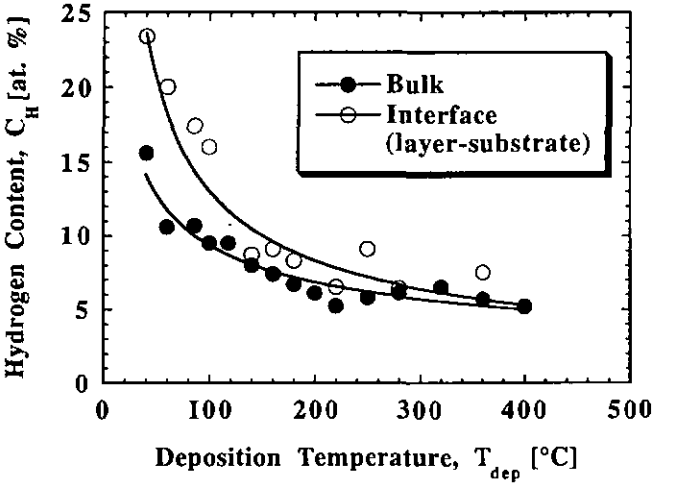

Fig. 3.1.1.3: Hydrogen content in the films (minimum bulk and maximum interface values) determined from ERDA measurements as a function of deposition temperature.

Harbeke et al. [Harbeke 1983] proposed **UV/visible reflection spectroscopy measurements** to determine empirically the near-surface roughness of amorphous and polycrystalline silicon films. In order to determine the near-surface roughness of our μc-Si:H samples, we measured the reflectance in the range of 200 to 450 nm. Fig. 3.1.1.4 shows the results for different values of T_{dep} in comparison with the reflectance of a <100> oriented polished single-crystal silicon wafer and a standard smooth amorphous layer.

The method previously developed for rapid characterisation of amorphous and polysilicon films is based on an observation of two reflection wavelengths: λ = 280 nm claimed to be influenced by degraded crystallinity and surface texture or "haze" and λ = 400 nm claimed to be influenced by surface texture only [Harbeke 1983]. The probing depths for our μc-Si:H films are estimated to be less than 100 Å at 280 nm and less than 1000 Å at 400 nm. Compared to these observations, the reflectance of the smooth a-Si:H layer shows - as expected - no peaks at all and an overall high value. The polished single-crystal Si shows in contrary two reflectance peaks and also an overall high value.

The μc-Si:H material deposited at the lowest temperature of 40 °C shows no peaks at all and very low reflectance indicating a poor quality porous and/or rough amorphous near-surface material. Increasing T_{dep} results in an increase of the overall reflectance and in the appearance of a peak at 280 nm. We thus tentatively conclude that by increasing T_{dep} the near-surface material becomes of better quality, i.e. more crystalline and less porous or rough (more smooth and compact), confirming thus all previously discussed characterisation methods. Finally, the material deposited at 320 °C shows a high crystalline contribution from the reflectance peak at 280 nm and an overall high reflectance indicating a high smoothness. The film deposited at the highest temperature of 400 °C (not plotted) shows a slight decrease of the overall reflectance and could indicate that too high deposition temperatures could possibly lead to degraded crystallinity; this hypothesis will be further checked by the structural characterisation techniques (Raman spectroscopy and X-ray diffraction).

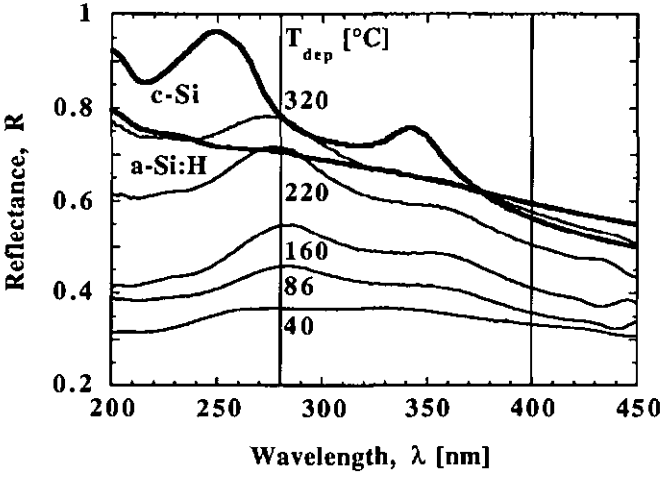

Fig. 3.1.1.4: Reflectance of undoped μc-Si:H deposited at various temperatures (from 40 to 320 °C), of a <100> oriented polished single-crystal silicon wafer and of a standard smooth amorphous silicon film versus wavelength.

Our experience in the growth of μc-Si:H thin films by VHF-GD leads us to the statement that μc-Si:H thin films mostly grow the same way from the bulk of the material until the top of the films. Only some few tens of Ångstroms of oxide cover the film surface. The "near-surface characterisation technique" just described gives us, thus, directly information on the bulk of our microcrystalline films. The two reflectance peak positions which are due to optical interband transitions [Harbeke 1983] are shifted to longer wavelengths for our μc-Si:H material compared to the polished <100> oriented single-crystal silicon. This indicates differences in the energy band diagrams between both types of materials.

The suspected increase in film crystallinity by an increase in T_{dep} could be subsequently verified. The dependence on T_{dep} of the structure of our μc-Si:H material was examined by Raman spectroscopy and X-ray diffraction measurements.

The **Raman spectra** of five different samples are shown in Fig. 3.1.1.5. It has been established [Brodsky 1977] that a disordered random network of Si (for example a-Si:H) which lacks long-range order yields a broad structure near 480 cm^{-1} in the spectrum associated with the transversal optic (TO) phonon mode. In contrast, a crystalline Si structure is represented by one sharp peak near 520 cm^{-1} (Γ_{25} (k = 0) line).

We have found that all our samples, even the one deposited at the lowest temperature of 40 °C, have a crystalline feature near 520 cm^{-1}: this is clearly seen in Fig. 3.1.1.5. The material deposited at 40 °C shows also an amorphous feature near 480 cm^{-1} implying clearly a coexistence of both amorphous and crystalline phases. Increasing T_{dep} results in an enhancement of the crystalline peak at the expense of the amorphous one that tends to disappear.

The plot of the position of the Raman crystalline peak frequency as a function of T_{dep} (not shown here but visible in Fig. 3.1.1.5) clearly shows a maximum at 520 cm^{-1} for films deposited at around 220 °C. An increase of the peak frequency of the crystalline component in the Raman spectra is said to be correlated with an increase of the crystallite size and a decrease of the lattice expansion [Iqbal 1982].

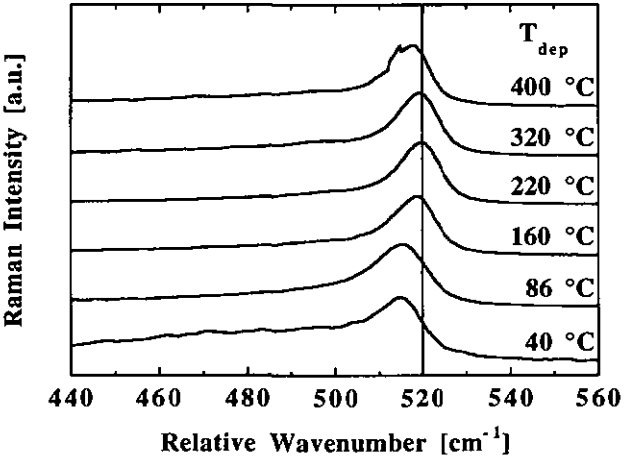

Fig. 3.1.1.5: Raman spectra of μc-Si:H samples as a function of deposition temperature.

The FWHM (full width at half maximum) of the Raman crystalline peaks (not shown here but visible in Fig. 3.1.1.5) shows a monotonous decrease from 7 to 5 cm^{-1} as a function of T_{dep}, where it saturates even for a further increase in T_{dep}. A linewidth decrease is associated with a decrease of the disorder at the boundaries of the crystallites which, in its turn, leads to an increased phonon lifetime [Iqbal 1982].

Thus, the decrease of the peak frequency of the crystalline component in the Raman spectra of films deposited at temperatures higher than 220 °C is suggested, from a similar study [Iqbal 1982], to be due to a decrease of the crystallite size (and/or to mechanical stress in the films). These results clearly confirm the reflectance analyses previously discussed.

The **X-ray diffraction measurements** contain signatures for different crystallographic planes from which one can derive information on preferential orientations of crystallites and the mean value of the grain size. The diffraction patterns of our μc-Si:H material (Fig. 3.1.1.6 for the film deposited at 220 °C) show two sharp peaks, characteristic of the <111> and <220> crystallographic planes, at the angular positions which satisfy the Bragg condition: $2\Theta = 28.45$ ° and 47.31 °, respectively. The other main crystallographic planes (<311>, <400>, <331> and so on) are not visible because of their too low intensities. The diffraction patterns observed correspond well with the diffraction pattern of Si powder indicating a homogenous distribution of crystallites in all directions (randomly oriented) with no preferential growth direction of the films. Moreover, the microcrystalline films are determined to be of c-Si cubic phase with a lattice constant a = 5.4309 Å.

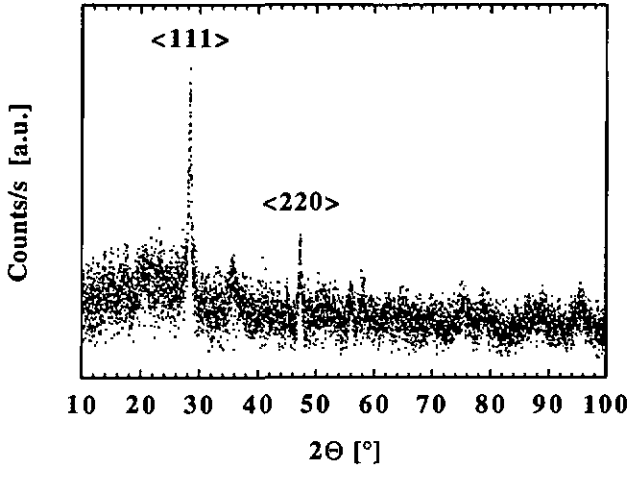

Fig. 3.1.1.6: X-ray diffraction pattern of the μc-Si:H film deposited at 220 °C.

For crystallites having a limited dimension, one can determine, by Scherrer's equation, the average size δ of the grains using the full width half maximum (FWHM) of a selected peak [Scherrer 1918]. This method yields the mean extension of the crystallites in the direction perpendicular to the chosen lattice plane. Based on this, we estimated the crystallite size of the different samples using the main peak at $2\Theta = 28.45$ ° for the <111> crystallographic plane (Fig. 3.1.1.7). We observe (see Fig. 3.1.1.7) when increasing T_{dep} a monotonous increase of δ from 100 Å to a saturation value of 250 Å reached at high temperatures. As reported by Veprek

[Veprek 1991] the evaluation by Scherrer's equation is correct only in the absence of mechanical stress in the film. Moreover, the peak broadening in the X-ray diffraction pattern due to internal mechanical stress is said [Veprek 1991] to become dominant at deposition temperatures above 300 °C for plasma deposited silicon films for which the crystallite size apparently approaches a constant value of 150 - 250 Å. For these films [Veprek 1991], the crystallite size evaluation from Scherrer's equation is, thus, no more correct for deposition temperatures above 300 °C.

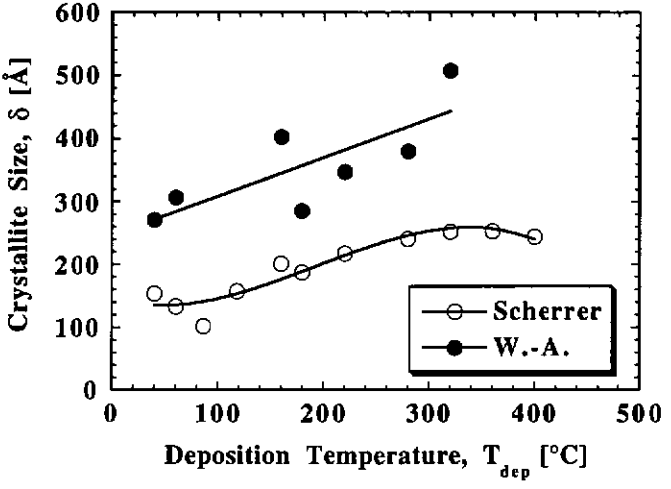

Fig. 3.1.1.7: Crystallite size determined by Scherrer's equation and Warren-Averbach's method as a function of deposition temperature.

To investigate this above mentioned problem more profoundly we undertook an independent evaluation of the crystallite size by using the Warren-Averbach method [Warren 1959] that performs a Fourier analysis of the peak profiles. This method - that works well for crystallite sizes in the range of 25 to 500 Å - leads to the average crystallite size of the material determined this time from both main diffraction peaks (<111> and <220>). Besides some scattering in the data, we observe (Fig. 3.1.1.7) - as expected - a monotonous increase of δ with T_{dep} in the studied temperature range of 40 to 320 °C. Because of computer evaluation problems some points are unfortunately missing here, especially those of the 2 especially interesting films deposited at 360 and 400 °C and, thus, nothing more can be said to the trend for higher temperatures. The values of δ are seen to be a little less than a factor two higher than those obtained by Scherrer's equation. This observation of higher values for δ obtained from Warren-Averbach's method is almost general; the differences observed in the evaluation of the crystallite size by using both above mentioned methods are due to different ways of evaluation, since, one more time, in our case only the <111> diffraction peak was used for the evaluation from Scherrer's equation while both <111> and <220> diffraction peaks were used for the evaluation from Warren-Averbach's method.

Thus, the apparent upper limit of the crystallite size as obtained from Scherrer's equation is possibly an artefact due to the finite contribution of internal mechanical stress in the films. It was also shown [Veprek 1991] that the presence of oxygen impurities in the plasma during the film deposition could be responsible for a structural transition to amorphous material. SIMS analyses shown in Fig. 3.1.1.2 show a slight increase in the oxygen content for films deposited at temperatures higher than 220 °C and this effect could therefore also explain the apparent upper limit of the crystallite size as obtained from Scherrer's equation. While the relatively low upper

deposition temperature limitation of the deposition system of 400 °C and the missing data - leading thus unfortunately to only very few films deposited at temperatures higher than 300 °C - hinders us in discriminating between these two possible explanations from these above discussed X-ray diffraction measurements, the UV/visible reflection spectroscopy analyses and the Raman spectroscopy analyses definitely support the second one.

Generally, **high resolution electron micrograph (HREM) images obtained from transmission electron microscopy (TEM)** enable one to see details of the film structures, namely: the crystalline and amorphous zones, crystallographic defects and grain boundaries. A micrograph image obtained by transmission of our μc-Si:H deposited at 200 °C is shown in Fig. 3.1.1.8. The brighter zones represent the crystallites satisfying the particular Bragg diffraction condition chosen for the taking of the picture. An evaluation of the average δ from TEM gives a value of about 200 Å which corresponds well to the value obtained from the X-ray diffraction measurements using Scherrer's equation (see Fig. 3.1.1.7).

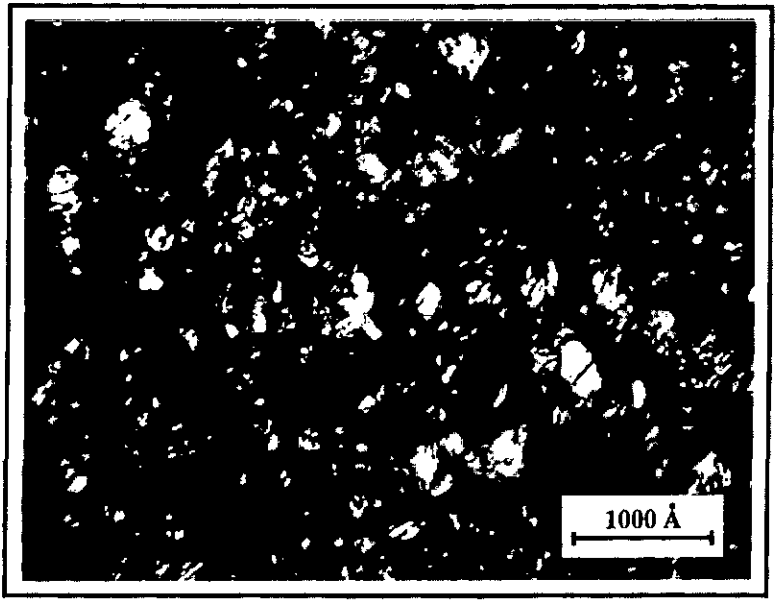

Fig. 3.1.1.8: High resolution electron micrograph (HREM) image obtained from TEM by transmission of a μc-Si:H film deposited at 200 °C.

Finally, as already mentioned at the beginning of this series study, the **deposition rate** shows a tendency to decrease slightly with increasing T_{dep} (from 0.6 - 0.48 Å/s when increasing T_{dep} from 40 - 360 °C for the chosen set of deposition parameters). An explanation for this may perhaps be found in the following effect: The deposition rate for μc-Si:H is generally smaller than the deposition rate for a-Si:H and therefore the observed and confirmed structural modifications towards more crystalline material (higher crystallinity) could possibly result in the observed decrease in the deposition rate.

3.1.1.3 Conclusions

Using the VHF-GD technique at 70 MHz, good quality μc-Si:H material is produced in a highly diluted silane glow discharge at low input discharge power and relatively low deposition temperatures.

The variation of T_{dep} for undoped layers in the wide range of 40 °C to 400 °C results in <n>-type μc-Si:H - as indicated by the low dark conductivity activation energies and thermopower experiment (not shown in this work) - tending for higher deposition temperatures towards more crystalline (higher crystallinity) and denser material: less hydrogen, less concentration of contaminants and unwanted dopants, smoother surface, larger crystallite size and also higher crystalline volume fraction, as concluded from all the electrical, optical and structural measurements presented above.

However, a decreased crystallinity is strongly suspected for temperatures higher than about 320 °C but has so far not been definitely confirmed by the author due to the relatively low upper system temperature limit of 400 °C leading to only very few experimental data for films deposited at temperatures higher than the critical value of 320 °C. A detailed and complete characterisation of a large number of films deposited in the temperature range of 300 to 500 °C would definitely confirm the above suggested hypothesis. Note that for our device applications of solar cells, the usual deposition temperatures are at present limited to about 220 °C, for the p-i-n's.

This deposition temperature series for undoped μc-Si:H allows us to obtain material with a wide range of electrical, optical and structural properties. A first application of our undoped μc-Si:H layers in an entirely μc-Si:H p-i-n solar cell (described in chapter 4) leads to the important observation that one can really extend the spectral response of the solar cell to longer wavelengths. These preliminary results published in part in [Flückiger 1992] show that μc-Si:H is a new promising solar cell material.

3.1.2 Comparison between standard 13.56 MHz UHV and 70 MHz VHF HV PECVD deposited film series

We report here on a comparison between two temperature series of "nominally" undoped μc-Si:H films, one deposited by standard 13.56 MHz ultra high vacuum UHV (modular multichamber system) and the other by "our" 70 MHz VHF high vacuum HV (single chamber system) PECVD techniques. The first one was carried out under UHV conditions (minimum chamber base pressure < $1x10^{-6}$ mbar) in a modular multichamber system preventing both the incorporation of residual impurities and cross contamination between different layers, the second one under HV conditions (minimum chamber base pressure of about $1x10^{-6}$ mbar) in a standard single chamber system. Particular attention has been devoted to differences and similarities between structural, compositional and electrical properties of the films deposited by the two different systems when the substrate deposition temperature was varied.

While by standard 13.56 MHz PECVD microcrystallite formation occurs only if the hydrogen dilution of silane is higher than 99 % and at deposition rates below 0.1 Å/s [Tsai 1988], the 70 MHz VHF PECVD method was demonstrated as being able of growing μc-Si:H films already at hydrogen dilution of silane higher than 95 %, at low substrate temperatures and at deposition rates as high as 0.7 Å/s [Flückiger 1992] (or even higher !).

The summarised results presented here are further treated and developed in detail elsewhere [Flückiger 1995a] where the plots are also shown; this results from a scientific collaboration between our group and the group of Prof. F. Demichelis of the Politecnico di Torino (Italy). The 70 MHz VHF HV PECVD deposited temperature series presented here was already treated and discussed in detail in chapter 3.1.1 (this work).

3.1.2.1 Experimental

Both sets of "nominally" undoped μc-Si:H films, those deposited by an ultra high vacuum standard 13.56 MHz PECVD [Madan 1993] system and those deposited by our high vacuum 70 MHz VHF PECVD system [this work, chapter 2], were deposited using a gas mixture of silane and hydrogen at different substrate temperatures. The detailed deposition parameters are described in Table 3.1.2.1.

	70 MHz VHF HV PECVD system (deposited in our laboratory)	Standard 13.56 MHz UHV PECVD system (deposited at Torino)
Inter-electrode distance, electrode surface and shape	15 mm, 133 cm^2, disk-like	25 mm, 100 cm^2, square
H_2 flow rate, SiH_4 flow rate and gas phase dilution (H_2/tot)	100 sccm, 3 sccm, 97 %	100 sccm, 1 sccm, 99 %
Pressure	40 Pa	100 Pa
RF input power and plasma power density	3 W, 8 mW/cm^2	4 W, 5 mW/cm^2 8 W, 13 mW/cm^2
Substrate temperature	60 - 320 °C	70 - 265 °C

Table 3.1.2.1: Deposition parameters of both sets of "nominally" undoped μc-Si:H films, those deposited at plasma excitation frequency of 13.56 MHz and those at 70 MHz.

As can be seen in Table 3.1.2.1, the deposition parameters are almost identical for both sets of films, except for some minor differences. The detailed experimental descriptions of the different characterisation techniques used to obtain the results described in the next part (3.1.2.2) as well as detailed plots illustrating the results can be found elsewhere [Flückiger 1992 and Flückiger 1994].

3.1.2.2 Summarised results and discussion

For a fruitful application of "truly intrinsic" (midgap material) μc-Si:H films as active layers in solar cells [Wang 1990 and Meier 1994a] certain technological problems, such as the achievement of a high deposition rate as well as that of a good film adhesion to the substrate have to be solved. We compare therefore deposition rates and substrate adhesion of μc-Si:H films deposited by both standard 13.56 and 70 MHz VHF PECVD techniques.

The **deposition rate** of the films deposited at the plasma excitation frequency of 70 MHz is about 0.7 Å/s (or even higher for higher input power densities), while that of films deposited at 13.56 MHz is as low as 0.1 Å/s for quite similar deposition conditions (see Table 3.1.2.1). This strong increase in the deposition rate at higher plasma excitation frequencies, by almost one order of magnitude, was already observed for the deposition of amorphous silicon [Curtins 1987] as well as for microcrystalline silicon [Prasad 1991 and Finger 1994].

The **adhesion** of the films to the substrate revealed to be good enough for the films deposited at 70 MHz to allow the growth of microcrystalline samples of a few micrometers thickness [Meier 1994a]. In contrary, for the films deposited at 13.56 MHz, the adhesion was not good enough, since problems of "peeling-off" occurred already when depositing 5000 Å thick films. An independent plasma excitation frequency study on μc-Si:H clearly showed through TEM analyses, that internal mechanical stress is larger at lower plasma excitation frequencies [Luysberg 1995]. Thus, the adhesion of the films to the substrate is certainly related to the internal mechanical stress of the films.

The **electrical properties** of both sets of films show certain minor differences. The values of the dark conductivity σ_d for all films, as deposited by both techniques, are orders of magnitude above those of device-quality a-Si:H films (for which $\sigma_d < 10^{-10}$ S/cm) and increase with T_{dep} (see Fig. 3.1.1.1 for the films deposited at 70 MHz). The values of σ_d for the films deposited at 13.56 MHz show a slight deviation from the monotonous increase up to the saturation value observed for those of films deposited at 70 MHz (see Fig. 3.1.1.1) and less than two orders of magnitude lower values. These observed differences are supported by the dark conductivity activation energies.

The **elemental composition** of the μc-Si:H films, deposited at both 70 and at 13.56 MHz plasma excitation frequency show the presence of oxygen for all films, with atomic concentrations lower than 3 %. Furthermore, the films deposited at 13.56 MHz show a slightly lower hydrogen content (about a factor two lower for the lowest T_{dep} of 86 °C with a relative difference tending to about 10 % for films deposited at high temperatures) as determined by resonant and nuclear reaction, ERDA and IR transmission spectroscopy. The hydrogen content for the films deposited at 70 MHz determined from ERDA measurements were already presented in Fig. 3.1.1.3 as a function of the deposition temperature. A monotonous decrease of C_H down to a saturation value of about 5 at. % when increasing T_{dep} was reported.

The microcrystallinity of all samples was verified by **Raman spectroscopy** and X-ray diffraction measurements. Both sets of films exhibit Raman spectra with a narrow peak around 520 cm^{-1} and a shoulder at about 480 cm^{-1}. As T_{dep} increases, the shoulder decreases suggesting that those films that contain even a certain crystallinity fraction at the lowest deposition temperatures are becoming more crystalline (higher crystalline volume fraction). Moreover due to the influence of the crystallite size (that increases with T_{dep}) [Iqbal 1982], the Raman c-Si peak is observed to shift from 514 to 520 cm^{-1}. No direct observable differences between both sets of films were obtained by Raman spectroscopy, as was also shown in a recent plasma excitation frequency study (13 - 120 MHz) of μc-Si:H films deposited at 200 °C [Hapke 1995].

The **X-ray diffraction** spectra were analysed for both sets of films, with T_{dep} ranging from 60 to 280 °C. In all the spectra, the main <111> and <220> diffraction peaks due to the crystal orientations are observed. The main difference between the two sets of films is a transition in the 13.56 MHz deposited film structure for T_{dep} > 200 °C: For temperatures below 200 °C, there is a predominance of the <111> diffraction peak which can be associated with a random distribution of the crystallite orientations, while for temperatures above 200 °C, the <220> diffraction peak - which is often correlated with a columnar growth [Prasad 1991] - becomes predominant. For the samples deposited at 70 MHz, the crystallite orientations remain mostly random for the range of T_{dep} investigated.

The **average crystallite size** δ analyses, as deduced from the <111> diffraction peak by using Scherrer's equation [Scherrer 1918], lead us to conclude the same trend of δ versus T_{dep} for both sets of films (see Fig. 3.1.1.7 for the films deposited at 70 MHz), except that the maximum crystallite size is higher (255 Å) for the films deposited at 70 MHz than the size observed (180 Å) for the films deposited at 13.56 MHz. Similarly, Finger et al. [Finger 1994] has shown in a plasma excitation frequency study of μc-Si:H deposited films, an increase of the average grain size determined by X-ray diffraction experiments with excitation frequency from 130 Å at 27 MHz to 320 Å at 120 MHz. Note that X-ray diffraction measurements only give an average grain size and the straightforward use of Scherrer's equation can severely underestimate the grain sizes [Veprek 1991].

All these differences just mentioned between the properties of μc-Si:H films deposited at both plasma excitation frequencies of 13.56 MHz and 70 MHz are summarised for more clarity in Table 3.1.2.2, presented hereafter.

Characterisation	70 MHz VHF HV PECVD system (deposited in our laboratory)	Standard 13.56 MHz UHV PECVD system (deposited at Torino)
Deposition rate	≥ 0.7 Å/s	≈ 0.1 Å/s
Film adhesion	Satisfactory; growth of films of a few micrometers thickness	Too low; problems of "peeling-off" already when depositing 5000 Å thick films
Electrical properties: σ_d	Monotonous increase when increasing T_{dep} up to the saturation value	Slight deviation from the monotonous increase and less than two orders of magnitude lower values
Hydrogen content	Monotonous decrease when increasing T_{dep} down to the saturation value	Same trend but slightly lower values; relative difference decreasing from 50 to 10 % when increasing T_{dep}
X-ray diffraction	Predominance of the <111> diffraction peak for the entire range of T_{dep} (60 to 280 °C), related to a random distribution of the crystallite orientations. Maximum δ of 255 Å, as evaluated by Scherrer's equation	Transition of the predominant diffraction peak from <111> to <220> for T_{dep} > 200 °C, suggesting a structural transition to a columnar growth. Lower maximum δ of 180 Å

Table 3.1.2.2: Differences between the properties of both sets of "nominally" undoped μc-Si:H films, those deposited at plasma excitation frequency of 13.56 MHz and those at 70 MHz.

All these differences mentioned above (and listed in Table 3.1.2.2) between the properties of μc-Si:H films deposited at 13.56 MHz and those of films deposited at 70 MHz can tentatively be related to differences in plasma chemistry, plasma physics and growth kinetic. As a matter of fact, results from plasma diagnostics [Howling 1992 and Heintze 1993a] and plasma impedance analysis [Kroll 1994] suggest that an ion bombardment with higher ion densities but lower average ion energies and a higher atomic hydrogen and radicals flux on the growth surface lead to favourable growth conditions for μc-Si:H at VHF plasma excitation. A higher gas phase dissociation in the bulk of the plasma is furthermore also suggested.

Thus, the higher deposition rate associated with the VHF plasma excitation can tentatively be explained by the higher ion, atomic hydrogen and radicals fluxes and the higher gas phase dissociation in the bulk of the plasma. The simultaneous increase in the growth rate and in the grain size of μc-Si:H deposited by VHF-GD at low deposition temperature is further suggested to be due to an effective selective etching of the disordered material creating, thus, more space to develop crystalline grains while at the same time also more space for faster growth of the crystallites becomes available [Finger 1994].

On the other hand, the bombardment of the growth surface with low average ion energies could reasonably contribute to the low value of internal mechanical stress suspected in the μc-Si:H films deposited at 70 MHz - as observed for a-Si:H [Kroll 1994a and Dutta 1992] and μc-Si:H [Luysberg 1995] - the same phenomenon could perhaps also explain the satisfactory film adhesion to the substrate and the onset of microcrystallinity already occurring at a hydrogen dilution of 95 %. This is probably not linked in such a simple manner, since, after all, stress and adhesion depend on many other factors. The film structure transition for the layers deposited at 13.56 MHz, and for T_{dep} > 200 °C from a homogenous growth (randomly oriented crystallites) to a columnar

growth (as suggested by the X-ray diffraction data of Flückiger et al. [Flückiger 1995a]) can possibly, also, be associated with the high-energy ion bombardment encountered at 13.56 MHz.

Finally, the observed difference in the grain size can possibly explain the slightly lower values of σ_d as observed for the films deposited at 13.56 MHz. Also, lower hydrogen content which is so low, as not being able to saturate all the defects and relax the strains at the crystallite intereonnections, can possibly lead to higher potential barriers at the grain boundaries, resulting, thus, in a deterioration of the electrical properties. Moreover, hydrogen that is known to be prevalently located at the surface of the silicon crystallites [Demichelis 1993], can decrease internal mechanical stress and improve the adhesion of the films to the substrate.

3.1.2.3 Conclusions

We have compared the structural, compositional and electrical properties of μc-Si:H films deposited by a standard 13.56 MHz UHV PECVD system in another laboratory with those of μc-Si:H films deposited by us with a 70 MHz VHF HV PECVD system, for deposition temperatures between 60 and 320 °C. The main advantages of the very high frequency-glow discharge technique at 70 MHz with respect to the deposition of microcrystalline films have been pointed out.

The deposition rate of films deposited at 70 MHz is revealed to be about on order of magnitude higher that of films deposited at 13.56 MHz and μc-Si:H films deposited at very high frequency show a better (and satisfactory) adhesion to the substrate even for thicknesses of some micrometers. Furthermore, improvement in the grain size and in the electrical properties for the films deposited at 70 MHz underlines the potential in choosing the VHF-GD technique for device deposition such as solar cells instead of the standard 13.56 MHz glow discharge method.

3.1.3 General conclusions

The effects of the deposition temperature and of the plasma excitation frequency on the film properties of "nominally" undoped μc-Si:H films were investigated, pointing out the main advantages to use the VHF-GD technique at 70 MHz, as developed at our laboratory.

Using the VHF-GD technique at 70 MHz, good quality μc-Si:H material is produced in a highly diluted silane glow discharge at low input discharge power and relatively low deposition temperatures. A variation in the deposition temperature leads to a wide range of film properties with films tending at higher deposition temperatures to be more crystalline (higher crystalline volume fraction) and to form a denser material. VHF-GD has been shown to produce μc-Si:H films at high deposition rates with low suspected mechanical stress and a satisfactory adhesion to the substrate: These being the essential conditions for the growth of thick μc-Si:H films as photovoltaic active layers in solar cells.

"Nominally" undoped films were shown to have the usual <n>-type character as most GD deposited films and have to be compensated by boron micro-doping for fruitful applications as a photovoltaic active material. This compensation mechanism as well as the film properties of compensated ("truly intrinsic" midgap material) μc-Si:H are treated in the next chapter (3.2).

3.2 Compensated films

Since the discovery in 1977 of the "Staebler - Wronski effect" [Staebler 1977] in hydrogenated amorphous silicon material (a-Si:H), a wide effort is being undertaken to obtain more stable material, especially for photovoltaic applications. Until now, this problem has not been fully solved. Preliminary work done with hydrogenated microcrystalline silicon (μc-Si:H) [Liu 1986 and Williams 1991] shows that this material does not degrade as much as a-Si:H and that it has the potential to become a new material for photovoltaic devices [Flückiger 1993, Meier 1994a and Williams 1991]. Moreover, microcrystalline silicon has, in general, lower optical absorption in the visible than amorphous silicon. It has, however, higher absorption in the infrared range [Flückiger 1993 and Meier 1994a]. Because of all these properties, fully microcrystalline p-i-n diodes may find their use within tandem structures, and it is towards this goal that we have studied "truly intrinsic" (midgap material) μc-Si:H layers.

As previously reported in chapter 3.1, we found that "nominally" undoped μc-Si:H has a slightly <n>-type character; this being already reported in earlier work [Wang 1990 and Willeke 1992]. Now, in the present study, we will try to obtain more insight into the doping compensation mechanism of μc-Si:H. Compensated layers are deposited by adding low quantities of diborane into the gas feed input of the plasma. The stability of such compensated μc-Si:H films was analysed under strong light illumination (fast degradation) and a detailed study of the electrical transport properties as a function of the doping level has been undertaken. The interpretation of our results is based on previous transport studies on microcrystalline silicon [LeComber 1983, Lucovsky 1993, Hapke 1993, and Rubino 1993]. The present study has already been partially published elsewhere [Flückiger 1995].

3.2.1 Experimental

In order to compensate the μc-Si:H material in the vppm (volume part per million) doping range (a technique we will henceforth call "micro-doping"), an additional mixing chamber was installed at the process chamber (see Fig. 2.1.1).The gases used were silane (SiH_4), hydrogen (H_2) and diborane (B_2H_6). The films were deposited at a dilution level of 3 % silane in hydrogen and a total gas flow of about 100 sccm. The micro-doping gas phase ratio (B_2H_6/SiH_4) was varied between 0 (undoped) and 10 vppm. The power measured at the power meter was 3 W. The substrate deposition temperature T_{dep} was 220 °C and the gas pressure was kept at 0.4 mbar. The film thicknesses were in the range of 0.4 μm and the deposition rates obtained were around 0.5 Å/s. These deposition parameters lead to high crystallinity films, with a crystalline volume fraction X_C of almost 90 % (not shown here). Furthermore, the crystallinity is expected not to be affected much by the micro-doping experiments [Finger 1993] and should hence be similar to that of the previously treated undoped μc-Si:H film series (3.1). The detailed experimental descriptions of the different characterisation methods mentioned in the next part (3.2.2) can be found elsewhere [Flückiger 1995].

3.2.2 Results and discussion

To be able to judge the results of the degradation studies we have first to understand the effects of the compensation experiments. The slightly <n>-type character of the "undoped" as-grown μc-Si:H (see 3.1) material (to be termed more precisely as "not intentionally doped") is compensated by systematically adding small amounts of diborane (micro-doping) into the gas phase, pushing thus the Fermi level (E_F) towards midgap.

Fig. 3.2.1 shows the **boron concentration** [B] (at/cc) in the films (bulk values) as a function of the micro-doping gas phase ratio (B_2H_6/SiH_4) obtained from SIMS (secondary ion mass spectroscopy) measurements. One can observe the pronounced onset of the boron incorporation into the films at a doping gas phase ratio of about 3 vppm. The concentrations of phosphorus, hydrogen and of major impurities incorporated into the films, are constant over all samples and are as follows: $C_P = 3x10^{16}$, $C_H = 3x10^{21}$, $C_O = 2x10^{19}$ (!), $C_C = 1.5x10^{18}$ and $C_N = 1x10^{16}$ (at/cc). As we will see later, the compensated film (lowest dark conductivity and highest dark conductivity activation energy) has a boron concentration of about $3x10^{16}$ (at/cc) for a micro-doping gas phase ratio of about 1 vppm, this value (boron concentration) corresponding to the phosphorus concentration mentioned above. So, besides the N and especially O contaminations, the phosphorous atoms present could possibly also contribute to the slightly <n>-type character of the "undoped" films. Another recent study done jointly by our group and the Jülich group [Finger 1993] dealing with compensation by the two types of dopants (P and B) showed, surprisingly, an optimum compensation for a 1 : 1 mixture of PH_3 and B_2H_6.

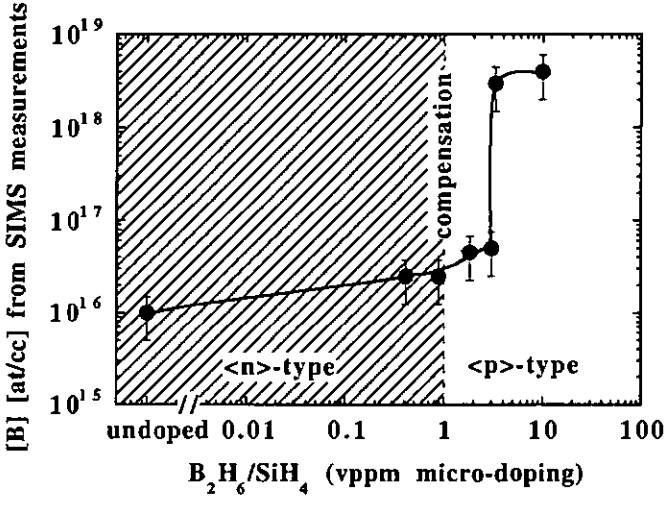

Fig. 3.2.1: Boron concentration [B] (at/cc) in the films (bulk values) measured by SIMS as a function of the micro-doping gas phase ratio (B_2H_6/SiH_4) in vppm (volume parts per million). The undoped film is arbitrarily placed at the left hand side of the x-axis.

Other groups [Wang 1991] have proposed as an alternate explanation, that the <n>-type character is due to the distortion of the network at the transition between crystallites and the surrounding amorphous matrix (or grain boundaries), leading thereby to a density of states

distribution that allegedly pins E_F at the grain boundaries near the conduction band of the crystallites. Whereas such an effect may also be present, we definitely suggest that the involuntary incorporation of contaminants and dopants is the main reason behind the <n>-type character of "undoped" or, rather, "not intentionally doped" films as already partially proposed in section 3.1.1.2 above.

Fig. 3.2.2 shows the effect of the compensation experiment on the **room temperature dark conductivity** and on the **dark conductivity activation energy** as a function of boron concentration [B] (at/cc) measured in the films by SIMS. It can clearly be seen that the Fermi level position reacts sensitively to the diborane partial pressure via the boron incorporation level. Micro-doping shifts the dark conductivity over a wide range from $2x10^{-3}$ (S/cm) for the undoped material to $3x10^{-8}$ (S/cm) at ~ $3x10^{16}$ B/cc. In the same way, the activation energy increases from 107 meV to the maximum value of 618 meV. Further doping leads to a very sharp increase of σ_d and to <p>-type material [Willeke 1992 and Wang 1990] and, for polycrystalline layers [Seto 1975], with values for E_σ that become once again smaller. (The electrical properties of the <n>-type material are studied in detail in [Richter 1981]).

In analogy with a study of boron doping in polycrystalline silicon [Seto 1975], such a sharp increase in the dark conductivity may be interpreted as being the result of the increase in carrier concentration and mobility. (Note that another recent study of our group [Finger 1993] dealing with compensation by the two types of dopants (P and B) did not lead to such a low dark conductivity value ($6x10^{-5}$ (S/cm)), as the one obtained here in the present work). The Arrhenius plot of the dark conductivity shows for higher temperatures (100 - 200 °C) a slightly steeper decrease than for temperatures below 100 °C. We plotted the lower values of E_σ - determined from the temperature range of 29 - 82 °C - which correspond to the RT conductivity points drawn in Fig. 3.2.2.

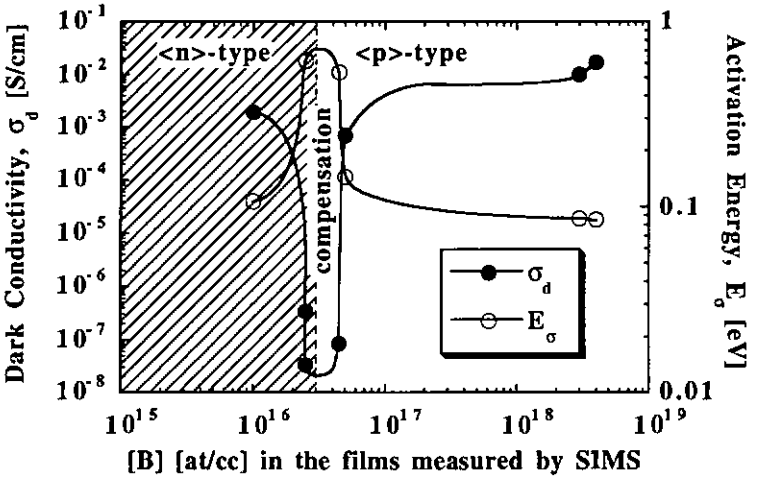

Fig. 3.2.2: Dark conductivity (at room temperature) and dark conductivity activation energy as a function of the boron concentration [B] (at/cc) measured in the films (bulk values) by SIMS. The compensation point is obtained at a doping gas phase ratio of about 1 vppm (B_2H_6/SiH_4), corresponding to a boron concentration (SIMS) of about $3x10^{16}$ (at/cc) in the film.

The doping gas phase ratio needed here to achieve the compensation of the material at ~ 1 vppm - corresponding to a boron concentration value of about $3x10^{16}$ at/cc - is significantly lower than those reported by [Williams 1991 and Wang 1990] using a remote plasma enhanced chemical vapour deposition (RPECVD) system; in the latter work, compensation was obtained for a boron concentration of $5x10^{17}$ (at/cc). Furthermore, the remote PECVD deposition leads to maximum values of E_σ around 0.7 eV [Williams 1991 and Wang 1990], i.e. slightly higher values than those found here (0.618 eV). This difference may be due to a higher bandgap prevailing in the RPECVD material - possibly, the higher bandgap arises from a lower crystalline volume fraction - or simply from differences in the σ_d temperature range for which the E_σ values were estimated.

In Fig. 3.2.3 we plot σ_{ill}/σ_d and σ_{photo} (at 100 mW/cm^2) as a function of the boron concentration (at/cc) in the films as measured by SIMS. To avoid confusion with the notation, we will write:

$$\sigma_{ill} = \sigma_{photo} + \sigma_d \qquad (1)$$

with σ_{ill} = conductivity as measured under illumination, σ_{photo} = photoconductivity (calculated from equation *(1)*) and finally σ_d = dark conductivity. σ_{ill}/σ_d shows a similar curve to the one for E_σ; the same is true for σ_{photo} and σ_d. σ_{ill}/σ_d shows a maximum value of about $6x10^3$ around compensation, whereas σ_{photo} exhibits a minimum of $1.5x10^{-4}$ (S/cm).

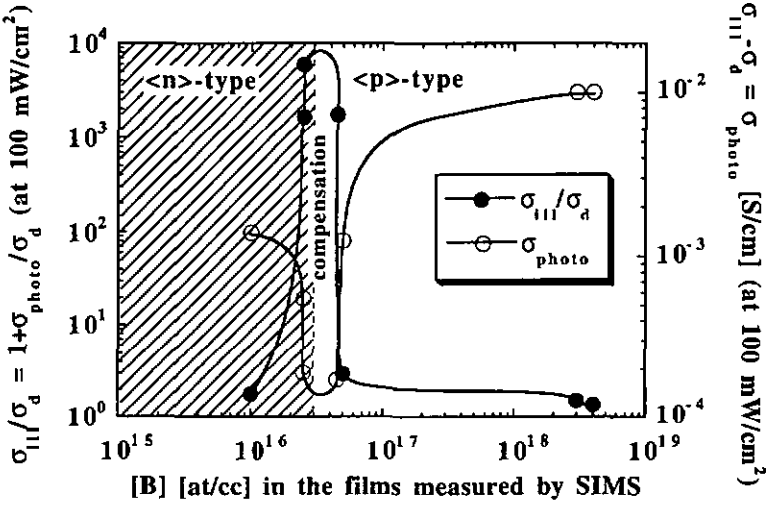

Fig. 3.2.3: σ_{ill}/σ_d and σ_{photo} (at 100 mW/cm^2) as a function of the boron concentration [B] (at/cc) in the films measured by SIMS. σ_{ill} is the measured value of conductivity under illumination, σ_d the dark conductivity and σ_{photo} the calculated photoconductivity (equal to $\sigma_{ill} - \sigma_d$).

This maximum of the photoconductive gain at 100 mW/cm^2 for our compensated μc-Si:H is a little higher than the one observed in [Lucovsky 1993] for both RPECVD and reactive magnetron sputtering technique deposited films and measured there under 0.5 AM1 illumination. These high values of photoconductive gain could be an indication that μc-Si:H can indeed be used as a photovoltaically active material.

In order to explain the minimum in photoconductivity obtained for compensated μc-Si:H, we propose the following line of thought. One may compare this minimum to a similar minimum

observed in a previous study [Pipoz 1992] for compensated amorphous silicon films. It was found there that a transition from one type of dominant free carrier to the other ($n_f \approx p_f$) is responsible for the minimum in photoconductivity observed on this particular compensated film. A similar effect may also prevail in the present series of μc-Si:H films.

Very generally, σ_{photo} is given by the (average) carrier density under illumination (this carrier density is at least in our case, for which the photoconductive gain is relatively high, i.e. $> 10^3$, much higher than the carrier density at thermal equilibrium) that is limited or governed by recombination. Now, recombination shows a maximum (both in the Shockley-Read-Hall (SRH) case, as well as for the three charge states model of the dangling-bonds developed by our group for compensated and slightly doped a-Si:H [Hubin 1994] which is the more appropriate case here) when $n_f \approx p_f$. (Very generally, recombination is always a two-carrier process involving holes and electrons and is approximately proportional to the product of n_f by p_f). Hence, if recombination is maximum, σ_{photo} is minimum.

Unfortunately, at present we do not have the needed transport measurements on these compensated films to be able to definitely confirm the above developed explanation.

The **absorption** in the subgap region as measured by PDS (photothermal deflection spectroscopy - the corresponding experimental set-up being described in detail in [Curtins 1988] -) is shown for the compensated film (0.9 vppm micro-doping gas phase ratio) in Fig. 3.2.4.

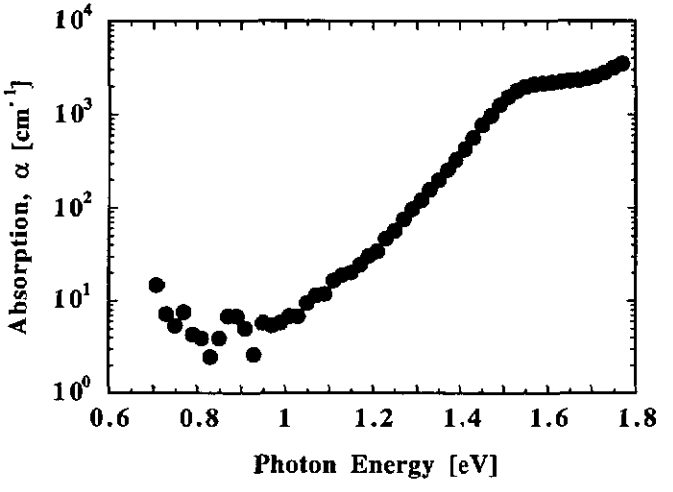

Fig. 3.2.4: Absorption of the compensated film (0.9 vppm micro-doping gas phase ratio) measured by PDS and calibrated through transmission/reflection data. The calibration of the PDS spectrum was done at 600 nm (2.07 eV).

The PDS spectra were calibrated at 600 nm from transmission and reflection spectroscopy measurements by neglecting the multiple reflections and using the expression T / (1-R) [Summonte 1993]. The low photon energy (< 1 eV) absorption value for this film is < 10 cm^{-1} and this is remarkably low for μc-Si:H material (see also [Meier 1994a] for the PDS spectrum of a 1.8 μm thick compensated μc-Si:H film). For comparison, a μc-Si:H film compensated by the use of two types of dopants, i.e. P and B (our previous series) shows an absorption value higher than 30 cm^{-1} [Finger 1993], whereas the high photon energy (> 1.5 eV) absorption is very similar for

both series. RPECVD compensated ("truly intrinsic" midgap material) μc-Si:H also shows a higher subgap absorption [Wang 1990].

We also measured (but did not plot) the absorption as a function of micro-doping in the region 0 - 3.3 vppm (gas phase ratio) and observed identical spectra with small variations in the low photon energy absorption values; these variations are less than a factor of three. Similarly, work done previously on compensated a-Si:H films by our own group [Sauvain 1993] showed also roughly constant deep defect densities (constant subgap absorption) as a function of the doping level (in the same range of low-level doping as studied here).

The subgap absorption has been related in μc-Si:H material both to deep defects and to free carrier absorption [Finger 1993]; we conclude, here, from the low values of subgap absorption observed on our set of films that they are not doped strongly enough to observe the effect of the free carriers. Furthermore, it has been concluded from IR transmission spectroscopy measurements on doped μc-Si:H material [Finger 1993] that the observed baseline shift is related to free carrier absorption. IR measurements on our compensated series (not presented here) indeed do not show a baseline shift, confirming, thus, that there is here no observable free carrier absorption.

Hence, the low value of subgap absorption measured for the compensated film clearly indicates the low level of deep defect densities obtained by us; this furthermore points out the real potential of this newly developed material as a photovoltaically active film in solar cell devices.

In order to tentatively explain the **temperature behaviour of the dark conductivity** of our set of micro-doped films (for the chosen limited temperature range of 29 - 82 °C for which the Arrhenius plots of σ_d show quite well a straight line), we will now use the usual simple expression for a thermally activated conductivity:

$$\sigma = \sigma_0 \exp(-E_\sigma / KT) \qquad (2)$$

with σ_0 = conductivity prefactor (characteristic conductivity of the transport in the extended states) and E_σ = effective activation energy.

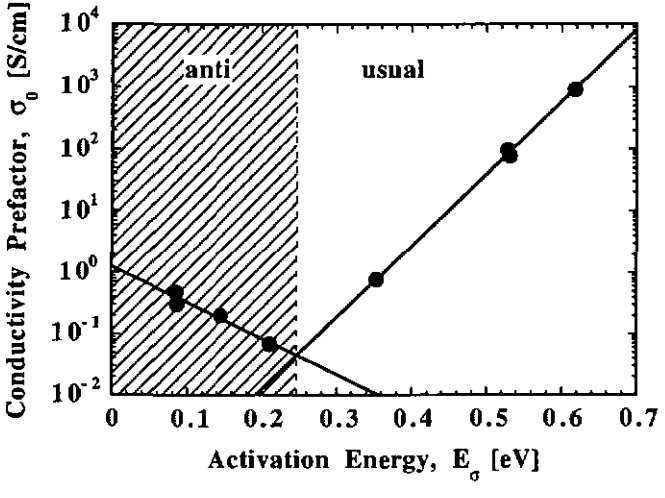

Fig. 3.2.5: Dark conductivity data: conductivity prefactor σ_0 as a function of the effective activation energy E_σ.

This procedure is based on the work of [Hapke 1993] for VHF-GD samples with E_F near midgap where we had showed - also supported by another work [Finger 1993] - that a simple activated behaviour for the electrical transport is not found when a wide temperature range is covered. Then, in Fig. 3.2.5 we can plot ln σ_0 versus E_σ for our set of films, and identify two different regimes. The data can be fitted by two exponentials demonstrating the "usual Meyer-Neldel behaviour" [Overhof 1983] as well as the so-called "anti Meyer-Neldel behaviour" (inversion of the slope) [Kikuchi 1988]:

$$\sigma_0 = \sigma_{00} \exp (E_\sigma / E_0). \quad (3)$$

These two regimes were already reported many times for μc-Si:H material and are now quite generally accepted [Lucovsky 1993, Rubino 1993 and Manfredotti 1993]. The critical E_σ threshold value of about 0.25 eV separates the two different transport regimes. For $E_\sigma \geq 0.25$ eV (compensation regime) we are in the "usual Meyer-Neldel behaviour" (positive slope) as explained by the statistical shift of E_F (the temperature variation of E_F is assumed to be linear for this region where E_F moves, with temperature and doping, in the band-tails) [Overhof 1983]. This behaviour is revealed to be the usual one for a-Si:H because of the low doping efficiency. The dominant transport in this regime, that takes place in the extended states across the internal potential barriers for μc-Si:H, is believed to be dominated by thermionic emission [Lucovsky 1993], in analogy with work on polycrystalline silicon layers [Seto 1975].

Contrary to this, for $E_\sigma < 0.25$ eV we are in the "anti Meyer-Neldel behaviour", where due to the very low E_σ values, the transport is believed to be dominated by tunneling from band states of the Si crystallites through the band-tail states of the intervening thin amorphous phase [Lucovsky 1993]. This second branch of the Meyer-Neldel plot was already predicted [Overhof 1983] for single phase heavily doped a-Si:H by numerical modelling of regions where E_F comes out of the exponential band-tails (for low and high E_σ) and assuming a simple thermally activated transport process in the extended states. However, this second branch is not directly accessible for a-Si:H because the Fermi level can not be moved into the band-tail states enough [Street 1985].

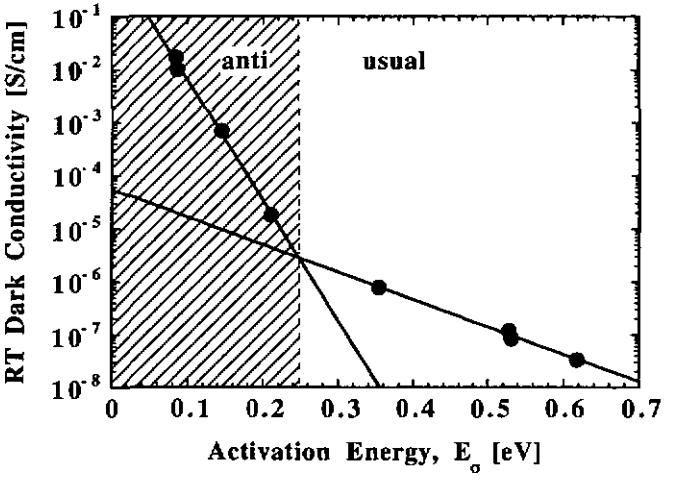

Fig. 3.2.6: Dark conductivity data: room temperature dark conductivity as a function of the effective activation energy E_σ.

In addition, the plot of σ_{RT} (room temperature dark conductivity) versus E_σ represented in Fig. 3.2.6 can again be fitted with two exponentials showing thereby (with equations (2) and (3)) the consistency of the Meyer-Neldel rule (see [Lucovsky 1993] for a more detailed description).

Substantial similarities between the electrical features of our μc-Si:H films deposited by 70 MHz VHF PECVD and the ones of μc-Si:H films obtained by several other techniques such as 13.56 MHz PECVD, RPECVD and LPCVD [Lucovsky 1993, Rubino 1993 and Manfredotti 1993] were observed with respect to differentiating between "usual Meyer-Neldel behaviour" and "anti Meyer-Neldel behaviour". However, our experimentally estimated critical E_σ value of about 0.25 eV separating both transport regimes is substantially higher than all other reported ones; the latter are lower than 0.1 eV [Lucovsky 1993, Rubino 1993 and Manfredotti 1993].

The transport study of μc-Si:H films, satisfying the "anti Meyer-Neldel behaviour" where E_F lies very high in the density of states (very low E_σ values) in a relatively flat region, is revealed to be a very complicated task since many different transport paths (thermally activated, tunneling and hopping) could take place simultaneously. Detailed electrical data on the carriers and on their mobility as a function of temperature from Hall and thermopower experiments, and a clear picture of the density of states distribution in the bandgap of microcrystalline material are essential.

During **light-soaking experiments**, the conductivity under illumination σ_{ill} of three different samples (illuminated from both sides) was simultaneously monitored (Fig. 3.2.7); the intensity of the sodium lamp used (about 500 mW/cm^2, ~ 1.5x10^{18} photons/cm^{2}s) was controlled by a photodiode in parallel. With the absorption coefficient of about 1x10^4 cm^{-1} at the wavelength of 590 nm of our light source a relatively uniform illumination throughout the entire μc-Si:H film (~ 0.4 μm thick) is achieved (decrease of light intensity in the middle of the film < 18 % with respect to the light intensity at the two edges). The temperature during the light exposure was 40 °C and was measured by an infrared thermometer.

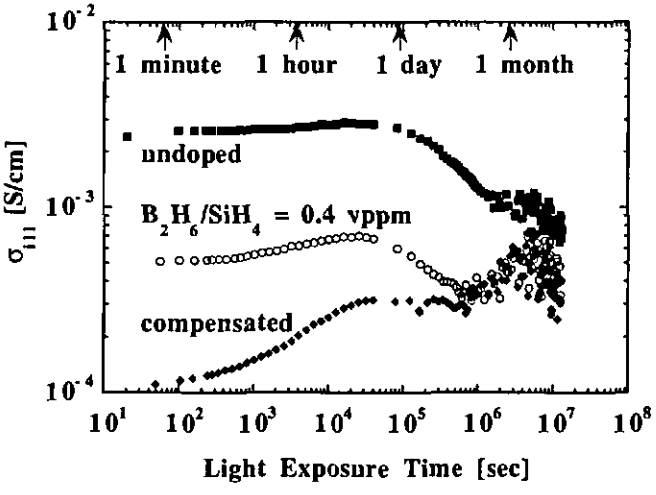

Fig. 3.2.7: σ_{ill} for three different samples (undoped, 0.4 vppm and compensated (0.9 vppm doping gas phase ratio)) from the compensated series as a function of the light exposure time (sodium lamp at 500 mW/cm^2, ~ 1.5x10^{18} photons/cm^{2}s). The films were illuminated from both sides.

The behaviour of the three samples is rather surprising. On the one hand the σ_{ill} value of the undoped material slowly decreases with long-term illumination (5 months); in contrast to this, on the other hand, for the compensated sample (0.9 vppm doping gas phase ratio) σ_{ill} seems even to increase slightly with time. The undercompensated probe (0.4 vppm doping gas phase ratio, slightly <n>-type) shows a small variation of σ_{ill} but remains more or less constant over the observed time period. Similarly, Williams et al. [Williams 1991] reported no Staebler-Wronski effect for the conductivity under weaker illumination (50 hours at 50 mW/cm^2) for compensated µc-Si:H deposited by RPECVD. From the plot (Fig. 3.2.7) it seems that all curves are converging after long-time illumination to the same point but this has to be further checked by a still longer illumination time (> 1 year !). Note that, after about 12 days of light exposure time an unexpected strong scattering of the σ_{ill} data plotted in Fig. 3.2.7 is observed. An analysis of the intensity of the sodium lamp used and of the temperature during light exposure as a function of the light exposure time shows no correlation with the observed scattering of σ_{ill}. This strong scattering of σ_{ill} - seldom observed during light-soaking experiments performed on a-Si:H films - remains unexplained by the author and has in the future to be further examined in order to be explained.

Analysing the net photocurrent:

$$\sigma_{photo} = \sigma_{ill} - \sigma_d \qquad (4)$$

before and after degradation we observe that the photocurrents for all three films (not shown here) are only slightly affected by long-term light exposure; furthermore, they reach, after degradation, similar values around 3×10^{-4} (S/cm). Thus, the variations of σ_{ill} in Fig. 3.2.7 could be mainly due to changes in the dark conductivity. In fact, the observed decrease of the dark current is accompanied by an increase in the activation energy (also reported elsewhere [Liu 1986]), meaning that E_F is pushed during degradation towards midgap.

From the above observations, we conclude that light-soaking has less effect (or even practically no effect) on compensated material; a low degradation rate was also found (probably not the same effect than for this case of µc-Si:H films), at least for the beginning of degradation, in a previous study of micro-doped a-Si:H films [Sauvain 1994].

Because the presented data are unfortunately the only ones we have on this specific degradation experiment, we are not yet able to clearly explain what happens. Instead, here are some suggestions based on different work done on a-Si:H and µc-Si:H. It is generally said about microcrystalline material that it degrades less than a-Si:H because of a self-limiting mechanism in the formation of the light-induced defects [Liu 1986 and Stutzmann 1984]. (These defects or dangling bonds act as dominant recombination centers in a-Si:H under illumination). It was further shown [Liu 1986] that the dangling bond defect density is proportional to the crystallite size δ, preventing, thus, for films with large crystallites ($\delta > 120$ Å) the creation of new detectable dangling bonds through light-soaking. The observed increase of defects by light-soaking - the defects are reported to be located at the grain boundaries [Wang 1991, Finger 1994a and Malten 1995] - pushes in our experiment the Fermi level towards midgap changing thus the properties of the films.

Thus as a conclusion from our work on micro-doped µc-Si:H and the ones mentioned above, we suggest that the degradation rate of µc-Si:H films depends mainly on the density of the already existing defects - what explains why generally µc-Si:H "degrades" less than a-Si:H - and on the position of E_F as prevailing in the initial state, what explains why the particular compensated film degrades the least from the micro-doped studied film series. Finally, first light-soaking experiments of an entirely µc-Si:H cell which photovoltaically active layer is a compensated ("truly intrinsic" midgap material) 1.7 µm thick µc-Si:H film [Meier 1994] indicate no observable degradation (see Fig. 4.3). This makes this newly developed µc-Si:H very attractive as a photovoltaically active stable material.

3.2.3 Conclusions

The VHF-GD process favours the deposition of microcrystalline silicon with a high crystallinity ($\delta \geq 200$ Å and $X_C \geq 90$ %) yielding thereby "nominally" undoped films having basically low activation energies (due to extrinsic impurities and contamination dopants). With low-level boron doping, "compensated" ("truly intrinsic" material) films can be deposited, with the Fermi level position at midgap.

Compensation of the initially <n>-type material could be achieved here by the introduction of a "micro-doping" technique. The very sharp compensation point obtained corresponds to maxima for the dark conductivity activation energy and the photoconductive gain (photo/dark current ratio) and to minima for the dark conductivity and for the photoconductivity.

The low value of subgap absorption determined from PDS experiment for the compensated film clearly indicates a low level of deep defects; this can be related to the high crystallinity and the good quality μc-Si:H film produced by the 70 MHz VHF PECVD process.

The author pointed out, from transport characterisation in the temperature range of 29 - 82 °C, the transitions from the "usual Meyer-Neldel behaviour" to the "anti Meyer-Neldel behaviour" occurring at a dark conductivity activation energy threshold value of 0.25 eV.

Light-soaking experiments with a high intensity, high pressure sodium lamp have shown clearly better stability for the new compensated μc-Si:H than for undoped films. In fact, for our series of films, the compensated one appears to be the most appropriate for solar cell applications - as a new promising stable photovoltaic active material - since it degrades the least, its dark conductivity is the lowest and its photoconductive gain is the highest. It is even suggested that μc-Si:H generally degrades less than a-Si:H due to a high defect density at the grain boundaries of the microcrystalline material that prevents the formation of new detectable defects by light-soaking. This statement has to be further checked by detailed and intensive studies and comparisons of both types of silicon material.

Using such compensated material for the implementation of entirely μc-Si:H p-i-n solar cells, the extension of the built-in field into the cell could lately be improved (better field uniformity) [Flückiger 1993], as compared to previously published results [Flückiger 1992] which used undoped μc-Si:H. Thanks to the confirmation of the better stability of such all μc-Si:H solar cells [Meier 1994a], microcrystalline silicon could become a new encouraging thin-film base material contributing to a solution to the photovoltaic problem provided the efficiency can be increased close to 10 %. The most realistic application of our microcrystalline material remains nevertheless the development of stable tandem structures with a standard amorphous p-i-n top cell and an entirely μc-Si:H p-i-n as bottom cell as reported in [Meier 1994a].

3.3 Boron doped films

Before having finally prepared solar cells using the compensated microcrystalline material already presented in (3.2), we first had to develop very thin appropriate <p>-type μc-Si:H and μc-SiC:H window layers; their detailed study will be given here (respectively in (3.3.1) and (3.3.2)). The <n>-type μc-Si:H material (thick and thin layers) was already studied in detail and presented elsewhere [Prasad 1990, 1991 and 1991a]. For solar cell applications, the most important features for a high quality <p>-type window layer are: its high transparency, its high conductivity and its overall ability of being an efficient emitter [Luft 1993]; it is towards these goals that we studied <p>-type microcrystalline silicon films.

3.3.1 <p> μc-Si:H film series

Our earlier studies have shown [Prasad 1990 and 1991] that by the VHF-GD technique at the plasma excitation frequency of 70 MHz, the input power for the growth of μc-Si:H can significantly be reduced, compared to conventional 13.56 MHz GD [Prasad 1991a and Flückiger 1992]. Also, the deposition temperature can be kept lower. Moreover, as already reported, doping efficiency for μc-Si:H is much higher than for a-Si:H [He 1983, Spear 1981 and Willeke 1992]. Thus, for thick <p> layers (0.3 μm) activation energies of 20 meV and dark conductivities of 30 (S/cm) can be obtained [Prasad 1991 and 1991a]. This very low value of E_σ and the high dark conductivity encouraged us to investigate the properties of very thin <p> μc-Si:H layers.

<p>-type μc-Si:H very thin films have proven to be excellent window and barrier layers for solar cells because of their high conductivity and transparency [Flückiger 1993 and Luft 1993]. However, due to the fact that boron in the gas phase hinders the nucleation of crystallites [Ghosh 1992 and Chou 1992], very thin films of <p> μc-Si:H have been difficult to deposit.

We present here results for very thin <p> μc-Si:H films (< 350 Å) deposited at low temperature (170 °C). First, the effect of boron doping on the growth and on the electrical properties of <p> μc-Si:H very thin films is investigated, leading to an optimised value of about 0.6 % for the diborane gas phase ratio (B_2H_6/SiH_4). The electrical, optical and structural properties of an optimised thickness series ranging from 100 to 350 Å are studied using thickness and conductivity measurements, transmission spectroscopy, transmission electron microscopy (TEM), Raman spectroscopy, grazing angle X-ray diffraction/reflection and spectroscopic ellipsometry measurements. Further, a columnar structure growth model for these very thin <p>-type μc-Si:H films will be proposed. This present study is partially published elsewhere [Flückiger 1993 and 1994].

3.3.1.1 Experimental

All films studied here were deposited with the same chamber history (the walls and electrodes being covered in the same manner with <p> μc-Si:H), so as to guarantee maximum reproducibility. To minimise a change in the surface of the thin films after deposition, they were all stored in an argon atmosphere.

The gases used were silane (SiH_4), hydrogen (H_2) and diborane (B_2H_6). The films were deposited at a dilution level of 1.6 % ($SiH_4/(SiH_4 + H_2 + B_2H_6)$) and a total gas flow of about

100 sccm. The doping ratio (B_2H_6/SiH_4) was varied between 0.1 and 0.9 %. The power measured at the power meter was 10 W. The substrate deposition temperature T_{dep} was 170 °C and the gas pressure was kept at 0.8 mbar. The film thicknesses were ≤ 350 Å (as measured and averaged over about twenty measurements) and the deposition rates obtained were ≤ 1.25 Å/s. The lowest thickness limit was about 100 Å for which low value the film was hardly visible by the eyes. Furthermore, the glass surface roughness is estimated (by the author) to be of 50 - 100 Å limiting thus a realistic film thickness to values higher than 100 Å. Due to the very low thicknesses encountered in this film series only few of the standard film characterisation methods could be performed. The uniformity of the films was checked by the eyes and estimated to be satisfactory for all films and for the entire surface, except for the borders due to the screening effect of the substrate holder during deposition.

The detailed experimental description of the different characterisation techniques mentioned in the next part (3.3.1.2) can be found elsewhere [Flückiger 1994].

3.3.1.2 Results and discussion

First, the effect of boron doping on the growth and electrical properties of very thin μc-Si:H films is investigated. Fig. 3.3.1.1 shows the **room temperature dark conductivity** σ_d as a function of the boron doping ratio (B_2H_6/SiH_4) in the range of 0.1 - 0.9 %, for different film thicknesses (range: 100 - 340 Å). The other deposition parameters were fixed (see (3.3.1.1)) and appropriately chosen from previous optimisations [Prasad 1991 and 1991a].

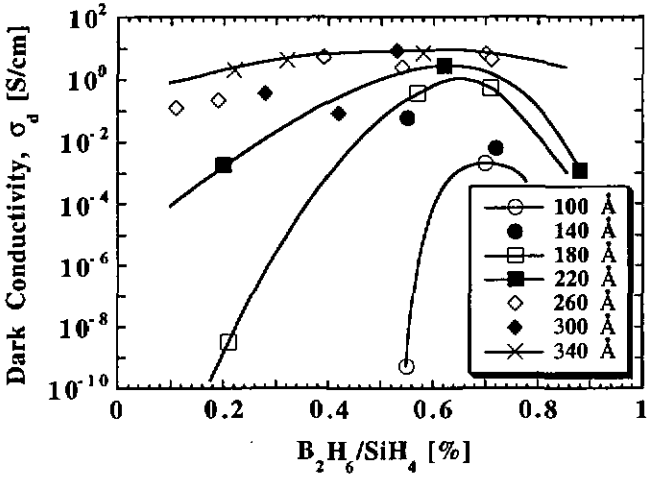

Fig. 3.3.1.1: Room temperature dark conductivity as a function of the diborane doping ratio for different film thicknesses.

While for the thickest films, the doping ratio does not influence σ_d very much, for very thin films the effect is drastic. To explain the shape of the curves of constant thicknesses, two competitive effects must be taken into account; first, by increasing the boron doping ratio slightly, the Fermi level E_F is pushed towards the valence band, thus increasing strongly σ_d. A further increase of the boron doping ratio to values higher than about 0.8 % (for the chosen set of deposition parameters) leads to structural changes of the material by amorphisation as was reported elsewhere [Prasad 1991 and Ghosh 1992].

In fact, it is now generally believed that diborane in the plasma gas phase favours the formation of amorphous material by increasing significantly the number of growth sites through hydrogen abstraction ("scavenging action") and reduction of the surface diffusion coefficient, enhancing thus, the film growth rate (as will be shown later) [Ghosh 1992 and Chou 1992]. It was proposed elsewhere [Prasad 1991 and 1991a], that in heavily doped samples, inactive boron atoms segregate to the grain boundaries where they hinder crystallite formation. Since, the doping efficiency in amorphous material is much lower than in μc-Si:H (due to a lower structural ordering) [He 1983, Spear 1981 and Willeke 1992], and furthermore, an increased doping for already degenerated films results in a reduced charge mobility (due to inactive boron atoms that create defects in the energy band), the conductivity of thin μc-Si:H films decreases strongly with boron doping higher than about 0.8 %.

The general trend of the decrease of σ_d with decreasing the film thickness at constant doping ratio is explained by a structural transition with the dominant phase changing from microcrystalline to amorphous material, as shown later. This effect is furthermore very sensitive to the diborane doping ratio as it can be observed in Fig. 3.3.1.1. The optimised boron doping ratio for what concerns both the electrical properties and the crystallinity of the deposited films seems to be in the range of 0.5 - 0.7 %; this boron doping ratio will be fixed at 0.6 % for the thickness series study presented hereafter.

The **deposition rate** r varies in this study of very thin <p> μc-Si:H films with the diborane doping ratio and also with the thickness of the films, as presented in Fig. 3.3.1.2; the latter effect will be specifically shown later in the study of the thickness series with constant doping ratio of 0.6 %.

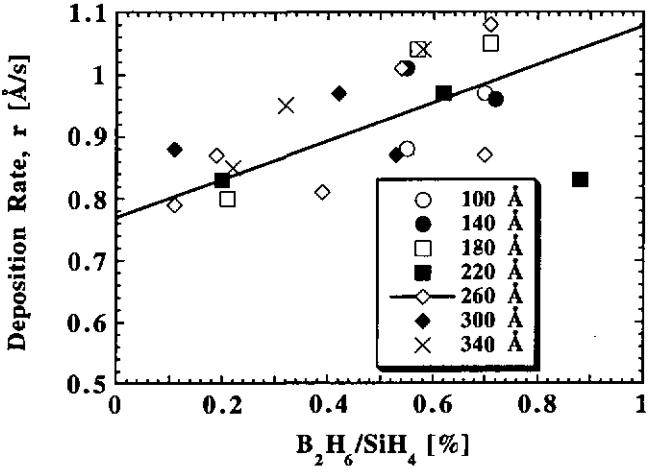

Fig. 3.3.1.2: Deposition rate as a function of the diborane doping ratio for different film thicknesses with the fitted line corresponding to films of thickness of about 260 Å.

For a constant film thickness of about 260 Å, the deposition rate increases from about 0.8 to 1.02 Å/s, quite linearly with the diborane doping ratio over the scanned range of 0.1 - 0.8 %. Similar findings were reported elsewhere [Prasad 1991, Ghosh 1992 and Chou 1992]. As was already claimed by the author, structural changes occur in the material (from μc-Si:H to a-Si:H) with an increasing boron doping ratio, resulting in an enhanced deposition rate, since, a-Si:H is well known to grow faster than μc-Si:H.

The increase of r with boron doping was also preliminary observed for a-Si:H, as reported by Perrin et al. [Perrin 1989]. It was claimed there, that diborane presumably strongly catalyses H_2 desorption for the growing film surface, leading thus, to a decreased H-coverage. The variation of r with doping complicates the study of the effects of the boron doping on the film properties since, as we will see it later, the film properties significantly depend on the film thicknesses for our very thin μc-Si:H films investigated.

From now on, we will concentrate on a thickness series of very thin <p> μc-Si:H films with fixed diborane doping ratio of 0.6 %. Fig. 3.3.1.3 shows the thickness of the films as a function of the deposition time (measured from the starting of the plasma). It is important to point out here that we are dealing with very thin films (d < 350 Å) and therefore, nearby the initial growth regime.

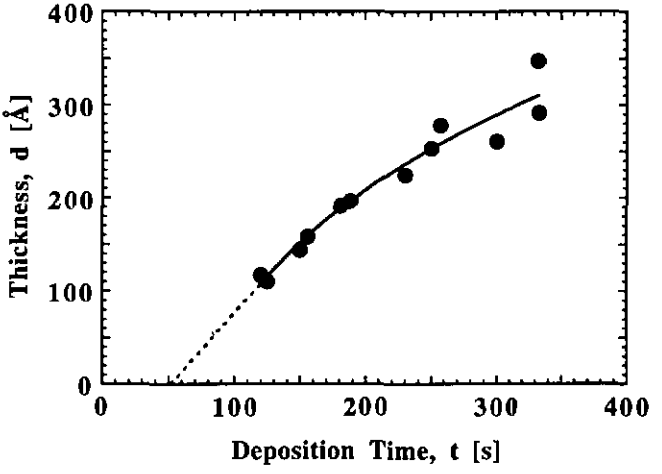

Fig. 3.3.1.3: Film thickness as a function of the deposition time for the <p> μc-Si:H thickness series (initial growth regime) with a fixed doping ratio of 0.6 %.

The shape of the curve is surely not a straight line (for our investigated film thickness range), meaning that in this region, the **deposition rate** is not constant. The extrapolation of the curve for the lowest thicknesses with a straight line leads to an "induction time" of about 1 minute. This value is suggested to correspond to the time needed for the initial nucleation. Due to the mentioned lack of very thin films with thicknesses ≤ 100 Å, this given value for the "induction time" is only a rough estimation. For increasing time, the effective deposition rate (calculated from the end of the "induction time") decreases from an estimated value of about 1.6 Å/s for the lowest thickness deposited film (~ 120 Å) and tends for thick films (> 500 Å) to the constant bulk deposition rate value of about 1.1 Å/s. This trend can be explained by considering the fact that the structure of the films is predominantly amorphous for very thin films and becomes

microcrystalline with hardly any a-Si:H phase, for thick films, as will be shown later by the detailed structural characterisation (TEM, Raman spectroscopy, X-ray diffraction/reflection and spectroscopic ellipsometry).

The presence of such an "induction time" for boron doped μc-Si:H films was already observed in an earlier work [Prasad 1991 and 1991a] and was reported to be of about the same value. Since, as we mentioned above, the deposition rate is a function of the diborane doping ratio it is then very probable that the "induction time" is also a function of the diborane doping ratio. These measurements of the deposition rate as a function of the diborane doping ratio and of the film thickness are very important for solar cell applications (window layers and tunnel junctions), since, very thin films of specific thicknesses (often lower than 200 Å) are required.

We already mentioned, by analysing the effects of the diborane doping on the room temperature dark conductivity (Fig. 3.3.1.1) for our set of <p> μc-Si:H very thin films, the general trend of the decrease in σ_d when decreasing the film thickness at constant doping level. Here, we specifically point out this observation for our thickness series of very thin μc-Si:H films with an optimised and fixed diborane doping ratio of 0.6 %. Fig. 3.3.1.4 shows the **room temperature dark conductivity** σ_d and the corresponding **dark conductivity activation energy** E_σ as a function of the film thickness. Since, the Arrhenius plot of the dark conductivity often shows for higher temperatures (100 - 200 °C) a slightly steeper decrease than for temperatures below 100 °C, we represent in Fig. 3.3.1.4 the lower values of E_σ, determined from the temperature range of 25 to 83 °C.

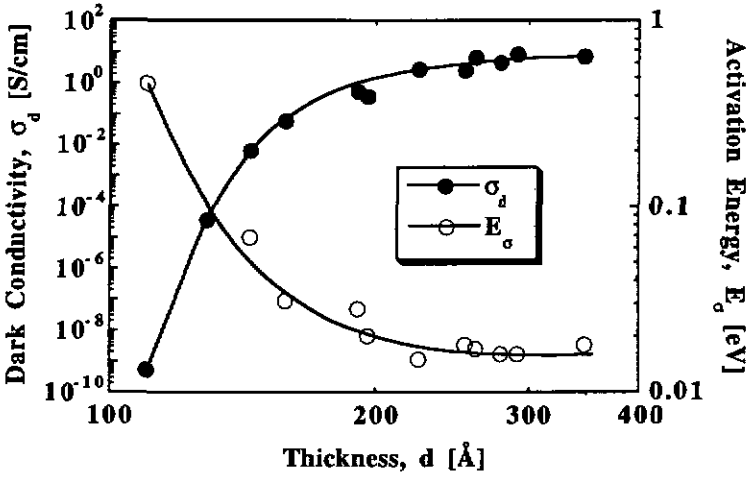

Fig. 3.3.1.4: Room temperature dark conductivity and dark conductivity activation energy as a function of <p> μc-Si:H film thickness for an optimised and fixed diborane doping ratio of 0.6 %.

σ_d remains still at really high values of 1 to 10 (S/cm) down to thicknesses of about 200 Å with corresponding very low activation energy values of lower than 20 meV, while beyond this thickness, the conductivity begins to fall and E_σ to increase. The conductivity reaches, even for thinner films (~150 Å), remarkably high values of > 10^{-2} (S/cm) which are well above those of doped a-SiC:H (~10^{-6} (S/cm)) or even doped a-Si:H (~10^{-4} (S/cm)). These observations of Fig. 3.3.1.4 are well known for both thin μc-Si:H and a-Si:H films used as window layers and

tunnel junctions in solar cells [Luft 1993, Li 1994 and Prasad 1991a] but such high σ_d and low E_σ values, as reached for our investigated very thin films, were seldom reported.

As we already showed, the diborane doping has a drastic effect on the film properties of very thin films and has to be carefully optimised. The entire problem lays on the ability of depositing highly doped μc-Si:H material, already for the early growth (initial growth regime) of the film, with a thinnest as possible or even vanishing amorphous interface layer. The already suggested phase transition from microcrystalline to amorphous material by decreasing film thickness will be confirmed later by detailed structural analyses (TEM, Raman spectroscopy, X-ray diffraction/reflection and spectroscopic ellipsometry). The rapid fall in σ_d for films thinner than ~ 150 Å is proposed to be attributed to a critical phase transition from microcrystalline to amorphous material. The crystallites become too small and too far away from one to an other - resulting in a low crystallite volume fraction - to allow a conduction path through crystallites by percolation. The amorphous phase becomes, thus, the dominant one for what concerns the transport properties.

These high conductivities and low activation energies reached for films thicker than about 150 Å are a reliable monitor for microcrystallinity and are consistent with the structural characterisation results shown hereafter.

The electrical measurements were carried out using Al contacts (1000 Å thick) with a 1 mm gap. The thinner the investigated films are, the more important influence of e.g. nucleation on size effects will become. A reliable and correct characterisation of such very thin films is therefore very difficult and strongly substrate-dependent. Possibly, conductivity and activation energy of the films would be seen not to change as strongly, if the films could be characterised by a sandwich configuration. Also, the solar cell device will probably show the thickness influence more evidently, but in this case the roughness of the TCO, too, will significantly influence growth and properties of the <p> μc-Si:H window layers.

The very thin <p> μc-Si:H layers were further characterised by spectral transmission measurements in the visible and near ultra-violet (UV) range of sun light.

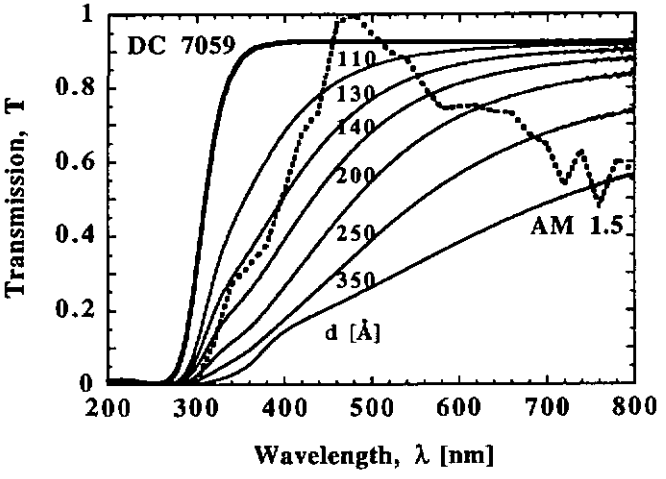

Fig. 3.3.1.5: Spectral transmission of a representative set of layers from the thickness series of <p> μc-Si:H films, deposited on glass substrates (Dow Corning 7059).

Fig. 3.3.1.5 shows the **transmission curves** obtained for some selected layers from the thickness series, deposited on DC 7059 glass; the transmissioo of the glass substrate alone is also plotted. For a relative comparison, the sunlight spectrum AM 1.5 is also given.

As it can be seen from Fig. 3.3.1.5, the glass alone acts as a "high-pass" filter, meaning that the wavelengths in the visible range (> 360 nm) are entirely transmitted, whereas the wavelengths lower than about 280 nm are fully cut. The ideal case of a glass transmission of 100 % is here experimentally not reached due to a set-up calibration deviation and reflection losses. Iostead, the measured transmissioo of the glass is about 93 %. The film transmission in the visible decreases rapidly when increasing the film thickness. Films between 110 and 140 Å still show a remarkable transparency in the important visible range of the sun light and show clearly the potential with their still sufficient conductivities as window layers in solar cells.

Electron diffraction (ED) patterns and **high resolution electron micrographs** (HREM) have been used to obtain structural information, in particular, on the crystallinity and crystalline surface coverage of the films. The films were deposited for these specific analyses on thin copper grids covered with a thin amorphous carbon layer. Fig. 3.3.1.6 shows ED patterns of three films selected from the thickness series (A - C: 110, 160 and 255 Å) and two corresponding HREM images (D - E: 110 and 160 Å).

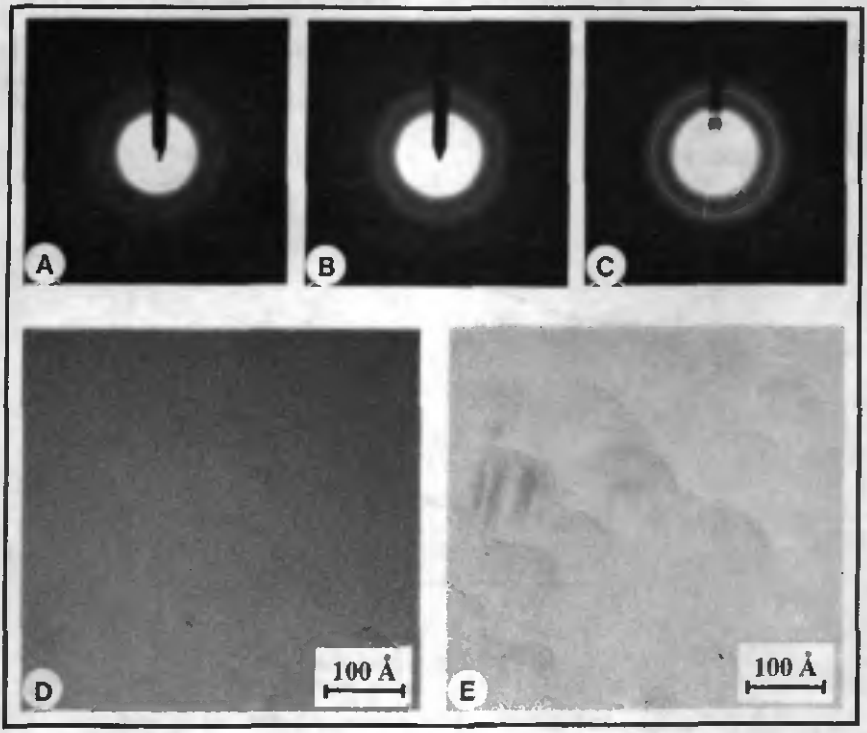

Fig. 3.3.1.6: ED patterns of three selected films from the thickness series (A - C: 110, 160 aod 255 Å) with two corresponding HREM images (D - E: 110 and 160 Å).

The ED pattern of the thinnest film (A) shows diffuse rings indicating low crystallinity and dominant amorphous phase. By increasing the thickness, the corresponding ED pattern shows intensity modulations on the outer rings related to an increase of the crystallinity. For the thickest film, the ED pattern (C) shows well-defined rings and sharp diffraction spots, an indication of film texture. The HREM image (D) shows only very few randomly growing spherically-shaped nanocrystalline clusters with sizes between 40 and 80 Å. The corresponding crystalline surface coverage value is low and estimated to be only 5 %. By increasing the thickness (HREM image (E)), the cluster size increases up to about 140 Å and an agglomeration phenomenon is observed. However, the spherically shaped clusters are separated by almost amorphous boundaries.

The HREM image (not shown here) pertaining to a thicker film (255 Å) clearly shows a large number of crystalline particles with different orientations, some of them agglomerating in clusters up to 400 Å. The coverage of crystalline material is estimated in that case to be about 80 % of the total surface. This value can still be higher since a single electron beam axis does not allow all the crystallites to be imaged. Small "stacking" or planar defects (e.g. break in plane ordering) - presumably originating from the coalescence of smaller nuclei - and interplanar spacings (risen through crystallographic orientations) can barely be resolved.

The **Raman spectra** of three films from the <p> μc-Si:H thickness series deposited on DC 7059 glass and measured with a liquid nitrogen cooled CCD camera at an excitation wavelength of 4579 Å are shown in Fig. 3.3.1.7. Generally, a disordered random network of Si (i.e. a-Si:H) which lacks long-range order yields a broad structure near 480 cm^{-1} in the spectrum, whereas in contrast, a crystalline Si structure is represented by one sharp peak near 520 cm^{-1} [Brodsky 1977]. Because of a background correction - necessary in this case of very thin films - that is not unique, quantitative conclusions based on a comparison of these results with those of thick samples are not possible.

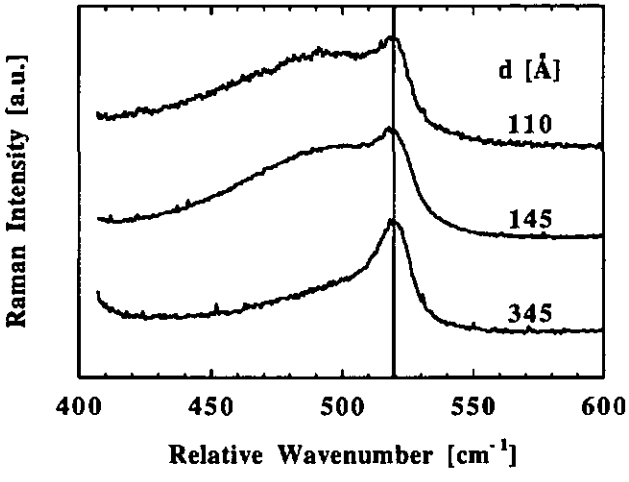

Fig. 3.3.1.7: Raman spectra of three films from the <p> μc-Si:H thickness series (110, 145 and 345 Å).

Surprisingly, the crystalline feature near 520 cm^{-1} is present for all three films, eveo for the thinnest one of only 110 Å. By increasing the thickness up to 345 Å, we can qualitatively see that the material becomes "typically microcrystalline", dominated by the microcrystalline phase with a negligible contribution from the amorphous phase. These results are in good agreement with the previously shown TEM analyses. We furthermore do not observe a strong variation of the Raman crystalline peak maximum position with increasing thickness suggesting thus no meaningful variations of the crystallite size [Iqbal 1982].

The **X-ray diffraction measurements** were performed using the $CuK\alpha$ line in the range of $2\Theta = 20 - 70°$, whereas for the reflectioo measurements, small variations of the source beam angle α were made near the total reflection angle. A fitting of the experimental data with the Fresnel equations leads to the following structural parameter values: film thickness, average Si density and surface/interface roughness.

The diffraction patterns (not represented in this work) of two analysed μc-Si:H films (d = 160 and 345 Å) by grazing angle X-ray diffraction show the Bragg reflections of polycrystalline Si with few or no orientation effects; the main peaks (listed hereafter by decreased peak heights) correspond to the <111>, <220> and <311> crystallographic planes. The observation of a certain crystallinity of the films is in good agreement with the previously presented TEM and Raman analyses. An estimation of the average size δ of the grains for the thickest film (345 Å) by Scherrer's equation [Scherrer 1918] from the <111> main peak leads to a value of about 60 Å for directions near the perpendicular to the surface plan. The estimated lattice constant a for that same film of 5.40 Å is a little bit smaller than the lattice constant of typical cubic pbase c-Si (5.43 Å). This observed deviation in the lattice constant is possibly caused by experimental errors.

Grazing angle X-ray reflection experiments done on three films (d = 110, 195 and 345 Å) show that the obtained thicknesses - from the fit to the data - are very near but somewhat lower than those measured by the α-step, probably because of the low resolution of the α-step measurement for such low thicknesses. The relative film thickness difference decreases from 33 to 6 % when increasing the film thickness from 110 to 345 Å. The root mean square rms roughness as determined from $(\langle z^2 \rangle)^{0.5}$ (with z defined as the average height of the features (that are at the origin of the roughness) as evaluated from a Gaussian shape and averaged on the entire film surface) is estimated to be between 0 and 35 Å for the interface (substrate/Si), and from 30 to 35 Å for the surface (Si/air) with no direct correlation with the film thickness. The quite low value of the estimated average Si density (50 - 80 %) for all analysed films leads us to infer an incomplete coalescence growth model where some voids are thought to fill the place left between the crystallite nuclei. This model will further be confirmed with detailed experimental data obtained from the following spectroscopic ellipsometry measurements.

The rotating-analyser spectroscopic ellipsometer used here is described elsewhere [Flückiger 1994 and references therein]. The fitting of the experimental data through a simple physical model, i.c., that of one or two films composed of a mixture of crystalline, amorphous, and void components, leads to values for the following structural parameters: the film thicknesses and volume fractions of each of the components. The results of the ex-situ **spectroscopic ellipsometry (SE) analysis** using the model of Fig. 3.3.1.8 are summarised in Table 3.3.1.1.

As expected from all the previously presented structural analyses (TEM, Raman spectroscopy and X-ray diffraction/reflection), the main result obtained here from the SE analysis is an increase of the crystalline volume fraction with increasing thickness of the films. While, the a-Si:H volume fraction stays nearly constant (~ 44 %), the void volume fraction decreases to less than 8 %. Thus, upon increasing the thickness, the films become less porous (more dense) and more crystalline.

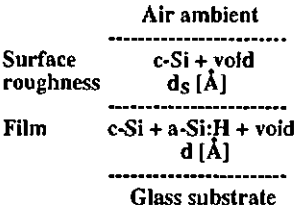

Fig. 3.3.1.8: Model for the SE analysis.

	Film			Surface roughness		
d [Å]	c-Si	a-Si:H	Void	d_S [Å]	c-Si	Void
14S	12	49	39	-	-	-
16S	16	45	39	-	-	-
19S	29	35	36	-	-	-
25S	42	44	14	38	29	71
34S	48	44	8	44	30	70

Table 3.3.1.1: Volume fractions (%) of the different phases (c-Si, a-Si:H and void) as a function of the sample thickness measured by α-step (column 1). Columns 2 - 4 correspond to the film and columns 6 and 7 to the surface roughness layer (see Fig. 3.3.1.8).

The total Si volume fraction (c-Si + a-Si:H) obtained thereby increases from 60 up to 90 % and is hence in good agreement with the previously discussed results (electrical properties, TEM, Raman spectroscopy and X-ray diffraction/reflection). As for the X-ray analyses, the obtained thicknesses from SE are very near - and again smaller - than the thicknesses measured by α-step, within a relative error of about 15 %. As shown in Table 3.3.1.1, a surface roughness film of about 40 Å can be detected on the top of the films of highest densities with thicknesses higher than 250 Å. Note that no amorphous phase was detectable in this film. This surface roughness - as also reported elsewhere [Shirai 1994] - is several times larger than the surface roughness observed in conventional device-grade a-Si:H and is directly related to the surface growth mechanism of microcrystalline material.

All these results possibly indicate a specific **columnar growth model**: The films grow as islands from well separated nucleation centers on the substrate, then extend vertically. Inverted "conical" structures - with a-Si:H and voids filling the space left in between - appear to characterise the growing films. Reaching a thickness of approximately 250 Å (as mentioned above), the films have their top layers almost covered with the conical structures that coalesce. A further increase of the thickness results in new nucleations on this partly covered c-Si layer, providing conditions for bulk material growth. As shown, the dark conductivity has nearly reached the saturation value for films thicker than 250 Å, this fact being in good agreement with the proposed growth model. This initial growth model proposed here for our <p> μc-Si:H very thin films was already observed and reported in other work [Collins 1989, Shen 1993 and Akasaka 1993]. Furthermore, a similar kind of preferential vertical growth (columnar structure) is very often observed for the deposition of thick <p> μc-Si:H films [Prasad 1991 and LeBerre 1993].

All above strongly correlated electrical and structural properties show the evidence of the existence of crystallites in our <p> μc-Si:H very thin films deposited on glass by VHF-GD even for the lowest thickness of 110 Å. Furthermore, by growing films, the crystallites are observed to coalesce quite quickly leading thus already for 250 Å thick films, to bulk material (for what concerns the electrical properties). These results clearly point out the potential of our <p> μc-Si:H very thin films deposited by the VHF-GD as window layers and tunnel junctions in solar cell devices. Finally, for these mentioned purposes, carbon was also added in the films; the electrical, optical and structural properties of these films will be discussed and compared in (3.3.2) with the previously shown <p> μc-Si:H films.

3.3.1.3 Epitaxial growth

We mainly discussed until now, the growth of <p> μc-Si:H very thin films deposited on DC 7059 glass, a substrate which allows almost all analyses and which is surely the most commonly used for standard film characterisation techniques. However, infrared (IR) spectroscopy analyses for example, require films deposited on c-Si and this is why we added, for all deposition runs, a small piece of <p>-type polished single crystal Si wafer (Czochralski CZ) with <100> orientation. By curiosity, we analysed the microstructure of the deposited <p> μc-Si:H films (on the c-Si substrate) in the growth direction; the results are shown hereafter. The deposition parameters are identically the same than the deposition parameters meotioned in (3.3.1.1) for the depositions on glass.

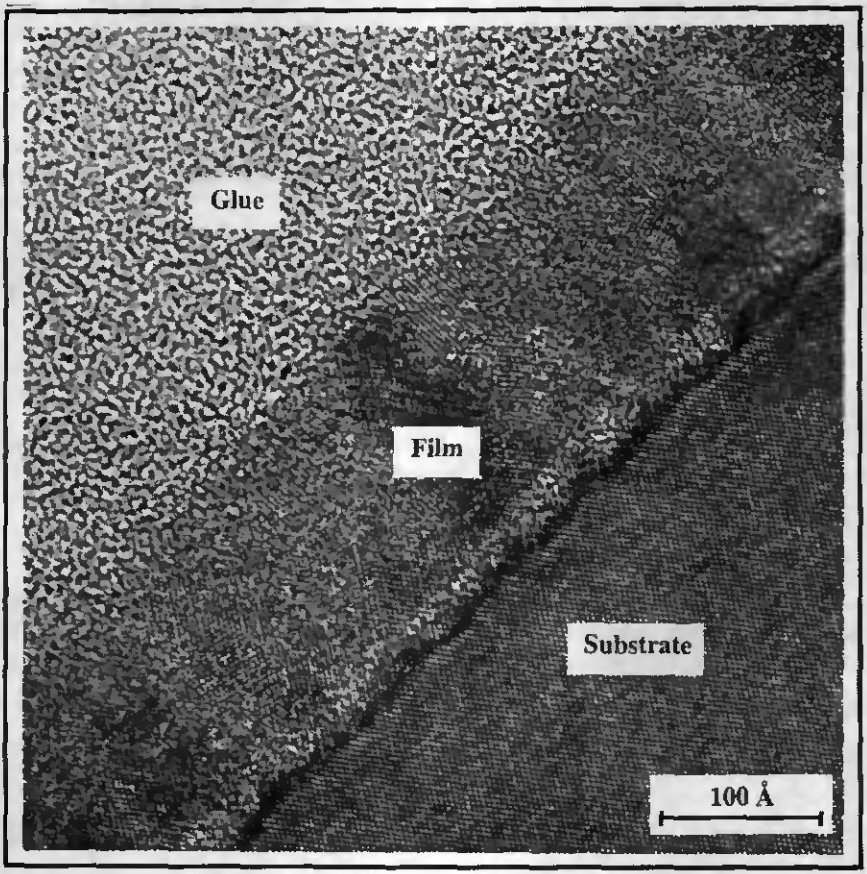

Fig. 3.3.1.9: Cross-sectional HREM of a thin <p>-type Si film deposited on c-Si; the epitaxial growth of the thin <p>-type Si film on the c-Si substrate is clearly visible.

Fig. 3.3.1.9 shows a cross-sectional high resolution electron micrograph (HREM) obtained by transmission electron microscopy (TEM) of a very thin <p> μc-Si:H film grown on c-Si; this film corresponds to the 255 Å thick film deposited on DC 7059 in the same run. Fig. 3.3.1.9 let us immediately recognise an **epitaxial type of growth** of the thin <p>-type Si film on the <100> c-Si substrate. The word "epitaxy" originates from the Greek words "epi" = "on" and "taxis" = "arrangement", meaning in other words the growth of a film with the same crystallographic orientation than that of the substrate on which the film is deposited. A consistent crystallographic relationship between the crystal lattices of the film and of the substrate is denoted. Here, in our case, we face a Si crystalline growth on a c-Si substrate.

The HREM image (see Fig. 3.3.1.9) clearly shows for the thin film, the crystallographic plans with a very thin or even no interface between the film and the substrate. Since, a bright contrast, possibly caused by strain, is observed at the interface, the thin film can clearly be distinguished from the Si substrate. Some very few small amorphous zones (a-Si:H or oxide) can barely be resolved at the interface. Also a detailed observation of the microstructure reveals some structural defects such as dislocations/stacking faults or twin boundaries, for the c-Si substrate as well as for the thin film.

An epitaxial growth for such a low deposition temperature of only 170 °C and the simple deposition technique as used here is seldom reported. Either, very high temperatures like the ones used by the CVD techniques (> 800 °C), or quite complicated deposition techniques (ECR-PECVD, RPECVD using fluorinated or other non-usual gases) are commonly used so far. Our observation of the epitaxial growth of a <p>-type Si very thin film on c-Si by the VHF-GD at low deposition temperatures can be attributed to some specific properties of the 70 MHz plasma excitation frequency GD technique used.

In fact, we believe that an ion bombardment with high ion densities but low average ion energies and a high supply of silane and hydrogen radicals [Howling 1992, Kroll 1994 and Heintze 1993a], which are thought to be essential for an efficient microcrystalline growth, are responsible for the observed epitaxial growth. Furthermore, as mentioned in 2.1.2, three treatment steps are performed, prior to deposition, in order to prepare the chamber surfaces and especially the substrate for deposition. We furthermore propose that the mentioned treatments etch away the native oxide from the upper surface of the c-Si substrate, leading thus to a clean and oxide free c-Si surface. This procedure is probably also a key issue for the growth of epitaxial layers on c-Si. Concluding, a suitable energetic particle bombardment can facilitate epitaxial deposition on epitaxial substrates by providing a clean, nascent substrate surface. Furthermore, an energetic particle bombardment during deposition acts primarily to enhance the surface and grain boundary mobility, what is favourable for the production of the grain structure.

This epitaxial growth of <p>-type Si at low temperatures, by our VHF-GD technique at 70 MHz plasma excitation frequency, including the pre-treatment steps, are patented [Flückiger 1994a]. Further extensive plasma excitation frequency studies relating some major plasma characterisation analyses to the epitaxially grown <p>-type Si film properties are under way and will be presented elsewhere [Torres 1995]. These findings open evidently a wide range of applications in opto-electronic and microelectronic devices, such as in the fabrication of advanced metal-oxide-semiconductors (MOS) and bipolar integrated circuit (ULSI) technology, for which the low temperature epitaxial growth is potentially advantageous. For example, dopant redistribution can be avoided at low temperature so that an abrupt dopant transition can be obtained. On the other hand, low temperature epitaxial growth reduces autodoping, wafer warping,

and system design cost. Furthermore, a greater liberty in the sequence of the deposition steps is introduced.

The VHF-GD technique, developed in our laboratory, shows many advantages for low temperature epitaxial growth, including batch-wafer processing, low cost, the absence of ultra-high (UHV) requirements, large area deposition, and the capability of low temperature growth assisted by plasma.

3.3.1.4 Conclusions

Starting from previously obtained results where the VHF-GD process has been shown to be a very suitable technique for preparing doped highly-conductive μc-Si:H layers, a down scaling of the film thickness to thicknesses lower than 350 Å could be successfully performed by carefully optimising the diborane doping ratio. We evidenced the existence of crystallites in our <p> μc-Si:H very thin films deposited on glass by VHF-GD even for the lowest thickness of 110 Å.

Detailed structural analyses obtained from a wide range of characterisation techniques lead to a suggested specific columnar growth model for the initial growth regime investigated. Such a preferential vertical growth is often mentioned as being the prevailing growth model for thick <p>-type microcrystalline silicon. Furthermore, an "induction time" of about one minute was observed for the initial growth regime, what has further to be taken into account for the deposition of very thin films of specific thicknesses as required for example for window layers in solar cells.

Structural analyses by cross-sectional TEM observations of a <p>-type Si very thin film deposited on c-Si surprisingly revealed an epitaxial growth. A series of three surface treatment steps are thought to be a key issue for the exhibited epitaxial growth. The possibility of growing epitaxial films further points out the ability of the 70 MHz PECVD-GD technique in growing good device-quality <p>-type Si films at low deposition temperatures. This epitaxial growth of very thin silicon films opens a wide range of potential applications in opto-electronic and microelectronic devices.

Thus, highly conductive and transparent very thin <p>-type doped μc-Si:H layers can now be prepared; they have the potential to become excellent window layers and tunnel junctions for solar cell applications. However, full p-i-n solar cells have yet to be fabricated, that incorporate these new layers.

3.3.2 <p> μc-SiC:H film series

Hydrogenated microcrystalline silicon, deposited at low temperatures by plasma methods, is a very promising material for photovoltaic [Torres 1994, Meier 1994a and Flückiger 1995] and for optoelectronic applications. Specifically, very thin films of <p>-type μc-Si:H have proven to be excellent window and barrier layers for solar cells because of their high conductivity and transparency (see (3.3.1) and [Luft 1993 and Li 1994]). <p> μc-SiC:H films are expected to show a much higher energy gap (than <p> μc-Si:H films) - since SiC crystallites have an energy gap of 2.8 - 3.0 eV - with still a high conductivity (due to the high doping efficiency of the crystallites). Due to the fact that boron and/or carbon in the gas phase hinder the nucleation of crystallites [Ghosh 1992 and Goldstein 1988], films of <p> μc-SiC:H are extremely difficult to deposit. In fact, only very few studies among a few others [Hattori 1988] report on <p> μc-SiC:H films containing SiC crystallites.

In the following, we tried to deposit this famous <p>-type μc-SiC:H material with our VHF-GD at 70 MHz. Unfortunately, as we will see it later, the deposition of SiC crystallites was not a real success or the detection of the SiC crystallites was under the instrumental limit of the used characterisation techniques. Nevertheless, we call our material μc-SiC:H while keeping in mind that no (or only very few) SiC crystallites are present in the films. In the present study, we report on the optimisation of nominally thin and very thin <p> μc-SiC:H films deposited at low temperatures. The individual effects of each of the deposition parameters (methane and diborane gas phase ratios, argon gas phase dilution, input power, deposition temperature and pressure) are investigated with respect to the structural, optical and electrical properties of the thin films of 0.1 - 0.6 μm thickness. Then, results on very thin <p> μc-SiC:H films (< 225 Å) deposited at low temperature (160 °C) are presented. The effect of boron doping on the growth and electrical properties of <p> μc-SiC:H very thin films is first investigated, leading to an optimised value of about 0.4 % ($B_2H_6/(SiH_4 + CH_4)$). Then, the growth and electrical properties of an optimised thickness series ranging from 110 to 225 Å are finally studied using thickness and conductivity measurements. The goal was to optimise the very thin <p> μc-SiC:H layers for use as highly conductive and high gap window layers in solar cells. The present study is partially published elsewhere [Flückiger 1995b].

3.3.2.1 Experimental

All films (42 films from 9 different series) were deposited in a single chamber reactor by the capacitively-coupled glow discharge method at a plasma excitation frequency of 70 MHz, as described in (2.1). To guarantee maximum reproducibility, all layers were deposited with the same chamber history.

The gases used were silane (SiH_4), hydrogen (H_2), diborane (B_2H_6), methane (CH_4) and argon (Ar). All films were deposited at a dilution level of 1.5 % ($(SiH_4 + CH_4)/(SiH_4 + CH_4 + H_2 + B_2H_6)$) and a total gas flow of about 100 sccm. The methane gas phase ratio ($CH_4/(SiH_4 + CH_4)$) was varied between 0 and 67 %, the diborane gas phase ratio ($B_2H_6/(SiH_4 + CH_4)$) between 0 and 0.9 %, and finally the argon gas phase dilution ($Ar/(Ar + H_2)$) between 0 and 44 %. The power measured at the power meter was varied from 5 to 50 W. The substrate deposition temperature T_{dep} was varied from 90 to 340 °C and the gas pressure from 0.2 to 1 mbar.

The film thicknesses were in the range of 0.1 to 0.6 μm for the thin film series and of 110 to 225 Å for the very thin film series (as measured and averaged over about twenty measurements). The deposition rates obtained were in the range of 0.2 to 1.2 Å/s. The lowest

thickness was about 110 Å, for which the film was hardly visible by the eyes. Furthermore, the glass surface roughness is estimated to be in the order of 50 - 100 Å, leading, thus, to the realistic deposition of films thicker than 100 Å. Due to the very low thicknesses of the following film series only few of the standard film characterisation techniques could be performed.

The detailed experimental descriptions of the different characterisation techniques mentioned in the next part (3.3.2.2) can be found elsewhere [Flückiger 1995b].

3.3.2.2 Results and discussion

To get a clear and overall view of the entire work presented here, the electrical and optical properties of all thin films (0.1 - 0.6 μm) are summarised in the two first plots. Then, the individual effects of each of the deposition parameters - methane and diborane gas phase ratios, power, deposition temperature, pressure and finally argon gas phase dilution - on the film properties will be shown.

Fig. 3.3.2.1 shows the **room temperature dark conductivity** σ_d and the **dark conductivity activation energy** E_σ as a function of the optical gap E_{04} (energy for which the optical absorption coefficient $\alpha = 10^4$ cm^{-1}), for all the thin <p> μc-SiC:H layers of thickness in the range of 0.1 - 0.6 μm. Since, the Arrhenius plot of the dark conductivity often shows for higher temperatures (100 - 200 °C) a slightly steeper decrease than for temperatures below 100 °C, we represent in Fig. 3.3.2.1 the lower values of E_σ, as determined from room temperature (RT) up to about 100 °C. Since the use of Tauc's gap is questionable in the case of microcrystalline films (because these films constitute a two phase material), the energy E_{04} is chosen as an arbitrary representation of the optical gap. UV/visible transmission and reflection spectroscopy measurements were performed to obtain the optical absorption coefficient α and the optical gap E_{04} of the films, by neglecting the multiple reflections and using the expression T / (1-R) [Summonte 1993].

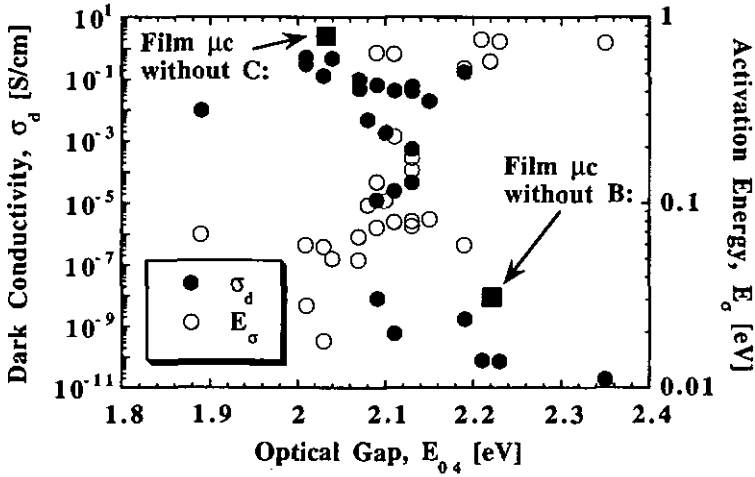

Fig. 3.3.2.1: Room temperature dark conductivity and dark conductivity activation energy as a function of the optical gap (E_{04}), for all deposited <p>-type silicon carbide thin films of thickness ranging from 0.1- 0.6 μm.

From Fig. 3.3.2.1, a wide range of film properties are obtained. Very generally, and as already observed in the case of amorphous films, a small increase of the optical gap results in a sharp decrease of σ_d together with an increase of E_σ [Luft 1993]. From later shown structural characterisation techniques (X-ray diffraction and Raman spectroscopy) films with $\sigma_d \leq 10^{-5}$ S/cm are revealed to be fully amorphous. In fact, an increase of E_{04} by increasing the methane gas phase ratio results very quickly in a structural transition from microcrystalline to amorphous material, as will be shown by the following detailed study of the individual deposition parameters. Amorphous material is well known to have dark conductivities by more than a factor of 4 lower than their microcrystalline counterparts. The very sharp decrease of σ_d when increasing E_{04} - as often reported - already leads us to suggest that no or only a small amount of carbon is incorporated into the crystallites [Lucovsky 1991], as it will further be discussed in this study; this fact will be confirmed by the structural characterisation analyses (X-ray diffraction and Raman spectroscopy). Nevertheless, very few groups have reported high dark conductivity ($> 10^{-3}$ S/cm) together with high optical gap (as high as 2.8 eV (Tauc's gap)) µc-SiC:H films, deposited mainly by ECR-CVD, and containing some SiC crystallites (see [Luft 1993] for an overview), so far.

For solar cell applications, as window layers for example, high conductivity and high optical gap films are requested. From Fig. 3.3.2.1 (see specifically the two microcrystalline films marked with an arrow: one without carbon and the other without boron), it becomes then evident that one has to do a compromise between the electrical and optical properties of the films (see also Fig. 3.3.2.2).

In view of the expected application of these <p> µc-SiC:H films as window layers in solar cells, Luft and Tsuo [Luft 1993 and references therein] proposed in a very elementary but fundamental model, that the built-in voltage (diffusion potential) V_{bi} of a simple p-i-n device is equal to the optical gap minus the dark conductivity activation energies for the <p> and <n> layers. Thus, a high optical gap together with low p and n dark conductivity activation energies will result in a high built-in voltage, and that in turn can result in a high open circuit voltage V_{oc}. We show in a very simplistic manner in Fig. 3.3.2.2 the quantity $E_{04} - E_\sigma$ as a function of E_{04} for all our thin <p> µc-SiC:H films with thicknesses ranging from 0.1 to 0.6 µm, being clearly aware that E_{04} is only representative of the optical gap and E_σ can differ from $E_a = E_F - E_V$ (for hole conduction). Moreover, because of the comparison of films with different optical gap values and different structures, real care has to be taken with the interpretations.

By slightly increasing E_{04}, one can obtain microcrystalline films with carbon having values of $E_{04} - E_\sigma$ that are a little higher than the values obtained for films without carbon (see the corresponding film marked with an arrow in Fig. 3.3.2.2) and, hence, should possibly lead to slightly higher V_{bi} and V_{oc} values in the p-i-n device. As already said previously, when increasing the optical gap too much, the films become amorphous, resulting in very low values of $E_{04} - E_\sigma$ (< 1.7 eV) mainly because of high E_σ values due to the low doping efficiency prevailing in amorphous Si [He 1983, Spear 1981 and Willeke 1992]. The importance of very low activated window and back contact layers are here clearly pointed out for solar cell devices.

Let us now compare two <p>-type carbide films deposited in our laboratory. The first one is a standard a-SiC:H film issued from a previous work [Crovini 1994] and commonly used in our high efficiency amorphous silicon solar cells, the second one is a µc-SiC:H film from this work. Both films have the same value for E_{04}, i.e. 2.13 eV. The quantity $E_{04} - E_\sigma$ is revealed to be about at least 300 meV higher for the microcrystalline film. This shows indeed, the potential for an efficiency increase of p-i-n devices by the newly developed <p> µc-SiC:H window layers. As predicted by Luft and Tsuo [Luft 1993], such an increase in $E_{04} - E_\sigma$ should theoretically lead in a gain in the V_{oc} of about 100 meV for a simple p-i-n structure device. Furthermore, the microcrystalline film has a σ_d-value that is a factor of 2×10^5 higher, and a E_σ-value that is a

factor of 5 lower; this, in its turn, should result in a better ohmic contact and lower serial resistance of the device.

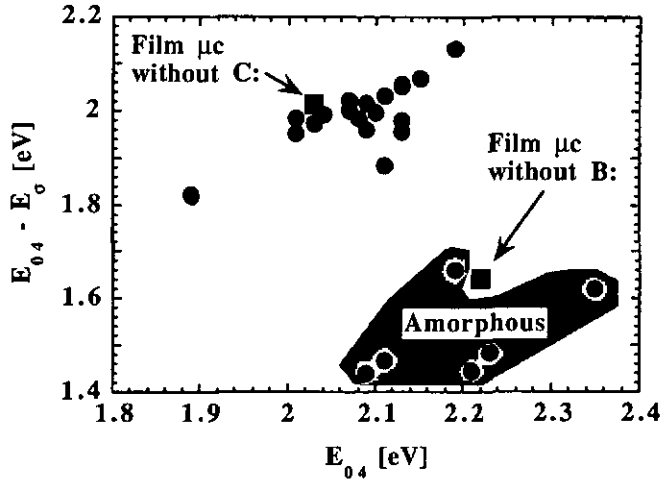

Fig. 3.3.2.2: E_{04} - E_σ as a function of E_{04}, for all thin <p>-type silicon carbide film series with thicknesses ranging from 0.1 - 0.6 μm.

Finally, one way to reduce the absorption losses in doped microcrystalline layers is, besides increasing the optical gap, to increase the doping efficiency. Increasing the doping efficiency reduces the total number of boron atoms (for <p>-type doping) in the film for a given electrical conductivity and reduces, thus, the optical absorption. Indeed, this further points out the potential of <p>-type microcrystalline material for window layer applications in p-i-n devices.

After this overview, we will now present the individual effects of each of the deposition parameters on the electrical and optical film properties. Then, we will describe the elemental composition and the structural properties of 5 selected films from all studied series. Starting from already optimised <p> μc-Si:H (see 3.3.1), CH_4 was added to the gas phase in order to increase the optical gap of the films.

The **methane series** is shown in Fig. 3.3.2.3, where σ_d at RT and E_{04} are plotted as a function of the CH_4 gas phase ratio. The other deposition parameters are fixed as follows: B_2H_6 gas phase ratio = 0.6 %, T_{dep} = 170 °C, p = 0.8 mbar and P = 10 W.

An increase of the CH_4 gas phase ratio results in a very sharp decrease of σ_d together with an increase of E_{04} as is commonly reported in another work [Luft 1993]. In fact, as already mentioned previously, and as will be shown by the structural characterisation analyses (X-ray diffraction and Raman spectroscopy), an increase of the carbon content in the films results in a structural transition from microcrystalline to amorphous material. At the above given deposition conditions, the critical CH_4 gas phase ratio is about 30 %.

A similar structural transition was already observed in a previously treated boron doping study (see 3.3.1). In fact, it is now well known and generally accepted, that B_2H_6 [Ghosh 1992] and/or CH_4 [Goldstein 1988] in the gas phase hinder the growth of crystallites. The E_{04} values obtained here, as a function of the CH_4 gas phase ratio, are surprisingly in the same range as those obtained

for a similar series of standard a-SiC:H, deposited by the same technique [Crovini 1994]. Very generally spoken, the optical gap mainly depends on the structure, on the elemental composition (H, O, C, ...) and on the doping level of the material. Here, in this methane series, all three probably contribute to the optical gap value. For low methane gas phase dilution (< 20 %), we first observe a slight decrease of E_{04}. In this regime, the structural effect (reduction of the crystallinity when increasing the methane gas phase ratio) is possibly dominant and could hence explain the slight decrease of E_{04}, since, microcrystalline material has generally a higher optical gap (E_{04}) than amorphous material.

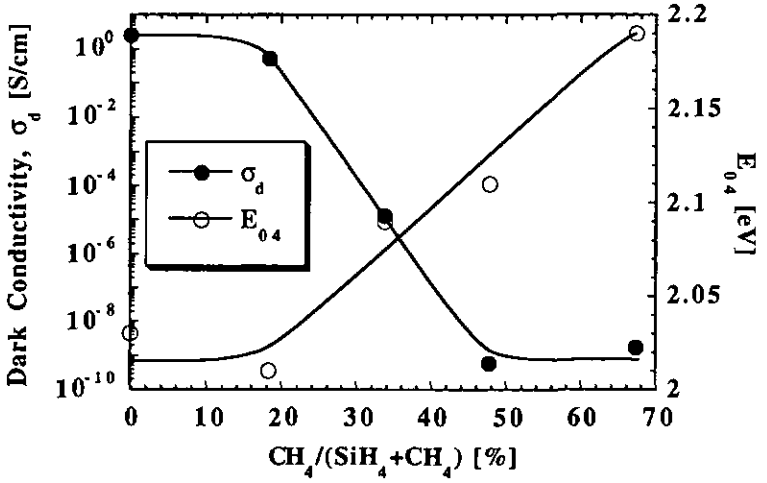

Fig. 3.3.2.3: Room temperature dark conductivity and optical gap (E_{04}) as a function of the methane gas phase ratio, for <p>-type silicon carbide films.

Lucovsky and Wang [Lucovsky 1991] proposed the following explanation to the observed limitation of the electrical transport in doped μc-SiC:H alloys (as is also observed here): Because the μc-SiC:H alloys are essentially composed of Si crystallites embedded in an a-SiC:H matrix, increasing the carbon content of the films to increase transparency will increase the effective band off sets at the conduction and valence band edges, thereby making transport via thermal emission over these barriers dominate over field-emission (tunneling) through the barriers.

The increase of the carbon content into the films by increasing the methane gas phase dilution is checked by secondary ion mass spectroscopy (SIMS) analyses, that are presented later on in this work. A further simple experimental check comes from the longer time needed to etch the film in a hot KOH solution, since KOH is known to etch Si much more rapidly than C.

The **boron doping** series is shown in Fig. 3.3.2.4, where σ_d at RT and E_{04} are plotted as a function of the B_2H_6 gas phase ratio. The other deposition parameters are fixed as follows: CH_4 gas phase ratio = 34 %, T_{dep} = 170 °C, p = 0.8 mbar and P = 10 W.

By increasing the dopant gas phase ratio from 0 to 0.1 %, σ_d increases drastically from 10^{-8} to the maximum value of 10^{-1} S/cm, while E_{04} decreases from 2.22 to the minimum value of 2.07 eV, due to an increase of the boron incorporation into the films. A further doping increase results in a structural transition from microcrystalline to amorphous material, as was also observed previously in the <p> μc-Si:H study (see 3.3.1). For the given deposition conditions, the critical

B_2H_6 gas phase ratio is about 0.5 %. The structural transition results in a pronounced decrease of σ_d, accompanied by a small increase of E_{04}. The shape of the curve of the RT dark conductivity is similar to the one obtained for <p> µc-Si:H films shown in 3.3.1, with a shift to lower values (of σ_d) since, as was inferred from Fig. 3.3.2.3, carbon lowers the electrical conductivity of the films.

The opposite trend of the optical gap by doping can be explained as follows: The initial rapid drop of the optical gap is directly related to the doping mechanism of the films, since doping shrinks the optical gap of the films. The slight increase in the optical gap, just following the rapid drop, is attributed to the structural transition from microcrystalline to amorphous material. Indeed, a-SiC:H films generally incorporate more C than µc-SiC:H films, for a constant methane gas phase ratio (see the SIMS analyses presented later on). This should lead to films with higher optical gap values.

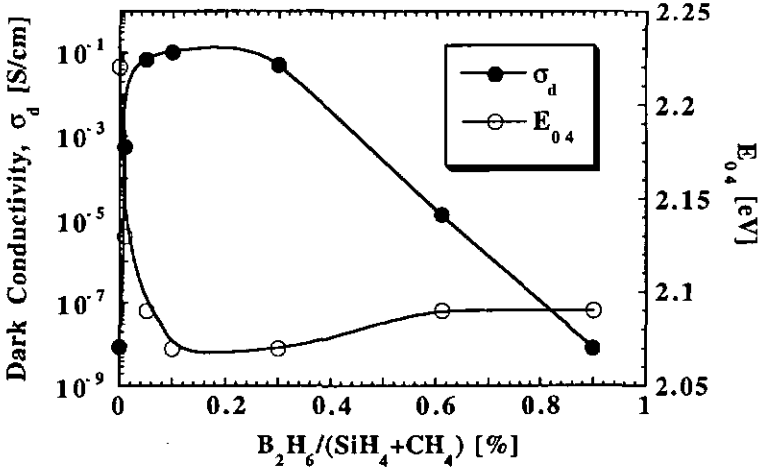

Fig. 3.3.2.4: Room temperature dark conductivity and optical gap (E_{04}) as a function of the diborane gas phase ratio, for <p>-type silicon carbide films.

As a conclusion, the more carbon is incorporated into the films, the less boron can be incorporated - and vice-versa - before the mentioned structural transition from microcrystalline to amorphous material occurs, since both elements hamper crystalline growth. One has therefore, to find a compromise between the electrical and optical properties, as one has to find a compromise between diborane and methane gas phase ratios.

Fig. 3.3.2.5 shows the power series where σ_d at RT and E_{04} are plotted as a function of the input discharge power, measured at the power meter. The effective plasma power for the range of 0 - 10 W can be extracted from Fig. 2.2.1. The other deposition parameters are fixed as follows: CH_4 gas phase ratio = 34 %, B_2H_6 gas phase ratio = 0.1 %, T_{dep} = 170 °C and p = 0.8 mbar.

An increase of the input discharge power from 5 to 50 W results in a structural transition from microcrystalline to amorphous material - as already observed for the methane and diborane series - with a critical value around 16 W, for the given deposition conditions. While σ_d drastically decreases from $5x10^{-1}$ to $2x10^{-11}$ S/cm, E_{04} increases from 2.04 to 2.34 eV. This "amorphisation" through an increase of the input discharge power is proposed to be due to changes in plasma properties, as already treated previously [Prasad 1990]. Higher input discharge

powers are suggested [Prasad 1990] to result in increased radical fluxes and in an increased ion energy bombardment onto the film growth surface, what in its turn favours rapid growth of amorphous material and hinders the formation of crystallites.

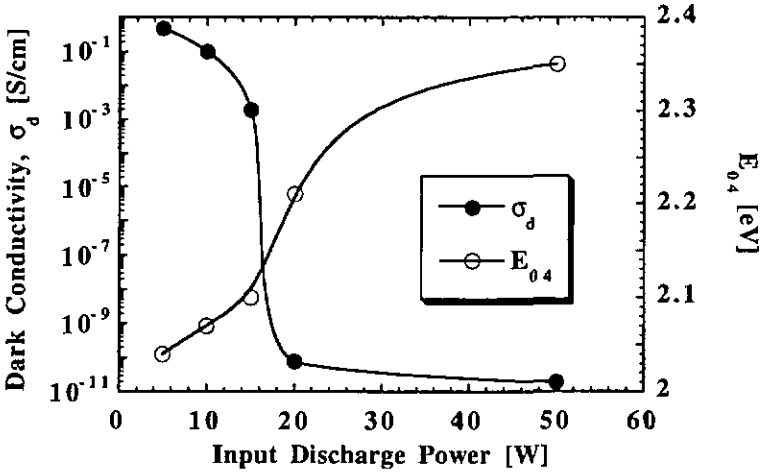

Fig. 3.3.2.5: Room temperature dark conductivity and optical gap (E_{04}) as a function of the input discharge power measured at the power meter, for <p>-type silicon carbide films.

Deposition temperature and pressure have less drastic influences on the electrical and optical film properties of <p> μc-SiC:H films. The **deposition temperature series** is shown in Fig. 3.3.2.6, where σ_d at RT and E_{04} are plotted as a function of the deposition temperature T_{dep}. The other deposition parameters are fixed as follows: CH_4 gas phase ratio = 34 %, B_2H_6 gas phase ratio = 0.1 %, p = 0.8 mbar and P = 10 W.

Very generally, the effect of T_{dep} on these carbide films is similar to effect of T_{dep} on standard microcrystalline films (see 3.1 for undoped and [Prasad 1991a] for doped films). The dark conductivity increases first rapidly by almost 4 orders of magnitude to reach the maximum value of about 1×10^{-1} S/cm at around 200 °C. A further increase of T_{dep} leads to a slight decrease of σ_d. As the author already suggested for undoped films in (3.1), the initial rapid increase of σ_d up to the maximum value is attributed to a structural transition from amorphous to microcrystalline material. The critical T_{dep} value is around 90 °C for the given deposition conditions.

The further slight decrease of σ_d, observed for the film deposited at the highest temperature of 340 °C, is suggested to be attributed to a reduction of the film crystallinity. This "amorphisation" at high deposition temperatures was already discussed in (3.1) for undoped films and was suggested elsewhere [Prasad 1991] for doped films. The monotonous decrease of the optical gap, for the entire temperature range studied, is in fact a well known trend; higher temperatures generally yield a shrinkage of the gap of the material. The mentioned structural transitions, as well as elemental composition variations due to increased deposition temperature could furthermore possibly contribute to the observed changes in the optical gap of the films.

For a device application of these films - such as window layers in p-i-n solar cells - the deposition temperature is often fixed (because of diffusion of B atoms at high temperatures) in the range of 170 - 220 °C. For this temperature range, our <p> μc-SiC:H films present both high dark

conductivity and high optical gap values; this is exactly what is expected for an efficient use of our <p> μc-SiC:H films as window layers in solar cells.

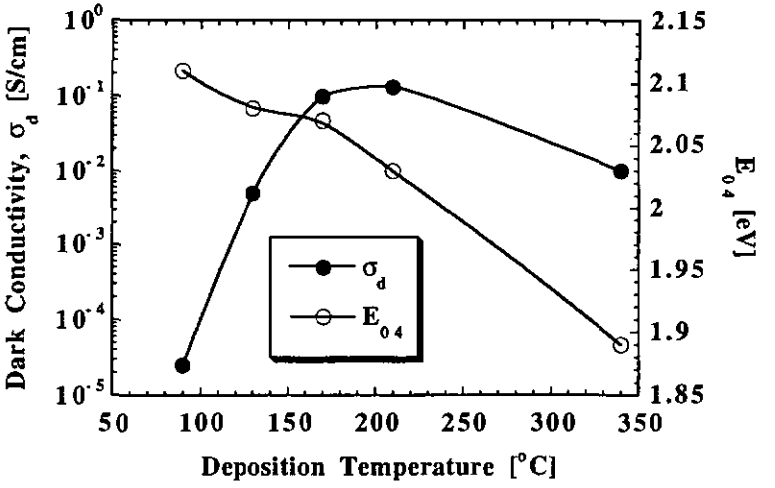

Fig. 3.3.2.6: Room temperature dark conductivity and optical gap (E_{04}) as a function of the deposition temperature, for <p>-type silicon carbide films.

The **deposition pressure series** is shown hereafter in Fig. 3.3.2.7, where σ_d at RT and E_{04} are plotted as a function of the deposition pressure. The other deposition parameters are fixed as follows: CH_4 gas phase ratio = 34 %, B_2H_6 gas phase ratio = 0.1 %, T_{dep} = 170 °C and P = 5 W.

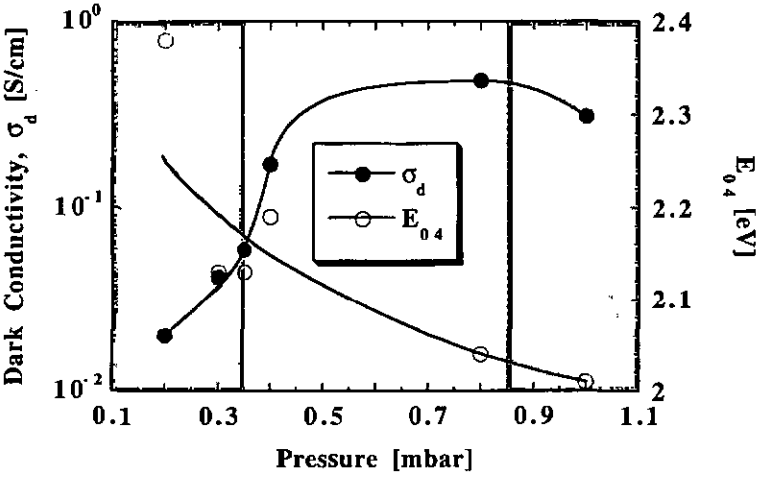

Fig. 3.3.2.7: Room temperature dark conductivity and optical gap (E_{04}) as a function of the deposition pressure, for <p>-type silicon carbide films.

The slight scattering of the E_{04} data observed in Fig. 3.3.2.7 is thought to be caused by some accuracy errors in their evaluation from the absorption plots in the visible wavelengths, which show specifically for non-uniform films strong interference fringes. Deposition pressure seems to have only very little effect on the film properties, except for the uniformity. In the pressure range of 0.35 to 0.85 mbar the films have a good to acceptable uniformity for their entire surface except for the borders due to the screening effect of the substrate holder during deposition, as simply observed by the eyes. Outside this range, the films are not uniform (see shaded zones in Fig. 3.3.2.7). There is a direct relation between the plasma confinement and the film uniformity, as again simply observed by the eyes. For the pressure range for which the films are uniform (i.e. 0.35 - 0.85 mbar), the plasma is well-confined between the two electrodes. Outside this range, for low pressures the plasma extends too much outside the electrodes, while for high pressures the plasma is too much localised and even separates in several distinct glow zones.

Deposition pressure has, to a much lower extent, the same trend of the electrical and optical film properties as the deposition temperature (compare Fig. 3.3.2.6 and Fig. 3.3.2.7). It seems from Fig. 3.3.2.7, that lower pressures yield to higher optical gaps and lower conductivities. The high conductivities obtained (> 10^{-2} S/cm) for the entire pressure range studied indicate that we are dealing here, in this study of the deposition pressure series, only with microcrystalline films. The shrinkage of the gap at high pressures - what possibly explains the increase in conductivity - is thought to be caused by changes in plasma physics, dynamics and chemistry. Films deposited at higher pressures are supposed to be of higher crystallinity, with a lower hydrogen and/or carbon content.

For solar cell applications, and more specifically for window layers, high conductivity and high transparency films are requested. Hence, films deposited at low pressure (i.e. around 0.4 mbar), with their both relatively high conductivity and high optical gap and their still acceptable uniformity, should best fit these requirements.

Finally, an **argon gas phase dilution series** was performed in the range of 0 to 44 % ($Ar/(Ar + H_2)$), with no observable effect on the film properties at all (!). The other deposition parameters were fixed as follows: CH_4 gas phase ratio = 36 %, B_2H_6 gas phase ratio = 0.1 %, T_{dep} = 160 °C, p = 0.35 mbar and P = 5 W. Higher Ar gas phase dilutions (> 80 %) seem to be needed, before one can induce any noticeable changes in the film properties [Kroll 1992]. For the given deposition conditions, the mass flow controllers unfortunately limited the dilution level to the studied range. Higher scale mass flow controllers have to be installed, in order to deposit films at higher Ar gas phase dilutions, for which the film properties are expected to change.

The results of the structural characterisation techniques (X-ray diffraction and Raman spectroscopy) and of the **secondary ion mass spectroscopy (SIMS) analyses** are shown hereafter, for 5 selected films from the above mentioned series. Table 3.3.2.1 resumes the deposition parameters, the film thicknesses and the SIMS analyses.

Films #1-3 belong to the methane gas phase ratio series, film #4 to the diborane gas phase ratio series and finally film #5 to the deposition pressure series. As expected, an increase of C_C is observed in the 3 first films, due to an increase of the methane gas phase ratio. Due to the mentioned "amorphisation" of the films for high CH_4 gas phase ratios, C_H is also slightly increased. Note that standard amorphous films show generally higher hydrogen contents than microcrystalline films.

A lowering of the diborane gas phase ratio for film #4 results in a decrease of the boron and oxygen content. This reduction of boron content is known from Fig. 3.3.2.4 and 3.3.2.5 to lead to higher crystallinity material, what possibly explains the related slight lowering of the oxygen content. By the way, it was unfortunately not possible to get a meaningful result for the boron concentration of film #3 because of sample charging problems that occurred during measurement.

Finally, a reduction of both deposition pressure and power for film #5 (relatively to film #4), seems not to change significantly the incorporation of contaminants and dopants. In fact, as it will be shown hereafter by the structural characterisation analyses (X-ray diffraction and Raman spectroscopy), the structures of films #4&5 are very similar.

Film #	$CH_4/(SiH_4+CH_4)$ [%]	$B_2H_6/(SiH_4+CH_4)$ [%]	P [W]	p [mbar]	d [Å]	C_H [at/cc]	C_O [at/cc]	C_C [at/cc]	C_B [at/cc]
1	0	0.6	10	0.8	5400	$6x10^{21}$	$2x10^{20}$	$2x10^{19}$	$2x10^{20}$
2	34	0.6	10	0.8	3200	$2x10^{22}$	$2x10^{20}$	$2x10^{21}$	$2x10^{20}$
3	67	0.6	10	0.8	4700	$2x10^{22}$	$2x10^{20}$	$7x10^{21}$	-
4	34	0.1	10	0.8	2800	$7x10^{21}$	$6x10^{19}$	$1x10^{21}$	$3x10^{19}$
5	36	0.1	5	0.35	2100	$7x10^{21}$	$9x10^{19}$	$1x10^{21}$	$2x10^{19}$

Table 3.3.2.1: Deposition parameters (methane and diborane gas phase ratios, power and pressure), film thicknesses and SIMS analyses (C_H, C_O, C_C, C_B) of 5 selected thin <p>-type silicon carbide films, from the previously mentioned series.

Fig. 3.3.2.8 shows the **X-ray diffraction patterns** of the same 5 selected films. Very generally, few diffraction peaks and low intensities are observed. However, Bragg reflections typical of polycrystalline Si are still visible for films #1, 4&5 with the observed diffraction peaks corresponding to the <111>, <220>, <311> and <331> orientations crystallographic planes. An evaluation of the corresponding lattice constants a yields values of about 0.02 Å bigger than for crystalline phase Si (5.43 Å). These differences could possibly occur due to film effects on the lattice constant evaluations, as for example a diffraction peak broadening due to the crystallite size or a diffraction peak shift caused by mechanical stress in the films.

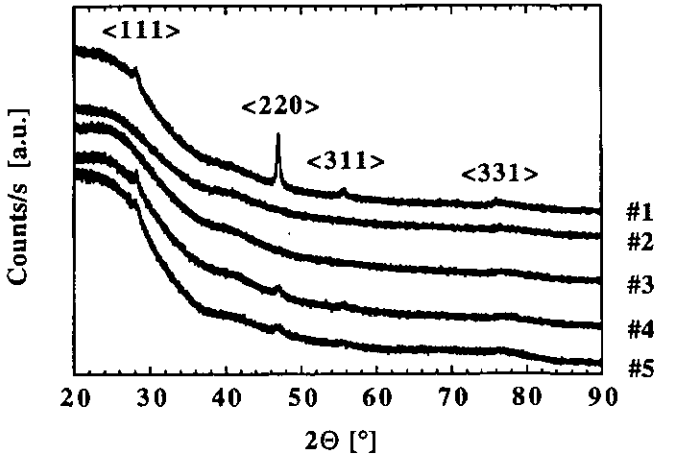

Fig. 3.3.2.8: X-ray diffraction patterns of the 5 selected <p>-type silicon carbide films.

An estimation of the average size ∂ of the grains by Scherrer's equation [Scherrer 1918], from the dominant diffraction peak <220> of film #1, leads to a value of about 230 Å. This <220> dominant diffraction peak differs from the <111> dominant diffraction peak observed for very thin <p> μc-Si:H films (see 3.3.1). Very often, a columnar growth (vertically extending needles) - related to the <220> diffraction peak - is observed for thick <p>-type microcrystalline silicon [Prasad 1991 and LeBerre 1993].

High content C and/or B films #2&3 (see Table 3.3.2.1) are revealed to be amorphous - due to the absence of diffraction peaks - as previously proposed. Thus, the vanishing diffraction peaks by increasing the methane gas phase fraction from 0 up to 67 % for films #1 to 3, clearly indicates the structural amorphisation. Nevertheless, films with moderate C and/or B contents #1, 4&5 (see Table 3.3.2.1) show a certain crystallinity. Also as expected, films #4&5 both possessing relatively high B and C contents show a lower crystallinity from the diffraction peak intensities than film #1, that has a much lower carbon content. From the structural point of view, films #4&5 seem not to differ much as was already suggested from the electrical and optical properties. Also as supposed, no crystalline phase SiC peaks [Miyajima 1992] are visible from the scanned 2Θ range, meaning that unfortunately the SiC crystalline phase does not exist or is only present to a negligible extent in our films.

Finally, the **Raman spectra** of the 5 selected films are shown in Fig. 3.3.2.9. Very generally, a disordered random network of Si (e.g. a-Si:H) which lacks long-range order yields a broad peak near 480 cm^{-1} in the spectrum, whereas in contrast a crystalline Si structure is represented by one sharp peak near 520 cm^{-1} [Brodsky 1977].

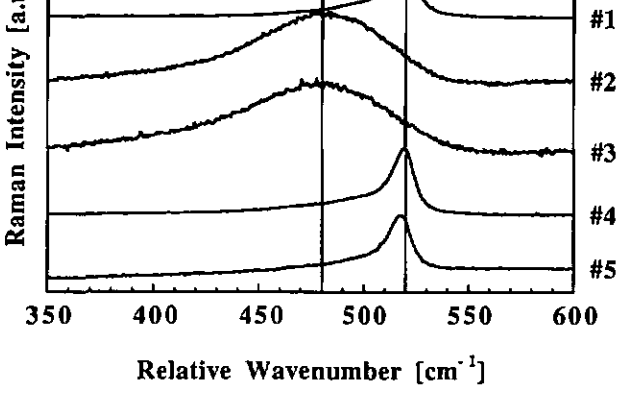

Fig. 3.3.2.9: Raman spectra of the 5 selected <p>-type silicon carbide films.

The crystalline feature near 520 cm^{-1} is present for films #1, 4&5 with a negligible to small contribution from the amorphous feature, while films #2&3 are revealed to be amorphous due to the broad structure near 480 cm^{-1}. Again, the structural amorphisation by increasing the methane gas phase ratio from 0 up to 67 % is clearly pointed out for films #1 to 3. Also, as inferred from the X-ray diffraction patterns, films #4&5, both with relatively high B and C contents, hardly show a lower crystallinity from the Raman crystalline peak than film #1 (that has a much lower

carbon content). Furthermore, as was already suggested, films #4&5 seem not to differ much from the structural point of view. A closer study of their spectra of Fig. 3.3.2.9, however barely shows for film #5 a lower position of the maximum of the crystalline peak than for film #4; this possibly iodicates a slightly lower crystallinity (of film #5) as already proposed in the previously studied pressure series.

No signals at 760 cm^{-1} and 790 cm^{-1} (outside the relative wavenumber range plotted in Fig. 3.3.2.9), which are the strongest characteristic Raman lines of (poly-) crystalline SiC in the range 100 - 1000 cm^{-1} [Feldman 1968], could be observed in the present films, so far. Such Raman signals have only been observed for samples annealed at 800 °C and for stoichiometric polycrystalline SiC [Carius 1994]. All these results from the Raman spectroscopy measurements are finally in good agreement with the previously-shown X-ray analyses. In fact, to our knowledge, only very few groups reported by Raman spectroscopy measurements the existence of crystalline phase SiC, for films deposited at low temperatures by a CVD technique [Hattori 1988].

Thus, by these Raman spectroscopy measurements we close this study of boron doped carbide microcrystalline silicon thin films. The effects of the deposition parameters on the electrical, optical and structural properties of thin <p> µc-SiC:H films were investigated, in order to optimise the film properties; the goal is to deposit high conductivity and high transmission films for window layer applications in solar cells. Reaching a compromise between the electrical and optical film properties by adjusting both diborane and methane gas phase ratios, <p> µc-SiC:H films are revealed according to a criteria used by Luft and Tsuo, to be potentially better, as solar cell window layers, than amorphous carbide and even µc-Si:H films. However, all the films presented so far are thin layers of thicknesses ranging from 0.1 to 0.6 µm, so as to facilitate their optimisation and characterisation; for device applications as window layers, these above studied films have to be thinner (≤ 200 Å) and it is towards this goal that we present hereafter results on very thin <p> µc-SiC:H films.

3.3.2.3 Very thin films

First, the effect of boron doping on the growth and electrical properties of very thin <p> µc-SiC:H films is investigated. Fig. 3.3.2.10 shows the **room temperature dark conductivity** σ_d as a function of the diborane gas phase ratio ($B_2H_6/(SiH_4 + CH_4)$) in the range of 0 - 0.6 %, for different film thicknesses (range: 110 - 210 Å). The other deposition parameters were fixed as follows and appropriately chosen from previous optimisations of thin <p> µc-SiC:H (see 3.3.2.2): CH_4 gas phase ratio = 34 %, T_{dep} = 160 °C, p = 0.35 mbar and P = 5 W.

Very generally, for all following results the trends for these very thin carbide films are identical with the trends observed for films without carbon (see 3.3.1). While, for the thickest films the boron doping influences σ_d only moderately, for very thin films the effect is drastic. To explain the shape of the curves of constant thickness of Fig. 3.3.2.10, two competitive effects must be taken into account; first, by increasing the diborane gas phase ratio slightly, the Fermi level is pushed towards the valence band (through an increase of the boron incorporation in the films), thus, increasing strongly σ_d. A further increase of the diborane gas phase ratio to values higher than 0.4 % (for which the σ_d curves show a maximum), leads to structural changes of the material by amorphisation, as was also reported elsewhere for non-carbide films [Prasad 1991 and Ghosh 1992] and shown here in chapter (3.3.1).

In fact, it is now generally believed and well accepted that diborane in the plasma gas phase favours the formation of amorphous material by increasing significantly the number of growth sites through hydrogen abstraction ("scavenging action") and reduction of the surface diffusion coefficient; this is said to enhance the film growth rate (as will be shown later) [Ghosh 1992 and Chou 1992]. Furthermore, it was proposed elsewhere [Prasad 1991 and 1991a], that in heavily doped samples inactive boron atoms segregate to the grain boundaries, where they hinder the formation of crystallites. Since the doping efficiency in amorphous material is much lower than in

μc-Si:H (due to a lower structural ordering) [Hc 1983, Spear 1981 and Willeke 1992], and furthermore an increased doping for already degenerated films results in a reduced charge mobility (due to inactive boron atoms that create defects in the energy band), the RT dark conductivity of very thin μc-SiC:H films decreases strongly with diborane gas phase ratios higher than 0.4 %.

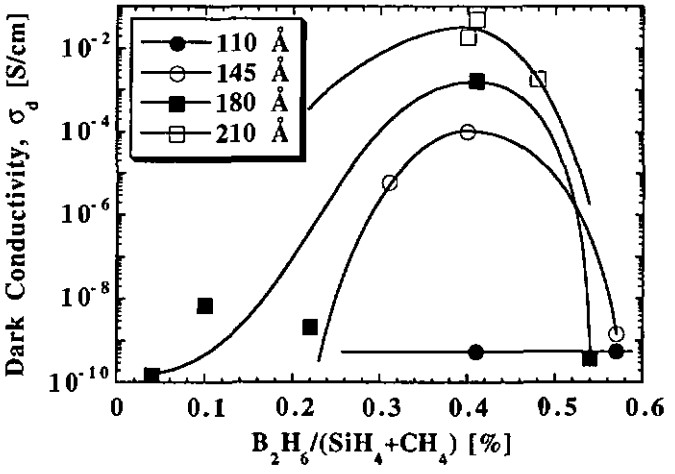

Fig. 3.3.2.10 Room temperature dark conductivity as a function of the diborane gas phase ratio, for different <p>-type silicon carbide film thicknesses.

The general trend observed of the decrease of σ_d with decreasing film thickness for a constant diborane gas phase ratio may be explained by a structural transition: The dominant phase changes from microcrystalline to amorphous material, as was already suggested for non-carbide films (see 3.3.1). This effect is furthermore very dependent on the diborane gas phase ratio, as it can be observed in Fig. 3.3.2.10. The optimised diborane gas phase ratio, for what concerns both the electrical properties and the crystallinity of the deposited films, seems to be around 0.4 %; this diborane gas phase ratio will be fixed at 0.4 % from now on, and for the thickness series studies presented hereafter.

The shape of the curves of the RT dark conductivity of these <p> μc-SiC:H very thin films are similar to the ones obtained for very thin <p> μc-Si:H films shown in Fig. 3.3.1.1, with a shift to lower values, since as inferred from Fig. 3.3.2.3, carbon lowers the electrical conductivity of the films. The optimised diborane gas phase ratio - corresponding to the maximum σ_d - is moreover slightly shifted to lower values, since carbon also hinders the formation of crystallites [Goldstein 1988].

The **deposition rate** r varies, in this study of very thin <p> μc-SiC:H films, with the diborane gas phase ratio and also with the thickness of the films, as presented in Fig. 3.3.2.11; the latter effect (deposition rate dependence on the film thickness) will be specified later, in the study of the thickness series with constant diborane gas phase ratio of 0.4 % (see Fig. 3.3.2.12).

For a constant thickness of about 180 Å, the deposition rate increases from about 0.26 to 0.34 Å/s quite linearly with doping over the scanned range of 0 - 0.6 %. Similar findings were reported elsewhere [Prasad 1991, Ghosh 1992 and Chou 1992], and shown in Fig. 3.3.1.2 for very

thin <p> μc-Si:H films. As the author already claimed, structural changes occur in the material (from μc-SiC:H to a-SiC:H) when increasing the diborane gas phase ratio, resulting in an enhanced deposition rate, since a-SiC:H is well known and generally accepted to grow faster than μc-SiC:H.

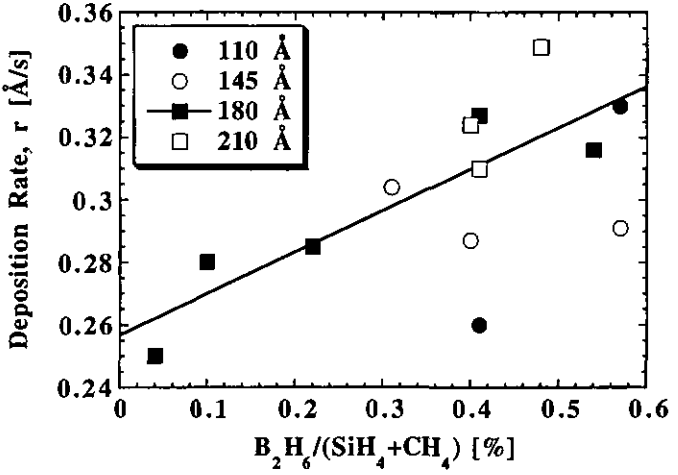

Fig. 3.3.2.11: Deposition rate as a function of the diborane gas phase ratio, for different <p>-type silicon carbide film thicknesses.

The increase of r by boron doping was preliminary observed for a-Si:H, as reported by Perrin et al. [Perrin 1989]. It was claimed there, that diborane presumably strongly catalyses H_2 desorption for the growing film surface, leading thus, to a decreased H-coverage. The variation of r with boron doping complicates the study of the effects of the boron doping on the film properties, since as shown later, the film properties significantly depend on the film thicknesses, for our very thin <p> μc-SiC:H films investigated.

From now on, we will concentrate on a thickness series of very thin <p> μc-SiC:H films, with the fixed diborane gas phase ratio of 0.4 %. Fig. 3.3.2.12 shows the thickness of the films as a function of the deposition time (measured from the starting of the plasma). It is important to point out here that we are dealing with very thin films (d < 230 Å), and therefore with the initial growth regime.

The shape of the curve is surely not a straight line (for our investigated film thickness range), meaning that for this regime of initial growth, the deposition rate is not constant. The extrapolation of the curve with a straight line for the lowest thicknesses leads to an "induction time" of about 200 seconds. This value is suggested (by the author) to correspond to the time needed for the initial nucleation. Due to the lack of very thin films of thickness ≤ 100 Å, this given value for the "induction time" is only a rough estimation. For increasing time, the effective deposition rate (calculated from the end of the "induction time") decreases from an estimated value of about 0.5 Å/s for the deposited film of lowest thickness (~ 110 Å), and tends for thicker films to the constant deposition rate value for bulk material. This trend can be explained by considering the fact that the structure of the films is predominantly amorphous for very thin films, and becomes microcrystalline with hardly any a-Si:H phase for thick films, as was previously shown by the detailed structural characterisation analyses (TEM, Raman spectroscopy, X-ray

diffraction/reflection and spectroscopic ellipsometry) of very thin <p> μc-Si:H films. The presence of such an "induction time" for boron doped films was observed in an earlier work [Prasad 1991 and 1991a] and inferred from in Fig. 3.3.1.3 for non-carbide films.

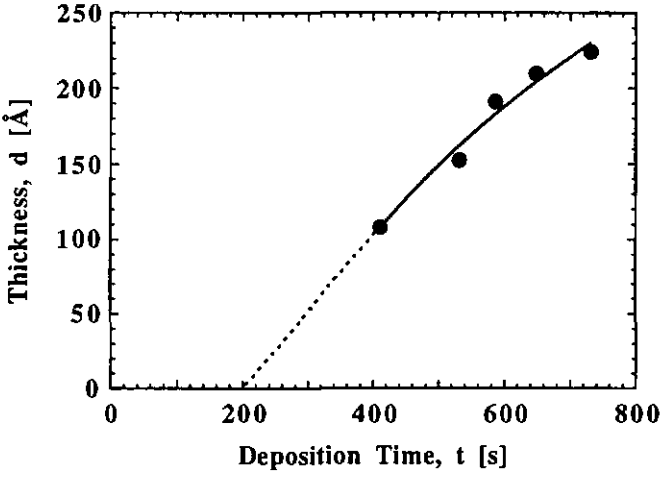

Fig. 3.3.2.12: Film thickness as a function of the deposition time, for the <p> μc-SiC:H thickness series (initial growth regime) with the fixed diborane gas phase ratio of 0.4 %.

Since the deposition rate is a function of the diborane gas phase ratio as we mentioned above, it is very probable that the "induction time" is also a function of the diborane gas phase ratio. In fact, the "induction time" generally depends on the entire set of deposition parameters and also on the type of substrates. These measurements of the deposition rate as a function of the diborane gas phase ratio and film thickness are very important for solar cell applications (window layers and tunnel junctions), for which very thin films of specific thicknesses (often lower than 200 Å) are required.

We already mentioned, while analysing the effects of the boron doping on the room temperature dark conductivity (Fig. 3.3.2.10) of our set of <p> μc-SiC:H very thin films, the general trend of the decrease of σ_d when decreasing the film thickness for a constant diborane gas phase ratio. Here, we specifically point out in Fig. 3.3.2.13 this observation, for our thickness series of very thin <p> μc-SiC:H films with the optimised and fixed diborane gas phase ratio of 0.4 %. Fig. 3.3.2.13 shows the **room temperature dark conductivity** σ_d and the corresponding **dark conductivity activation energy** E_σ as a function of the film thickness. Since, the Arrhenius plot of the dark conductivity often shows for higher temperatures (100 - 200 °C) a slightly different slope than for temperatures below 100 °C, we represent in Fig. 3.3.2.13 the values of E_σ as determined from the temperature range from room temperature (RT) up to about 100 °C.

σ_d remains still at high values, higher than 10^{-2} S/cm down to thicknesses of about 200 Å, with corresponding low activation energy values of about 100 meV, while beyond this thickness the conductivity begins to fall and E_σ to increase more rapidly. The conductivity reaches, even for thinner films (~150 Å), quite remarkably high values of > 10^{-4} S/cm, which are still above those of thick doped a-SiC:H (< 10^{-6} S/cm) or even thick doped a-Si:H (10^{-5} _ 10^{-4} S/cm). The relation between σ_d and the film thickness (Fig. 3.3.2.13) is well known for both the very thin microcrystalline and amorphous Si films used as window layers and tunnel junctions in solar cells

[Luft 1993, Li 1994 and Prasad 1991a], but such high σ_d and low E_σ values, as reached for our investigated very thin <p> µc-SiC:H films, were seldom reported.

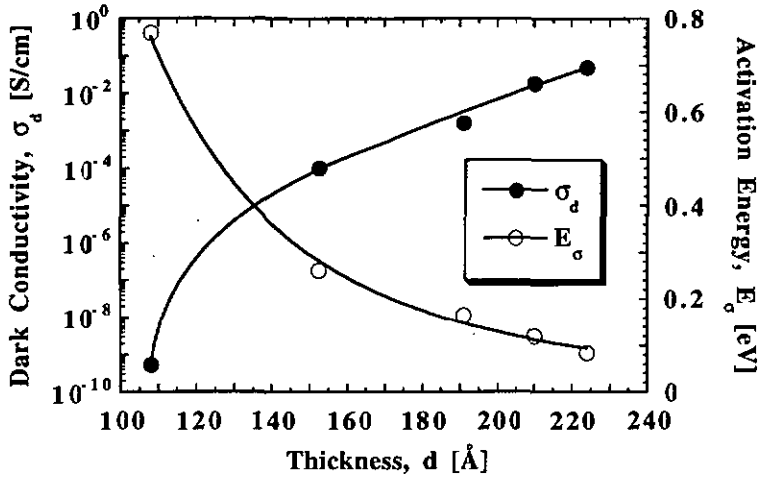

Fig. 3.3.2.13: Room temperature dark conductivity and dark conductivity activation energy as a function of <p>-type silicon carbide film thickness, for the optimised and fixed diborane gas phase ratio of 0.4 %.

As we already showed, the boron doping has drastic effects on the film properties for very thin films and has therefore, to be carefully optimised. The entire problem lays on the ability of depositing highly doped µc-SiC:H material, already for the early growth (initial growth regime) of the films, with a thinnest as possible or even vanishing amorphous interface layer. The already suggested structural transition from microcrystalline to amorphous material, when decreasing the film thickness, was previously confirmed by detailed structural analyses (TEM, Raman spectroscopy, X-ray diffraction/reflection and spectroscopic ellipsometry) of very thin <p> µc-Si:H films (see 3.3.1). The rapid fall in σ_d for films thinner than ~ 150 Å is proposed by the author to be attributed to a critical structural transition from microcrystalline to amorphous material; the crystallites become too small and too far away distanced from each other - resulting in a low crystallite volume fraction - to allow a conduction path through the crystallites by percolation. The amorphous phase becomes the dominant phase for what concerns the electrical properties of the films.

These very thin <p> µc-SiC:H layers were further characterised by spectral transmission and reflection measurements in the visible range. The film transmission in the visible (not shown here) decreases rapidly by increasing thickness, as was previously inferred from Fig. 3.3.1.5 for a thickness series of <p> µc-Si:H films deposited onto DC 7059 glass. Furthermore, an increase of the doping level results in a decreased transmission of the films, due to a shrinkage of the optical gap. Therefore, it is for our very thin film series deposited onto glass, with variations of both the thickness and the doping level, almost impossible to quantitatively sort the best optimised film, for what concerns its application as window layer in solar cells.

Moreover, films deposited in the final device are known to show often different properties by comparison with films deposited onto glass, due to several effects that are inherent to the deposition of devices, such as substrate-dependence of the growth, contamination from the

chamber walls, deposition parameter range limitations (e.g. temperature because of dopants post-diffusion) and so on. One has therefore really to optimise the very thin films in the device, with the experience inferred from such studies of films deposited on glass.

3.3.2.4 Conclusions

Starting from previously obtained results, where the VHF-GD process at 70 MHz plasma excitation frequency has shown to be a very suitable technique for preparing at low temperatures doped highly conductive μc-Si:H layers, methane was added to the plasma gas phase in order to increase the optical gap of boron doped μc-Si:H films and, thus, decrease the absorption losses (when such layers are used in p-i-n solar cells). For small CH_4 fractions, thin μc-SiC:H films could be obtained, which are revealed according to a criteria used by Luft and Tsuo, to be potentially better, as solar cell window layers, than amorphous carbide films and even μc-Si:H films.

In the context of the 70 MHz VHF-GD technique and the gases used in this work, there is so far no evidence from detailed structural analyses and electrical properties for the appearance of crystalline phase SiC. Furthermore, we show that a "too" high methane and/or diborane gas phase ratio, as well as a "too" high input discharge power leads to amorphous material. The other deposition parameters checked (temperature, pressure and argon gas phase dilution) have sensitively less drastic influences on the film properties. Thus, a wide range of film properties were obtained with structure ranging from microcrystalline to amorphous.

For a concrete application of these <p> μc-SiC:H films as window layers in solar cells, a down-scaling of the film thicknesses to values lower than 230 Å could be successfully performed, by carefully optimising the diborane gas phase ratio. An "induction time" of about 200 seconds was observed for the initial growth regime; this has further to be taken into account for the deposition of very thin films of specific thicknesses, as required for example for window layers in solar cells. Moreover, the structure of the growing films is predominantly amorphous for the early beginning of the deposition and becomes microcrystalline with hardly any amorphous phase when increasing film thickness.

Thus, down to thicknesses of about 150 Å, highly conductive and highly transparent very thin <p>-type μc-SiC:H layers can now be prepared; they could become excellent window layers and tunnel junctions for solar cell applications. However, full p-i-n solar cells have yet to be fabricated, that incorporate these new layers.

3.3.3 General conclusions

We optimised in this chapter <p>-type microcrystalline silicon films for window layer applications in p-i-n solar cells, for which high conductivities and high transparencies are required. Since very generally, the electrical and optical properties of the films show opposite trends, a compromise had to be found. By varying the deposition parameters, a wide range of film properties were obtained for film structures ranging from microcrystalline to amorphous.

Methane was added to the plasma gas phase, in order to increase the optical gap of the films. We showed, that as with boron doping, a "too" high methane gas phase ratio leads to amorphous material. A careful optimisation of both methane and diborane gas phase ratios leads to microcrystalline films with excellent properties for window layers in p-i-n solar cells.

The film thicknesses were reduced to the lowest value of about 100 Å (limited by the characterisation techniques) in order to really deal with films of thicknesses encountered in p-i-n devices. Even for the lowest thicknesses, the films showed a certain crystallinity. After an "induction time", depending sensitively on the deposition parameters, the films were observed to follow an "inverted conical" growth structure. The initial structural transition from amorphous to microcrystalline material was further observed at the critical thickness of about 150 Å.

Compared to amorphous silicon carbon alloy the newly developed <p> μc-Si:H or <p> μc-SiC:H show enhanced window layer properties and should lead to an increase solar cell performance. However, the influence of the substrate on the microcrystalline silicon growth remains open, the electrical and optical properties were obtained for films deposited on glass substrates.

Thus, as for undoped films, the VHF-GD at the plasma excitation frequency of 70 MHz shows to be also very efficient in depositing highly conductive and highly transparent boron doped microcrystalline films, at both low input powers and deposition temperatures. However, in the context of the VHF-GD technique and the gases used in this work, there is unfortunately so far no evidence for the appearance of crystalline phase SiC.

3.4 General conclusions to the film series studies and outlook

Detailed studies on undoped, compensated ("truly intrinsic" midgap material) and boron doped μc-Si:H film series were presented, the goal being their optimisations for solar cell applications. The 70 MHz plasma excitation frequency PECVD technique used in this work is revealed to be very favourable for the rapid growth of high crystallinity microcrystalline layers. Furthermore, lower input plasma powers and substrate temperatures could be used, in comparison with the standard 13.56 MHz plasma excitation frequency; the space of deposition parameters seems simply to be extended for the growth of high quality microcrystalline Si films.

The benefits of the 70 MHz GD are proposed to be related to differences in plasma chemistry, physics and kinetics. As a matter of fact, results from plasma diagnostics and impedance analyses suggest that a higher but less energetic ion flux to the growth surface - due to a lower self-bias potential, lower sheath voltages and lower sheath thicknesses - lead to a favourable growth of μc-Si:H under VHF conditions.

A temperature series of undoped μc-Si:H films - that are revealed to have the usual <n>-type character, as most GD deposited films - clearly points out the differences in the properties of μc-Si:H films deposited at the plasma excitation frequencies of 13.56 and 70 MHz . An increase of the growth rate and grain size with no adhesion problems were mainly observed under VHF conditions. Higher plasma excitation frequencies seem also to lead to μc-Si:H films showing less defects. The variation of the deposition temperature leads to a wide range of film properties with films tending for higher temperatures to denser and more crystalline material.

Thus, the VHF-GD at the plasma excitation frequency of 70 MHz has shown to produce μc-Si:H at high deposition rates (~ 0.7 Å/s or even higher !) with a satisfactory adhesion to the substrate; these are two essential conditions for the rapid growth of some micrometers thick μc-Si:H films as active layers in solar cells. The <n>-type character observed for nominally undoped films is however undesirable for the above mentioned applications as photovoltaically active layers in solar cells and it is towards this goal that compensation experiments were undergone. By a stepwise microdoping of the plasma gas phase in the vppm range compensated films could be obtained with the Fermi level position at midgap. Detailed absorption measurements indicate a low subgap absorption for these films, which could be a sign of a low defect density. Light-soaking experiments with an intense high-pressure sodium lamp have clearly shown better stability for the new compensated μc-Si:H than for undoped films. In fact, from the series of films studied, the compensated one appears to be the most appropriate for solar cell applications - as a new promising stable photovoltaically active material - since it degrades the least, its dark conductivity is the lowest and its photoconductive gain is the highest. We even further suggest that μc-Si:H generally degrades less than a-Si:H.

Finally, for p-i-n solar cell applications, highly conductive and highly transparent <p>-type microcrystalline very thin films (100 - 200 Å) were optimised. The effects of the main deposition parameters on the film properties were studied. A particular attention was brought on the initial growth regime for very thin films of thicknesses as requested for the applications as window layers and tunnel junctions in solar cells. A careful optimisation of mainly the diborane and methane gas phase ratios lead to highly conductive and highly transparent microcrystalline films, even for low thicknesses of about 150 Å. The substrate-dependent growth under microcrystalline

silicon plasma conditions was confirmed by the observation of an epitaxial growth of a <p>-type Si very thin film deposited onto c-Si. This further points out the new potential application of the VHF-GD technique for the deposition of epitaxial layers for c-Si based heterojunction solar cells.

All these developed and optimised films (compensated and boron doped) have yet to be incorporated in solar cell devices (e.g. single, double or even triple p-i-n's, heterojunctions and n-i-p's) and optimised for the device performances. Very surely, some new problems inherent to the fabrication of the devices will have to be faced. This is fully another task, since the films are no more an entity by themselves but belong to a full device, for which each constituting film has a specific role and where furthermore the interactions between these up to now independently analysed films become crucial.

To conclude, this presented thesis work of film development and optimisation for some specific devices applications can be compared to the establishment of the playing rules of a given complex game. The next step would be to use the rules for playing the game ... (!)

4 APPLICATIONS OF MICROCRYSTALLINE SILICON THIN FILMS TO PHOTOVOLTAIC DEVICES (SOLAR CELLS) AND TO MICROELECTRONIC DEVICES

In the present work, we mainly focused so far on the research and optimisation of microcrystalline silicon thin films for multiple applications to photovoltaic devices (solar cells). We will now, in this chapter, mention the realised applications (in our laboratory mainly done by co-workers) of the developed μc-Si:H thin films to several kinds of solar cells. Other potential applications of microcrystalline silicon thin films and of our VHF-GD technique at a plasma excitation frequency of 70 MHz to large area microelectronics are also very briefly given.

4.1 Photovoltaic devices

Very generally, microcrystalline Si and SiC thin films are incorporated in our solar cells mainly as window layers, tunnel junctions, and even as photovoltaically active layers. In the world-wide quest for higher sunlight conversion efficiencies of a-Si:H based photovoltaic solar cells, a number of approaches appear promising: 1) the use of multiple junction devices (tandem or triple cells), 2) the use of highly conductive and transparent p- and n- layers, and 3) the reduction of interface recombination losses. Microcrystalline silicon with its general weaker absorption (in the visible range), enhanced infrared response and higher conduction (than a-Si:H) is useful in all these approaches [Luft 1993].

4.1.1 Completely microcrystalline Si p-i-n-type solar cells

This part will exhibit the real importance of this innovative work by pointing out the tremendous potential of the newly developed compensated microcrystalline silicon (see 3.2) as **photovoltaically active material** in entirely microcrystalline silicon p-i-n solar cells and that in contrast with the established general viewpoint.

Indeed, different characterisation methods such as electron spin resonance (ESR) [Liu 1986] and field effect measurements [LeComber 1983] suggested for the microcrystalline silicon material a defect-rich region at the grain boundaries or amorphous zones, with defect densities in the order of 10^{17} - $5x10^{18}$ cm^{-3}, distributed energy-wise over the whole energy gap. These high defect densities together with low photoconductive gains probably hindered up to now the use of undoped μc-Si:H material for solar cell applications as photovoltaically active material.

Until this work, only very few studies have been done concerning μc-Si:H in p-i-n cells as photovoltaically active material [Wang 1990 and Faraji 1992], probably because of the suspected high defect densities as mentioned above. However, our investigations on films deposited by VHF-GD at a plasma excitation frequency of 70 MHz (this work) led to the general recognition of the fact that compensated ("truly intrinsic" midgap material) μc-Si:H is more stable under light exposure than a-Si:H (see 3.2). This fact has already been shown by other groups [Liu 1986 and Williams 1991].

As it is now well known, microcrystalline silicon shows a weaker absorption for the short wavelengths than amorphous silicon; however, in the near infrared (for $h\nu > E_g$) it has an enhanced absorption [Wang 1990, Meier 1995 and Beck 1995]. On the other hand, we found, as shown in Fig. 3.2.4 and Fig. 4.1, a significantly lower subgap absorption (for $h\nu < E_g$) of our compensated material as compared to that found by other groups. The subgap absorption of our compensated μc-Si:H reaches values even as low as those obtained for good amorphous material in the annealed state [Meier 1995 and Beck 1995]. Fig. 4.1 shows the absorption spectra of a 1.8 μm thick compensated μc-Si:H film as measured by PDS [Meier 1995]. One of the recent constant photocurrent method (CPM) measurements executed by the Prague group (M. Vanecek and N. Beck) of our compensated μc-Si:H layers is also given in Fig. 4.1, for comparison.

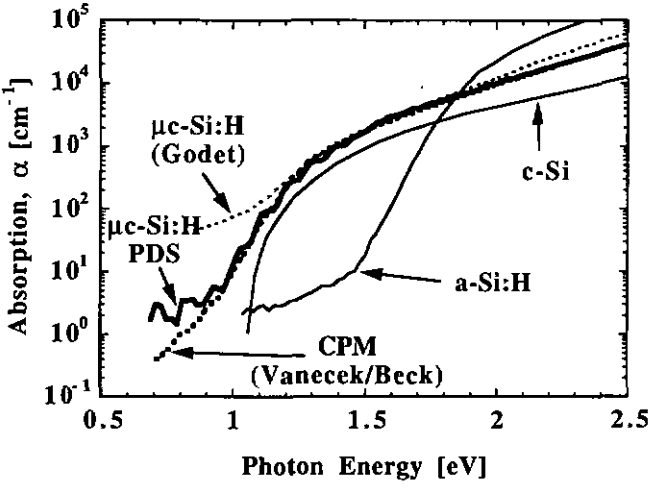

Fig. 4.1: Absorption spectrum of a 1.8 μm thick compensated μc-Si:H film as measured by PDS and transmission/reflection spectroscopy [Meier 1995]. A recent measurement obtained by the CPM technique (by M. Vanecek and N. Beck [Beck 1995]), for our compensated material is also plotted. For comparison, the μc-Si:H spectrum given in another work [Godet 1987], together with those of amorphous and crystalline silicon are also added.

It clearly follows that, compared to a-Si:H, the μc-Si:H absorption opens a real potential in additionally making use of the sun's spectrum in the near infrared to a higher extent and, thus, increasing the short circuit current density (J_{SC}) of the cell; however, to this end, the active layer thickness has to be increased or more sophisticated light trapping has to be applied than usually done. Spectral response (SR) measurements of our entirely μc-Si:H p-i-n cells [Flückiger 1993 and Meier 1994a] (see also Fig. 4.2) confirm clearly the higher infrared absorption. Fig. 4.2 shows moreover the very pronounced effect of the micro-doping of the <i> layer on the cells and on their spectral responses [Meier 1994a]. All three cells presented have the same <p> and <n> layers and the same <i> layer except for the micro-doping. Very surprisingly, we also found [Meier 1994] that in cells with thicknesses as high as 1.7 μm, practically all photogenerated carriers could be collected, which is in contrast with the case of a similarly thick amorphous p-i-n cell. This last point further clearly confirms the real potential of our compensated μc-Si:H when used as photovoltaically active material in solar cells.

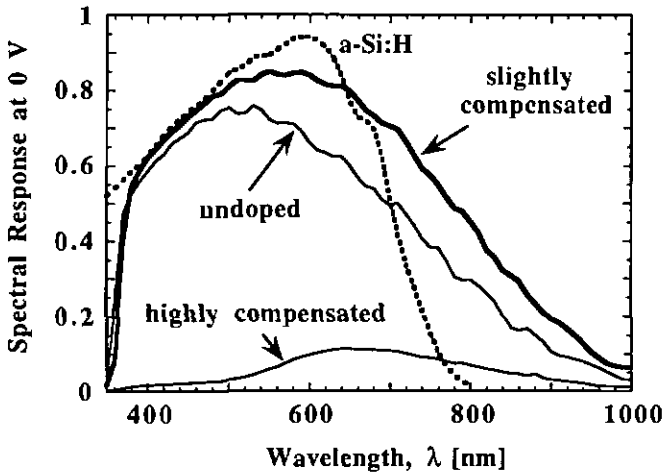

Fig. 4.2: Influence of micro-doping of the <i> μc-Si:H on the spectral response of entirely μc-Si:H cells (1.6 μm thickness) [Meier 1994a]. For comparison, the spectral response of a standard a-Si:H cell is also plotted.

Under AM1.5 conditions, we obtained, for our best μc-Si:H cells [Meier 1994], a short circuit current density of 21.9 mA/cm^2, which is significantly higher than the highest value ever reported for amorphous silicon solar cells and which is clearly consistent with the data obtained from the absorption spectra. The best cells of 1.7 μm thickness show an efficiency of 4.6 % (for an active area of 5 mm^2), whereas the obtained open circuit voltages (V_{OC}) were only between 340 and 390 mV and the fill factors (FF) between 40 and 60 %. The potential in further increasing the efficiency lies in an increase of the active layer thickness in order to obtain higher short circuit current densities, in the optimisation of the p-i interface for achieving higher V_{OC} values and finally in the optimisation of the back contact reflector for the infrared light. We showed previously in another study [Flückiger 1993] that V_{OC} values of 600 mV are in fact obtainable by introducing a-Si:H buffer layers. However, these cells (at least so far) have very low fill factors and possess a "bend" in the active region of the I-V curves; the latter is thought to be caused by a band spike at the p-i interface due to the higher gap of the amorphous buffer layers. This problem is still unsolved and more work in this field has to be done in the future. It is as yet not clear whether the introduction of amorphous buffer layers can lead to high V_{OC}-values without introducing the disturbing "bend" in the I-V curve.

The most important problem of stability under long-term light-soaking conditions was also investigated for our completely microcrystalline cells [Meier 1994]. The degradation experiment was undertaken, as is recommended by the National Renewable Energy Laboratory (NREL, USA) for amorphous silicon solar cells: 100 mW/cm^2 AM1.5, 1000 h, 50 °C. The microcrystalline cells were exposed to an AM1.5 light source of 90 mW/cm^2 over more than 640 h. The surprising result of Fig. 4.3 [Meier 1994] (somewhat expected from film degradation studies) shows almost no degradation; the precise characterisation by SR and standard current voltage (I-V) measurements of the microcrystalline cells before and immediately after the degradation (without an annealing) results in the following changes (including fluctuations of the apparatus): $\Delta V_{OC} < 2$ %, $\Delta J_{SC} < 1$% and $\Delta FF < 2$%.

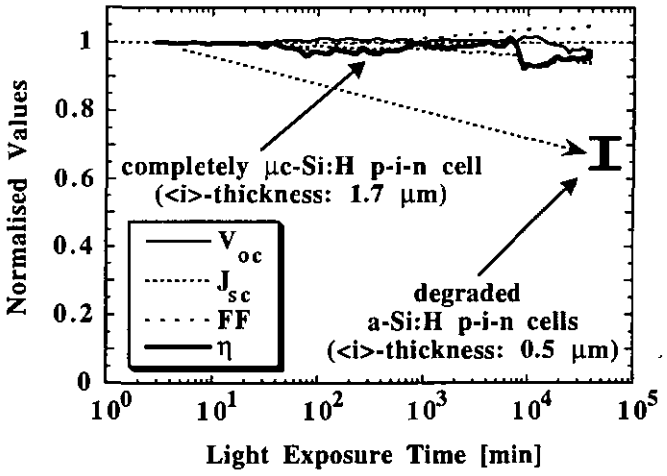

Fig. 4.3: Stability behaviour of an entirely μc-Si:H p-i-n solar cell under long-term light exposure (~ 90 mW/cm^2 AM1.5, T = 47 °C). For comparison, typical results of degraded a-Si:H single p-i-n cells (> 10 % initial efficiency) obtained by the same degradation light source are also plotted.

Compared to high efficiency amorphous cells (> 10 % initial efficiency) there seems to be no degradation due to light-soaking present in the entirely μc-Si:H solar cells. The stability of the conductivity under illumination σ_{ill} in compensated μc-Si:H films when light-soaking is performed has already been found from film degradation studies (see Fig. 3.2.7). The comparison with a-Si:H solar cells might yet not be deemed as being representative, as the conversion efficiency of our μc-Si:H cells is only 4.6 % , and as it is known, that a-Si:H cells of e.g. 5 % initial efficiencies are less affected by light-soaking than high efficiency cells (> 10 % initial efficiency). On the other hand, one has to note that our fully microcrystalline cells do have (unlike a-Si:H cells with 5 % efficiency) reasonable values of FF and high values of J_{sc}, which are both indeed not affected by light-soaking.

Finally, voltage-dependent spectral response measurements were performed on our completely microcrystalline p-i-n solar cells in order to get insight on the carrier transport mechanism [Meier 1994]. The carrier collection behaviour seems to lie between that of a-Si:H and c-Si leading us to suggest that the carrier-collection mechanism is partly diffusion-supported [Meier 1994]. The existence of this transport mechanism is also well supported by the observation of a strong peripheral effect in our μc-Si:H cells, as seen is light beam induced current (LBIC) measurements; this strong peripheral effect has in fact to be carefully taken into account for accurate efficiency measurements [Meier 1994].

Fig. 4.4 shows a cross-sectional SEM (scanning electron microscopy) picture of a completely microcrystalline p-i-n-solar cell (2.1 μm thick) deposited onto SnO_2 coated glass and covered with an ITO/Ag layer acting as back-reflector. The vertically needle-like extending crystallite growth within the cell is clearly visible. It is important to note here that due to the observed preferential columnar growth, the electrical properties obtained by a coplanar electrode configuration (i.e. by the usual configuration) may possibly differ much from those obtained for a sandwich configuration of the film. Let us keep in mind that the properties relevant for the cells are those of the vertical transport.

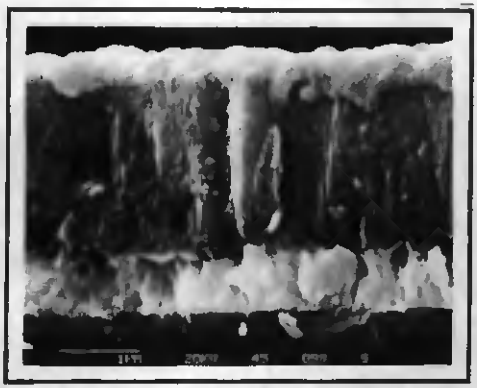

Fig. 4.4: Cross-sectional SEM picture of a completely microcrystalline p-i-n-solar cell (2.1 μm thick) deposited onto SnO_2 coated glass and covered with an ITO/Ag layer.

Due to the increased infrared sensitivity of the microcrystalline material, the combination of entirely μc-Si:H p-i-n bottom cells with conventional a-Si:H top cells is a promising concept to realise high efficiency, all-silicon thin film solar cells. So far, and for the first time, tandem cells with an initial efficiency of 9.1 % and a matched current density of 11.5 mA/cm^2 (see Fig. 4.5) have been realised in our laboratory [Meier 1994a]. The I-V characteristics of this new tandem cell shown in Fig. 4.6 demonstrate furthermore that, indeed, the fabrication of VHF-deposited μc-Si:H solar cells is fully compatible with the amorphous silicon technology.

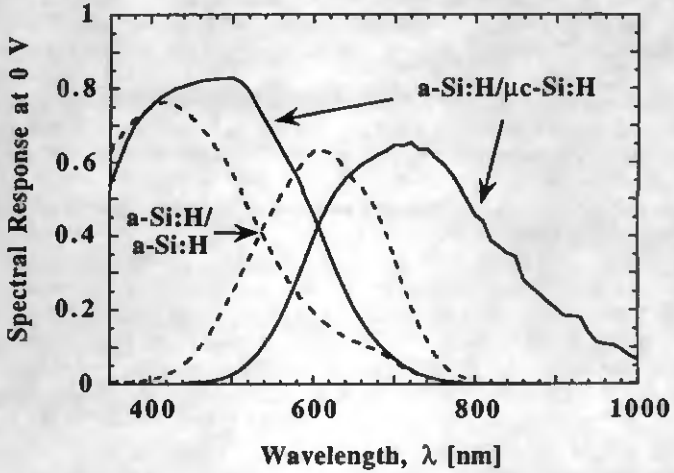

Fig. 4.5: Spectral response of the a-Si:H/μc-Si:H tandem cell in comparison with a standard a-Si:H/a-Si:H tandem cell [Meier 1994a]. The J_{sc} values under AM1.5 conditions are 11.5 mA/cm^2 for the μc-Si:H bottom cell and 11.6 mA/cm^2 for the a-Si:H top cell (active area of 8.7 mm^2).

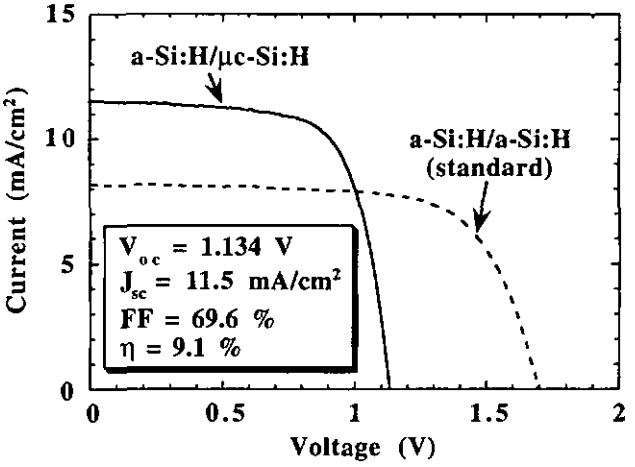

Fig. 4.6: I-V characteristics under AM1.5 conditions of the a-Si:H/μc-Si:H tandem cell, in comparison with a conventional a-Si:H/a-Si:H tandem cell [Meier 1994a].

Because of the relatively low open circuit voltage of our completely μc-Si:H solar cell (< 400 mV), as already mentioned previously, the performance of a-Si:H/a-Si:H/μc-Si:H triple stacked cells is expected to be even superior over that of tandem cells. Such triple cells were thus recently fabricated for the first time in our laboratory and show, for the best cells, an efficiency of 9.5 % under AM1.5 conditions [Meier 1995a].

The combination of the μc-Si:H cells with standard a-Si:H cells obviously leads to Staebler-Wronski degradation effects under light exposure. However, the amplitude of the degradation is expected to be clearly reduced with respect to that of pure a-Si:H stacked cells due to the absence of degradation in the microcrystalline films (see Fig. 3.2.7) and cells (see Fig. 4.3) and due to thinner a-Si:H cells [Meier 1995a].

The highest deposition rate of approximately 1 Å/s, obtained by our VHF-GD technique at the plasma excitation frequency of 70 MHz, is still far too low for the industrial production of a 1.7 μm thick solar cell. This is, in our personal point of view, presently the main bottleneck for the use of microcrystalline silicon as a commercial photovoltaically active solar cell material. However, good hope is still kept since higher plasma excitation frequencies and, especially other deposition techniques (e.g. hot wire) are known to be now able to further increase the deposition rate of μc-Si:H.

4.1.2 n-i-p-type amorphous Si solar cells with <p> μc-Si:H window layer

The detailed practical experience shows that <p>-type microcrystalline silicon window layers are also successfully used in n-i-p-type amorphous Si solar cells, leading to relatively high V_{oc} values (890 mV without buffer layers) and to better cell efficiencies than for cells based on conventional <p>-type amorphous window layers [Goetz 1995]. These n-i-p solar cells deposited on metal substrates have three striking advantages compared to the conventional p-i-n technology on glass: First, cost reduction can be expected because of omitting expensive textured TCO on glass. Second, a wider choice of surface textures of the metal substrates offers the possibility of further optimised light trapping. Third, deposition temperatures for the <i> layers higher than 250 °C are generally possible, since the most critical interface (i-p) is deposited last.

4.1.3 c-Si based heterojunction structure solar cells

In the field of heterojunction solar cells, we demonstrated the emitter, passivation and back surface field (BSF) properties of microcrystalline silicon layers deposited on <p>-type crystalline silicon [Keppner 1994 and Torres 1994]. Surface passivation is of essential importance in order to increase the total solar cell efficiency by enhancing the open circuit voltage V_{oc}. So far, mainly oxides and nitrides grown at high temperatures were used. The PECVD technique at the plasma excitation frequency of 70 MHz showed to be a non-destructive deposition technique for the growth of a-Si:H and μc-Si:H thin films onto c-Si surfaces. Note that c-Si cells are very sensitive to surface damages through increased surface recombination velocity, leading as major consequence, to a reduction in the value of V_{oc}. In our heterojunction cells relatively high values of V_{oc} could be obtained (up to 635 mV). Furthermore, very efficient surface passivating a-Si:H films and highly doped <p>-type layers could be deposited for the creation of a back surface field. The serial resistances of the cells were significantly reduced by the inherent high conductivity of the <n>-type μc-Si:H we used. The detailed scientific results concerning our heterojunction solar cells are fully described elsewhere [Keppner 1994 and Torres 1994].

4.1.4 Summary

In Table 4.1 are listed, as a summary, all different types of solar cells fabricated in our laboratory using one or more microcrystalline Si thin films developed and optimised in this thesis work. References to publications are also given for further detailed descriptions.

Silicon solar cell structures	References
p(μc)-i(a)-n(μc)	Work under way ...
p(μc)-i(μc)-n(μc)	[Flückiger 1992, 1993, Meier 1994, 1994a, and 1995]
n(μc)-i(a)-p(μc)	[Goetz 1995]
p(a)-i(a)-n(μc)-p(μc)-i(a)-n(μc)	Work under way ...
p(a)-i(a)-n(μc)-p(μc)-i(μc)-n(μc)	[Meier 1994a, 1995 and 1995a]
p(a)-i(a)-n(μc)-p(a)-i(a)-n(μc)-p(μc)-i(μc)-n(μc)	[Meier 1995a]
n(μc)-i(a)-p(c)-i(n)-p(μc)	[Keppner 1994 and Torres 1994]

Table 4.1: Enumeration of all different types of solar cells fabricated in our laboratory using one or more microcrystalline Si thin films developed and optimised in this thesis, with the corresponding references to publications. The abbreviations used for crystalline, microcrystalline and amorphous are, respectively: "c", "μc" and "a".

4.2 Microelectronic devices

As already mentioned by the author in (3.3.1.3), our findings of epitaxial growth of <p>-type Si at low temperature by our VHF-GD technique at the plasma excitation frequency of 70 MHz open a wide range of potential applications for opto-electronic and microelectronic devices, such as for the fabrication of advanced metal-oxide-semiconductors (MOS) and for the bipolar integrated circuit (ULSI) technology. For example, dopant redistribution can be avoided at low temperature so that an abrupt dopant transition can be obtained. On the other hand, low temperature epitaxial growth reduces autodoping, wafer warping, and system design cost. Furthermore, a greater liberty in the sequences of deposition steps is introduced.

The VHF-GD technique, developed in our laboratory, shows many advantages for low temperature epitaxial growth, including batch-wafer processing, low cost, the absence of ultra-high (UHV) requirements, large area deposition, and the capability of low temperature growth assisted by plasma.

Hydrogenated amorphous silicon films are now widely used in opto-electronic devices (solar cells, flat panel displays and contact image sensors) and electronic devices (thin film transistors (TFT's)) [Kanicki 1991]. The factors limiting their applications are the low charge carrier mobility, low electrical conductivity and poor electrical reliability (due to light induced degradation) even at room temperature, generally related to the intrinsic network structure. Changing intrinsic network of a-Si:H into microcrystalline phase could be the most effective way to improve the characteristics of the devices mentioned above, since μc-Si:H shows higher effective carrier mobility and stable electrical properties.

Polycrystalline silicon and microcrystalline silicon TFT's with high effective charge carrier mobility have recently received considerable interest for their use in flat-panel display devices for example, in place of a-Si:H TFT's. Materials with better performance are required for the TFT's used for display addressing (active matrix display) to integrate the driving electronics and to reduce the number of connections to the screen. Also, due to display sizes that become larger and larger, higher and higher drain currents of TFT's are requested.

Low temperature processed TFT's incorporating <n>-type μc-Si:H source and drain contacts and boron-compensated ("truly intrinsic" midgap material) μc-Si:H channel layers were thus fabricated and reported [He 1993] to exhibit low threshold voltages (1.1 V) together with high effective channel charge carrier mobilities (6.5 cm^2/Vs). The substitution of a-Si:H by μc-Si:H in TFT's results in the following performance improvement, i.e. a reduction of the threshold voltages and an increase of the effective channel carrier mobilities [He 1993, Hsu 1994 and Parsons 1994]. However, practically the substitution of a-Si:H by μc-Si:H remains still a challenge from the technological point of view and a lot of work has still to be done in this field in the future. Also, the use of microcrystalline material for TFT's active layers might induce a degradation of the on/off current ratio as was reported by Hsu et al. [Hsu 1994]. The low value of R_{off} might moreover possibly restrict the applications of μc-Si:H TFT's to displays.

4.3 Conclusions

We mentioned here the realised applications in our laboratory of the developed μc-Si:H thin films to several kinds of solar cells and to large area microelectronic devices.

The presented results have shown that compensated ("truly intrinsic" i.e. midgap material) μc-Si:H has the potential to become a new photovoltaically active thin film material which merits much broader investigations. The entirely μc-Si:H cell is the first thin film device, exclusively based on silicon alone, that shows an enhanced sensitivity in the infrared above 800 nm. The limits of the V_{oc}, J_{sc} and FF of the completely μc-Si:H solar cell are still far from optimisation and rest still open for improvement. The highest potential in further increasing the cell efficiency is related to obtaining higher V_{oc} values.

The results show furthermore that the substitution of conventional a-Si:H or costly a-SiGe:H by a μc-Si:H bottom cell within a multi-junction configuration opens new ways for increasing the efficiency of silicon thin film solar cells. The growth of entirely microcrystalline cells is revealed to be fully compatible with the growth of amorphous silicon, when using the VHF-GD technique at 70 MHz. The still far too low maximum deposition rate of approximately 1 Å/s, obtained by our VHF-GD technique at the plasma excitation frequency of 70 MHz is presently the main bottleneck for the use of microcrystalline silicon as a commercial photovoltaically active solar cell material.

The potential applications of μc-Si:H thin films to other solar cell devices such as n-i-p's and heterojunctions were furthermore also briefly pointed out.

Finally, the VHF-GD technique opens a wide range of potential applications for opto-electronic and microelectronic applications for which low temperature growth of thin films (a-Si:H, μc-Si:H and even epitaxial) is advantageous. In the field of large area microelectronics, polycrystalline silicon and recently microcrystalline silicon with their high effective charge carrier mobility have received considerable interest for their use in flat-panel display devices in place of a-Si:H TFT's.

5 GENERAL CONCLUSIONS TO THE PRESENTED WORK

It was shown in a previous thesis work [Prasad 1991], that by using the VHF-GD technique at the plasma excitation frequency of 70 MHz, good quality undoped and doped microcrystalline silicon was obtained under very favourable conditioos of deposition, i.e. low substrate temperature (150 - 200 °C) and low input discharge power (25 - 75 mW/cm^2). Even at low silane gas phase concentrations (< 4 %), the deposition rates were shown to be higher by a factor of 3 to 5 than the deposition rates reported for the standard plasma excitation frequency of 13.56 MHz. The RT dark conductivities were also higher than those reported earlier for the doped specimens.

The still actual world-wide quest for higher sunlight conversion efficiencies of a-Si:H based photovoltaic solar cells leads us to optimise and develop in this thesis work microcrystalline silicon thin films for multiple photovoltaic applications in solar cells. Microcrystalline silicon with its weaker absorption (in the visible range) and higher conduction (than a-Si:H) is useful in this approach [Luft 1993 and references therein]. It has been shown by other groups [e.g. Yang 1994] that μc-Si:H window layers lead to very high open circuit voltages (> 1 V !) for a-Si:H based solar cells and, thus, to increased cell efficiencies.

All films presented in this work, belonging to a set of nearly 200 films from different series, were deposited by the author alone. The system used for the deposition of the films (presented in chapter 2) was already realised but had to be carefully characterised, for what concerns some major physical parameters (e.g. effective plasma power, deposition temperature of the substrate, effective gas fluxes, and so on). Only after a good understanding of the deposition technique together with the plasma and vacuum physics, the different film series could be deposited and carefully compared. Once the films were developed and optimised for specific solar cell applications (as for example photovoltaic active material, window layers, tunnel junctions, and passivating films), incorporation into different solar cell devices was successively performed in the same laboratory by co-workers.

A nominally undoped μc-Si:H deposition temperature series revealed the strong <n>-type character of the films, supposed to be caused mainly by oxygen contamination. By increasing the deposition temperature, a wide range of film properties were obtained, corresponding to films ranging from almost a-Si:H to μc-Si:H having an estimated crystalline volume fraction higher than 95 %. A comparison of two deposition temperature series of nominally undoped μc-Si:H films deposited by a standard 13.56 MHz UHV and our 70 MHz VHF HV PECVD technique revealed certain essential differences in the film properties. The main advantages of the films deposited under VHF conditions are the better adhesion of the growing films to the substrates and the higher deposition rates of enhanced crystallite size material. Very generally, higher crystalline volume fraction, denser and less defective μc-Si:H material is obtained, yielding better optical and electrical properties.

The plasma excitation frequency of 70 MHz as used in this work for the deposition of the films is understood to be responsible for the above mentioned results. A hydrogen rich plasma is suspected to be produced from the high power transfer efficiency in the bulk of the plasma and the high dissociation rate, as deduced from the high deposition rates. In combination with the low sheath potentials and the low sheath thicknesses, a high flux of hydrogen, ions and radicals with moderate energies are produced at the growing film/plasma interface. This is thought to establish

the required equilibrium or growth conditions between deposition and etching, which results in the formation of high-quality μc-Si:H.

Compensation experiments by boron doping in the vppm range (so-called "microdoping") were undergone to get ride of the usual <n>-type character of nominally undoped μc-Si:H films for a solar cell application as photovoltaic active material. "Truly intrinsic" μc-Si:H with Fermi level at midgap was thus obtained, exhibiting a maximum in the photoconductive gain and dark conductivity activation energy, a minimum in the dark conductivity and photoconductivity and no observable Staebler-Wronski effect under strong light-soaking experiments. No feasible explanations were found, so far, for the observed degradation kinetics as a function of boron microdoping. For what concerns the transport properties, a theoretical explanation was tentatively proposed, which is based on the well-known grain boundary trapping model [LeComber 1983], originally developed for polycrystalline silicon [e.g. Seto 1975]. All μc-Si:H p-i-n solar cells, incorporating the optimised compensated film as photovoltaic active material, showed by the way, an enhanced stability to light-soaking experiments and an increased infrared absorption (above 800 nm) [Meier 1994]. Furthermore, these mentioned cell properties clearly call for the incorporation of the all microcrystalline Si cell as a bottom cell in a tandem or even triple structure a-Si:H based solar cell, since, the whole growth process of the all μc-Si:H p-i-n cell reveals to be fully compatible with the standard amorphous p-i-n cell preparation [Meier 1995 and 1995a].

Boron doped μc-Si:H and μc-SiC:H thin and very thin films were deposited and optimised for solar cell applications as window layers and tandem junctions; these applications request highly conductive and highly transparent films. The problem of the deposition of highly doped and highly crystalline films was studied for the early growth step (initial growth regime). Detailed structural analyses lead to the suggestion of a specific "inverted conical" growth model for the initial growth regime of the films. A boron doping optimisation for very thin films ($d < 350$ Å) leads to <p>-type μc-Si:H window layers with excellent electrical and optical properties. Like boron atoms, carbon atoms in the plasma gas phase showed to sensitively hamper the growth of crystallites. However, by carefully optimising the diborane and methane plasma gas phase ratios, very thin <p> μc-SiC:H films could be deposited, that are revealed to be - according to a criteria introduced by Luft and Tsuo [Luft 1993] - potentially better than standard a-SiC:H or even μc-Si:H films for window layers in solar cells. These films have so far made their first proof in a-Si:H based n-i-p structure cells deposited on aluminium substrates: V_{OC}-values as high as 890 mV (without buffer layer) were obtained and were reported to be even higher than those obtained for cells with <p> a-SiC:H window layers [Goetz 1995]. The optimised <p> μc-Si:H very thin films were applied with success in heterojunction solar cells based on c-Si wafers as window and passivation layers [Keppner 1994 and Torres 1994]. Unfortunately, in the context of our VHF-GD at the plasma excitation frequency of 70 MHz and the gases used in this work, there is, so far, no evidence of crystalline phase SiC for our <p> μc-SiC:H films.

The influence of the substrate on the growth of very thin <p> μc-Si:H films was briefly evidenced: After three specifically developed surface treatment steps and under specific growth conditions, the film growth on a c-Si substrate was revealed to be epitaxial. This obvious epitaxial growth by using the VHF-GD at 70 MHz has strong consequences for potential applications of epitaxially grown Si films on heterojunction solar cells as window and passivation layers. Both the pre-treatment procedure and the deposition itself are under way to be patented [Flückiger 1994a].

Regarding ahead to the deposited microcrystalline material leads us to state that a lot is realised from the technological point of view, while only few is, so far, really understood from the point of view of physics (e.g. transport theories, degradation kinetic models, and so on). Seeing that this new type of material gently over-passes a-Si:H and some exotic type of alloy using Ge, As and C, the author strongly recommends to really attribute more time for the understanding of the basic phenomena and physics that govern μc-Si:H material. Moreover, our 70 MHz PECVD technique has clearly pointed out some major advantages from the technological and film properties point of views, by comparison with the standard 13.56 MHz plasma excitation frequency. An enhanced plasma excitation frequency over 70 MHz [Finger 1994] already revealed some further advantages; this is why one should, from now on, scan in detail the very high frequency range for the quest of a more optimal plasma excitation frequency for the deposition of μc-Si:H.

6 ANNEXES

6.1 Cleaning procedures

6.1.1 Glass substrates

The used glass was the "Dow Corning 7059".

6.1.1.1 Manual cleaning

Solution: concentrated "Vizir" (commercial solution for the washing of clothes)
Brushing: each substrate using a standard soft paint brush and following only one direction movement
Rinsing: each substrate individually with cold running water
Rinsing: the whole lot of substrates under deionised running water

6.1.1.2 Cleaning using ultrasonic baths

Bath 1: solution of 0.8 % "Deconex" in deionised water (80 ml of "Deconex" in 10 l of deionised water)
temperature: 70 °C
duration: 3 minutes with ultrasound
Bath 2: ordinary water
temperature: room temperature
duration: 10 minutes without ultrasound
Bath 3: deionised water shower
temperature: room temperature
duration: 1 minute without ultrasound
Bath 4: solution of 0.8 % "Trulit S" in deionised water
temperature: 60 °C
duration: 3 minutes with ultrasound
Bath 5: deionised water shower
temperature: room temperature
duration: 10 minutes without ultrasound

6.1.1.3 Drying

Take each substrate one by one, while leaving the others under a deionised water shower. Dry them immediately with a nitrogen flow.

6.1.2 Crystalline silicon substrates

The silicon substrates (<100> orientation) are already clean enough when received from the wafer manufacturer so they are simply rinsed with deionised water and then immediately dried with a nitrogen flow before being loaded into the vacuum chamber.

6.1.3 Stainless steel parts: substrate holder with screws and rf electrode plate

- remove the silicon powder using paper tissues
- dip the pieces (until total etching of the deposit) in CP6 acid (CP6 = 1/2 HNO_3 (65 %) + 1/4 HF (40 %) + 1/4 CH_3COOH (98 %); should be stored in teflon bottles)
- rinse them with ordinary running water for 10 to 15 minutes
- rinse in deionised water
- heat the pieces in hot deionised water with ultrasound, while frequently renewing the water
- dry the pieces using a nitrogen flow.

6.2 Characterisation techniques

We describe here the different methods used for the characterisation of the electrical, optical and structural properties of the studied films. Table 6.2.1 enumerates these techniques and the information they provide.

Characterisation techniques	Information
Stylus step profiling	Film thickness
Electrical conductivity	Conductivity (σ_d, σ_{ill} and σ_{photo}) and dark conductivity activation energy
UV/visible spectroscopy	Transmission, reflection and optical absorption for the UV/visible range
Photothermal Deflection Spectroscopy (PDS)	Subgap optical absorption
IR transmission spectroscopy	Bond vibration absorption modes, free carrier absorption
Secondary Ion Mass Spectroscopy (SIMS)	Dopants and contaminants concentrations
Elastic Recoil Detection Analysis (ERDA)	Hydrogen content profiles
Spectroscopic Ellipsometry (SE)	Film constituents volume fractions, thicknesses and surface roughness
X-ray diffraction/reflection	Average crystallite size and grain orientations, film constituents volume fractions, thicknesses and roughness
Raman spectroscopy	Crystalline volume fraction, bond angle disorder
Transmission Electron Microscopy (TEM)	Details of structure: crystallites, grain boundaries and defects
Light-soaking	Degradation kinetics of the electrical properties

Table 6.2.1: Enumeration list of all different techniques used for the characterisation of the electrical, optical and structural properties of the films, with the related information they provide.

6.2.1 Stylus step profiling

The precise evaluation of the film thickness is of great importance as it is further used for the determination of other film properties such as the conductivity or the optical absorption. The film thickness is accurately measured and averaged over about 20 measurements, using a stylus step profilometer (Tencor Instruments: Alpha Step 200) over steps etched out for the films deposited on glass. The steps are produced very close to the area used for other measurements, so that errors due to film non-uniformity (thickness variations) are minimised.

To create the steps, first the entire specimen except the areas to be etched out are covered with a protective commercial lacquer (Plastik 70). Once dried in ambient air, the sample is dipped in a hot (50 - 80 °C) diluted KOH solution (10 M = 560 g/l). The KOH attacks and etches away the exposed parts of the film. As the etch rate for the silicon film is much faster than for the glass or for the protective lacquer, one obtains with care very neat steps. The lacquer is then removed and the specimen cleaned by rinsing with acetone and dried using a nitrogen flow. The stylus step profiling is then carried out across the steps. The precise film thickness is obtained by applying standard levelling procedures. The obtained precision for the specifically chosen measurement conditions is about 5 to 20 Å.

6.2.2 Electrical conductivity

The electrical conductivity is an important and useful physical parameter, measured to evaluate and optimise our films. The measurement is performed in a dark vacuum chamber under a nitrogen atmosphere of about 10 mbar, so as to ensure a good thermal contact between the sample holder plate and the film.

Two, 1000 Å thick, parallel aluminium electrode stripes (coplanar contact configuration) of 8 mm length and separated by a 1 mm gap are thermally evaporated (Joule effect) on the film. The specimen is then mounted on the temperature controlled sample holder and loaded into the vacuum chamber. A fully computer controlled measurement cycle is initiated consisting of three steps: 1) a rapid heating ramp to the selected backing temperature (usually between 150 and 200 °C, corresponding to the deposition temperature minus 20 °C), 2) a dwell of 1h30 at constant temperature and finally, 3) a constant rate cooling ramp of 0.8 °C/h down to room temperature. The importance of the thermal cycle lies in having the specimen in a reproducible state (called "annealed") before measuring the electrical properties.

The electrical measurements are performed continuously during the entire thermal cycle using a Keithley Electrometer 617. The electrical conductivity is calculated from the geometry of the contacts, the film thickness and the measured resistance. The ohmic behaviour of the aluminium contacts is previously verified and the dark conductivity and conductivity under illumination (at 60 or 100 mW/cm^2) by a halogen lamp source are measured.

The dark conductivity activation energy is finally extracted from the Arrhenius plot of the dark conductivity (σ_d plotted in a logarithmic scale as a function of 1000/T (in K^{-1})). The slope of the so obtained curve yields the activation energy, assuming a simple thermally activated transport model.

6.2.3 UV/visible spectroscopy

Transmission (T) and reflection (R) measurements in the UV/visible range for wavelengths ranging from 300 to 700 nm (4.13 to 1.77 eV) were carried out at room temperature for films deposited on 7059 Dow Corning glass using a commercial computer controlled spectrophotometer (model Lambda 17 from Perkin-Elmer). The film surface was positioned towards the light source beam. The spectrometer uses a double beam technique, one beam is taken as the reference while the other beam traverses the specimen. The computer controlled detection is performed by a photomultiplier. The reflection measurement mode uses an Ulbricht's integration sphere.

The evaluation of the absorption coefficient α is performed from transmission and reflection data by using the simplified expression $T/(1-R) = \exp(-\alpha d)$ (where d is the film thickness), while neglecting all multiple reflections and taking into account only the dominant reflection at the air-film interface [Summonte 1993]. The absorption coefficient values are determined by taking the algebraic average over the interference fringes of the resulting α vs λ plot. Note that this evaluation method should yield interference free absorption spectra if both transmission and reflection measurements were performed exactly on the same place on the specimen (without moving the specimen for both T and R evaluations); this was unfortunately not possible in our case for the used spectrometer set-up.

6.2.4 Photothermal Deflection Spectroscopy (PDS)

PDS is an optical method, sensitive to very low absorptions, used to measure the absorption spectrum in the range of 600 to 1400 nm (2.07 to 0.89 eV). The system set-up and measurement technique are described in detail elsewhere [Curtins 1988] and therefore not treated again here. The measurement results provide the relative changes in the absorption coefficient as a function of the wavelength of the incident beam. The data are then calibrated using the absorption coefficient (absolute value) obtained for a wavelength of 600 nm from the UV/visible spectroscopy data. The error in the measurement of α, estimated from the signal to noise ratio, is less than 100 % at an absorption of 1 cm^{-1} and is expected to be even smaller for higher values.

6.2.5 IR transmission spectroscopy

The infrared (IR) absorption gives information on the atom bonding vibration modes occurring in the material via phonon excitation. The absorption signatures at the different energy positions for amorphous and microcrystalline silicon materials are described in detail elsewhere [Brodsky 1977, Demichelis 1993 and Curtins 1986]. In the case of doped specimens, the background transmission is reduced due to the overall absorption increase originating from free carriers [Finger 1993]. From IR spectra, relative quantification of hydrogen and oxygen concentrations of the films were performed.

The infrared transmission measurements are performed on films deposited on crystalline substrates (<p>-type wafers), using a commercial Fourrier Transform - Infra Red (FT-IR) spectrometer (model 1720 X from Perkin-Elmer). The spectrometer scans over the wavelength range of 400 to 7900 cm^{-1} (0.05 to 0.98 eV). Prior to measurement, a standard background correction is performed using a piece from the same c-Si wafer as used as substrate for deposition.

6.2.6 Secondary Ion Mass Spectroscopy (SIMS)

The concentrations of dopant (P and B) and contaminant (H, C, N and O) atoms in the films deposited on glass have been evaluated by SIMS by the Evans Europa Cascade Scientific Ltd. (U. K.), specialists in materials characterisation. The method is based on the mass resolution detection (counts as a function of time) of secondary ions extracted from the film surface by a primer highly energetic (KeV range) ion beam (O_2^+ for B and Cs^+ for H, C, N, O and P). Calibration is performed using silicon implant standards. Final treated data yield concentration depth profiles. The overall accuracy of the concentrations should be within 15 % and the highest resolution limit of the system is about $1x10^{15}$ at/cm^3 (for B).

6.2.7 Elastic Recoil Detection Analysis (ERDA)

ERDA is a well-adapted and non destructive method to determine the hydrogen concentration profile of the films. ERDA consists in measuring, using a semiconductor detector (SiBS), the energy spectrum of the protons which have been elastically hit by incident alpha particles (from a 3 MeV Van de Graaff electrostatic accelerator) and recoil in a defined direction. The energy spectrum is a function of the H-concentration profile which is to be determined and of other physical parameters. The film H-concentration profile was obtained from the proton energy spectrum by fitting a computed energy spectrum to the experimental one. The procedure was checked by measuring the H-concentration profile of a hydrogen standard. A more detailed experimental set-up description is presented elsewhere [Tang 1990].

The measurements were performed by Dr. O. Greim from the Institute of Physics, University of Neuchâtel (Switzerland).

6.2.8 Spectroscopic Ellipsometry (SE)

SE is a powerful and non destructive optical method used to determine the optical and structural properties of the films deposited on glass substrates (in our case), such as film thicknesses and volume fractions of each of the film components (crystalline, amorphous and void), by the fitting of the experimental data with a more or less simple physical model.

The samples have been measured using a rotating-analyser spectroscopic ellipsometer consisting of the following sequence of optical elements: 75 Watt xenon light source, monochromator, shutter for background correction, collimator, fixed polariser, sample holder, 54 Hz rotating analyser, and photomultiplier detector. Ellipsometric (Ψ, Δ) spectra from 1.5 to 5.0 eV are collected at a 70 ° angle of incidence with background correction and data reduction steps. The analysis of the (Ψ, Δ) spectra, to determine the sample structure, was performed using a multilayer optical analysis. Fitting the calculated and experimental spectra for the proposed structure yields the structural parameters. The Bruggeman Effective Medium Approximation (EMA) is used to determine the effective dielectric function of any composite films in the sample structure. Detailed set-up description and analyses are presented elsewhere [Nguyen 1993].

All SE analyses were performed by Dr. H.V. Nguyen and Prof. R.W. Collins from the Materials Research Laboratory of Pennsylvania State University, University Park (USA).

6.2.9 X-ray diffraction/reflection

The X-ray diffraction/reflection technique is commonly used to obtain structural information of the samples. The diffraction results contain signatures (at the angular positions which satisfy the Bragg reflection conditions) for different crystallographic planes from which one can derive information on preferential crystallite orientations and the mean value of the grain size, while the reflection results (fitting of the experimental data with the Fresnel equations) lead to structural parameters such as film thickness, average Si density and root mean square surface/interface roughness. For the reflection measurements, small variations of the source beam angle α were made near the total reflection angle.

X-ray diffraction measurements have been performed by Dr. J. Pohl at the Physics Institute of Konstanz University (Germany) using a commercial Siemens D5000 X-ray diffractometer (Bragg-Brentano-Geometry). The used $Cu_{K\alpha 1}$ radiation has a wavelength of 1.5406 Å. Specimens having an area of about 1 to 4 cm^2 are fixed on the sample holder and rotated by the Θ angle during measurement. The diffracted rays are recorded for 2Θ angles ranging from 10 to 100 °.

For the very thin films of thicknesses < 350 Å, yielding the necessity of a higher sensitivity, grazing angle X-ray measurements have been carried out by Dr. M. Brunel at the Crystallographic Laboratory of the CNRS, Grenoble (France). The detector was scanned in the 2Θ range of 20 to 70 °.

6.2.10 Raman spectroscopy

The Raman spectroscopy measurement is useful to determine the structural properties of the material. The first order Transversal Optic (TO) phonon spectrum, resulting from the inelastic scattering of the incident beam, is measured. The frequency shift of the scattered photons yields information on the vibration energies and structure of the molecules. Raman spectroscopy is thus a sensitive probe for changes in the local bonding environment. Due to very small frequency shifts of the scattered radiation from the incident one, monochromatic incident light and a powerful monochromator are requested.

Generally, a disordered random network of Si (i.e. a-Si:H) which lacks long-range order yields a broad structure near 480 cm^{-1} in the spectrum, whereas in contrast a crystalline Si structure is represented by one sharp peak near 520 cm^{-1} [Brodsky 1977]. In the case of μc-Si:H, one obtains a profile which can be deconvoluted into the two above mentioned components. The first component is understood to result from the disordered regions of grain boundary like zones and the second one from the crystallites.

The measurements of films deposited onto glass have been performed by Dr. R. Carius, Dr. P. Hapke and Dr. M. Tzolov from the Research Center Jülich (Germany). They have been carried out at room temperature in a backscattering geometry, and in the case of very thin films of thicknesses < 350 Å, the spectra have been corrected for the baseline and substrate. A 25 to 100 mW incident beam, having different discrete wavelengths of 4579, 4960 and 5140 Å, has been used from an Ar-laser source to illuminate the samples. The scattered lines are recorded in the range of 360 to 1060 cm^{-1} with respect to the incident radiation, using a scanning photon counting system (liquid nitrogen cooled CCD camera: Photometrix 9000) attached to a double monochromator (Spex 1404 spectrometer). The system resolution is 0.2 cm^{-1}.

6.2.11 Transmission Electron Microscopy (TEM)

TEM is a complementary and quite necessary technique to fully characterise the structure of the deposited films. High Resolution Electron Micrographs (HREM) obtained from TEM enable one to reach details of the film structure such as the crystalline (effective grain size and volume fraction) and amorphous zones, crystallographic defects and grain boundaries. Structural details are also obtained from the film-substrate interface for cross-sectional views.

The selected area Electron Diffraction (ED) patterns obtained at the focal plane of the microscope provide further information on the film structure. An amorphous phase results in a diffraction pattern with broad diffused halos, while sharp rings with distinct dots are observed in the case of randomly oriented polycrystalline material. Finally, a pattern exhibiting a periodic structure of bright diffraction spots is characteristic for a large crystalline area of crystallographic orientations parallel to the electron beam.

Planar views have been obtained for films deposited on thin copper grids or NaCl substrates, while cross-sectional views resulted from films deposited onto c-Si substrates after a fastidious sample preparation by cleavage. The measurements have been performed by Dr. M. Morris from the Institute of Structural Metallurgy of the University of Neuchâtel (Switzerland), Dr. A. Catana from EPF Lausanne (Switzerland), Dr. M. Luysberg from the Research Center Jülich (Germany), and Dr. V. Shklover from the Laboratory for Crystallography ETH Zürich (Switzerland).

6.2.12 Light-soaking

The light-induced degradation experiment was undergone by the long-term exposure of the films to a 400 W intensive high-pressure sodium vapour lamp (λ = 590 nm). The advantage of a high pressure lamp by comparison to a low pressure lamp is to widen the Na emission line. The half-width of the yellow emission line is around 80 nm, what should favour the uniformity of the light absorption throughout the entire film thickness. With the absorption coefficient of about $1x10^4$ cm^{-1} for our µc-Si:H material at the wavelength of this light source of 590 nm, we obtain a relatively uniform illumination throughout the entire film (transmission ≈ 70 % for a film thickness d of about 0.4 µm). The light intensity measured at the sample during light-soaking experiment and controlled by a photodiode in parallel was around 500 mW/cm^2 (~ $1.5x10^{18}$ photons/cm^2 s) and the temperature (measured by an IR thermometer) kept at 40 °C by controlled air-cooling. The film electrical conductivity under illumination σ_{ill} was continuously monitored during the entire degradation time.

7 REFERENCES

Akasaka 1993	T. Akasaka, Y. Araki, M. Nakata and I. Shimizu, Jpn. J. Appl. Phys. **32**, 2607 (1993)
Beck 1995	N. Beck, J. Fric, Z. Reme, A. Poruba, M. Vanacek, J. Meier, R. Flückiger, A. Shah and J. Pohl, submitted to ICAS 16, Kobe (Japan), September 4-8 1995
Brodsky 1977	M.H. Brodsky, M. Cardona and J.J. Cuomo, Phys. Rev. B **16** (8), 3556 (1977)
Carius 1994	R. Carius and M. Tzolov, private communication, 1994
Carlson 1977	D.E. Carlson, IEEE Trans. Elec. Dev. **24** (4), 449 (1977)
Carlson 1988	D.E. Carlson, R.R. Arya, M.S. Bennett and A. Catalano, Semiannual Report for the period 2/1/1987-7/31/1987, STR-211-3375, Solar Energy Research Inst., 1988; NTIS Accession No. DE89000843
Chatham 1989	H. Chatham and P.K. Bhat, Mat. Res. Soc. Symp. Proc. **149**, 447 (1989)
Chou 1992	J.-S. Chou, W.-J. Sah, S.-C. Lee, T.-C. Chang and J.-C. Wang, Materials Chemistry and Physics **32**, 273 (1992)
Collins 1989	R.W. Collins and B.Y. Yang, J. Vac. Sci. Technol. B **7** (5), 1155 (1989)
Crovini 1994	G. Crovini, F. Demichelis, C.F. Pirri, E. Tresso, J. Meier, S. Dubail and A. Shah, Mat. Res. Soc. Symp. Proc. **336**, 481 (1994)
Curtins 1986	H. Curtins and S. Veprek, Sol. State Comm. **57** (4), 215 (1986)
Curtins 1987	H. Curtins, N. Wyrsch and A.V. Shah, Elec. Lett. **23** (5), 228 (1987)
Curtins 1987a	H. Curtins, N. Wyrsch, M. Favre, K. Prasad, M. Brechet and A.V. Shah, Mat. Res. Soc. Symp. Proc. **95**, 249 (1987)
Curtins 1987b	H. Curtins, N. Wyrsch, M. Favre and A.V. Shah, Plasma Chem. and Plasma Process. **7**, 267 (1987)
Curtins 1988	H. Curtins and M. Favre, in Amorphous Silicon and Related Materials, edited by H. Fritzsche (World Scientific Publ. Co., 1988), p. 329
Demichelis 1993	F. Demichelis, G. Crovini, C.F. Pirri and E. Tresso, Phil. Mag. B **68** (3), 329 (1993)
Dutta 1992	J. Dutta, U. Kroll, P. Chabloz, A. Shah, A.A. Howling, J.-L. Dorier and Ch. Hollenstein, J. Appl. Phys. **72** (7), 3220 (1992)
Faraji 1992	M. Faraji, S. Gokhale, S.M. Choudhari, and M.G. Takwale, Appl. Phys. Lett. **60** (26), 3289 (1992)
Feldman 1968	D.W. Feldman, J.H. Parker, W.J. Choyke and L. Patrick, Phys. Rev. **173** (3), 787 (1968)
Finger 1990	F. Finger, V. Viret, A. Shah, X.-M. Tang, J. Weber and W. Beyer, Mat. Res. Soc. Symp. Proc. **192**, 583 (1990)
Finger 1993	F. Finger, R. Carius, P. Hapke, K. Prasad and R. Flückiger, Mat. Res. Soc. Symp. Proc. **283**, 471 (1993)
Finger 1994	F. Finger, P. Hapke, M. Luysberg, R. Carius and H. Wagner, Appl. Phys. Lett. **65** (20), 2588 (1994)
Finger 1994a	F. Finger, C. Malten, P. Hapke, R. Carius, R. Flückiger and H. Wagner, Phil. Mag. Lett. **70** (4), 247 (1994)

Flückiger 1992	R. Flückiger, J. Meier, H. Keppner, U. Kroll, A. Sbah, O. Greim, M. Morris, J. Pohl, P. Hapke and R. Carius, Proc. of 11th EC PVSEC, 617 (1992)
Flückiger 1993	R. Flückiger, J. Meier, H. Keppner, M. Götz and A. Shah, Proc. of 23rd IEEE PVSC, 839 (1993)
Flückiger 1994	R. Flückiger, J. Meier, A. Shah, A. Catana, M. Brunel, H.V. Nguyen, R.W. Collins and R. Carius, Mat. Res. Soc. Symp. Proc. **336**, 511 (1994)
Flückiger 1994a	R. Flückiger, H. Meier and P. Torres, F Patent No. 94'12329, October 11 1994
Flückiger 1995	R. Flückiger, J. Meier, M. Goetz and A. Shah, J. Appl. Phys. **77** (2), 712 (1995)
Flückiger 1995a	R. Flückiger, J. Meier, G. Crovini, F. Demichelis, F. Giorgis, C.F. Pirri, E. Tresso, J. Pohl, V. Rigato, S. Zandolin and F. Caccavale, Mat. Res. Soc. Symp. Proc. **358**, 751 (1995)
Flückiger 1995b	R. Flückiger, J. Meier, A. Shah, J. Pohl, M. Tzolov and R. Carius, Mat. Res. Soc. Symp. Proc. **358**, 793 (1995)
Ghosh 1992	S. Ghosh, A. De, S. Ray and A.K. Barua, J. Appl. Phys. **71** (10), 5205 (1992)
Godet 1987	C. Godet, Ph. D. thesis, Univ. Paris-Sud, Centre D'Orsay, 1987
Godyak 1990	V.A. Godyak and R.B. Piejak, J. Vac. Sci. Technol. A **8** (5), 3833 (1990)
Goetz 1995	M. Goetz, private communication, 1995
Goldstein 1988	B. Goldstein, C.R. Dickson, I.H. Campbell and P.M. Fauchet, Appl. Phys. Lett. **53** (26), 2672 (1988)
Hapke 1993	P. Hapke, F. Finger, R. Carius, H. Wagner, K. Prasad and R. Flückiger, J. Non-Cryst. Solids **164-166**, 981 (1993)
Hapke 1995	P. Hapke, F. Finger, M. Luysberg, R. Carius and H. Wagner, Mat. Res. Soc. Symp. Proc. **358**, 745 (1995)
Harbeke 1983	G. Harbeke, E. Meier, J.R. Sandercock, M. Tgetgel, M.T. Duffy and R.A. Soltis, RCA Review **44**, 19 (1983)
Hattori 1987	Y. Hattori, D. Kruangam, T. Toyama, H. Okamoto and Y. Hamakawa, Tech. Digest of 3rd Int'l PV Sci. & Eng. Conf., 171 (1987)
Hattori 1988	Y. Hattori, D. Kruangam, T. Toyama, H. Okamoto and Y. Hamakawa, Appl. Surf. Science **33/34**, 1276 (1988)
He 1993	S.S. He, M.J. Williams, D.J. Stephens and G. Lucovsky, J. Non-Cryst. Sol. **164-166**, 731 (1993)
He 1983	Y. He, Y. Yen, R. Wu and K. Chen, J. Non-Cryst. Sol. **59&60**, 831 (1983)
Heintze 1993	M. Heintze, W. Westlake and P.V. Santos, J. Non-Cryst. Sol. **164-166**, 985 (1993)
Heintze 1993a	M. Heintze and R. Zedlitz, J. Non-Cryst. Sol. **164-166**, 55 (1993)
Howling 1991	A.A. Howling, Ch. Hollenstein, P.-J. Paris, F. Finger and U. Kroll, Proc. of XX ICPIG, 1089 (1991)
Howling 1992	A.A. Howling, J.-L. Dorier, Ch. Hollenstein, U. Kroll and F. Finger, J. Vac. Sci. Technol. A **10** (4), 1080 (1992)
Hsu 1994	K.-C. Hsu, B.-Y. Chen, H.-T. Hsu, K.-C. Wang, T.-R. Yew and H.-L. Hwang, Jpn. J. Appl. Phys. 33, 639 (1994)

Hubin 1994	J. Hubin, Ph. D. thesis, Institute of Microtechnology, University of Neuchâtel, 1994
Iqbal 1980	Z. Iqbal, A.P. Webb and S. Veprek, Appl. Phys. Lett. **36** (2), 163 (1980)
Iqbal 1982	Z. Iqbal and S. Veprek, J. Phys. C: Solid State Phys. **15**, 377 (1982)
Kanicki 1991	J. Kanicki, in Amorphous and Microcrystalline Semiconductor Devices: Optoelectronic Devices, edited by J. Kanicki (Artech House, Norwood, 1991)
Kausche 1989	H. Kausche, K. Prasad and R. Plättner, Proc. of 9th EC PVSEC, 595 (1989)
Keppner 1994	H. Keppner, P. Torres, R. Flückiger, J. Meier, A. Shah, C. Fortmann, P. Fath, G. Willeke, K. Happle and H. Kiess, Solar Energy Materials and Solar Cells **34**, 201 (1994)
Keppner 1995	H. Keppner, U. Kroll, J. Meier and A. Shah, submitted to J. Solid State Phenomena, May 1995
Kikuchi 1988	M. Kikuchi, J. Appl. Phys. **64** (10), 4997 (1988)
Komuro 1984	S. Komuro, Y. Aoyagi, Y. Segawa and S. Namba, J. Appl. Phys. **56** (6), 1658 (1984)
Kroll 1992	U. Kroll, F. Finger, J. Dutta, H. Keppner, A. Shah, A. Howling, J.-L. Dorier and Ch. Hollenstein, Mat. Res. Soc. Symp. Proc. **258**, 135 (1992)
Kroll 1994	U. Kroll, Y. Ziegler, J. Meier, H. Keppner and A. Shah, Mat. Res. Soc. Symp. Proc. 336, 115 (1994)
Kroll 1994a	U. Kroll, Ph. D. thesis, Institute of Microtechnology, University of Neuchâtel, 1994; ISBN # 3-89191-905-0
LeBerre 1993	M. LeBerre, M. Lemiti, P. Pinard, E. Bustarret, W. Grieshaber, J.-C. Bruyère and M. Bruncl, Mat. Res. Soc. Symp. Proc. **283**, 573 (1993)
LeComber 1983	P.G. LeComber, G. Willeke and W.E. Spear, J. Non-Cryst. Sol. **59&60**, 795 (1983)
Li 1994	Y.-M. Li, F. Jackson, L. Yang, B.F. Fieselmann and L. Russell, Mat. Res. Soc. Symp. Proc. **336**, 663 (1994)
Liu 1986	H. Liu and M. Xu, Solid State Comm. 58 (9), 601 (1986)
Lucovsky 1991	G. Lucovsky and C. Wang, Mat. Res. Soc. Symp. Proc. **219**, 377 (1991)
Lucovsky 1993	G. Lucovsky, C. Wang, M.J. Williams, Y.L. Chen and D.M. Maher, Mat. Res. Soc. Symp. Proc. **283**, 443 (1993)
Luft 1993	W. Luft and Y.S. Tsuo, in Hydrogenated Amorphous Silicon Alloy Deposition Processes, edited by A.M. Hermann (Marcel Dekker, New York, 1993)
Luysberg 1995	M. Luysberg, P. Hapke, F. Finger and R. Carius, presented at MRS Spring Meeting, San Francisco (CA), April 17-21 1995, unpublished
Madan 1993	A. Madan, P. Rava, R.E.I. Schropp and B. von Roedern, Appl. Surf. Science **70/71**, 716 (1993)
Malten 1995	C. Malten, F. Finger, P. Hapke, T. Kulessa, C. Walker, R. Carius, R. Flückiger and H. Wagner, Mat. Res. Soc. Symp. Proc. **358**, 757 (1995)
Manfredotti 1993	C. Manfredotti, F. Fizzotti, G. Amato, L. Boarino and M. Abbas, Mat. Res. Soc. Symp. Proc. **283** , 507 (1993)
Matsuda 1990	A. Matsuda and T. Goto, Mat. Res. Soc. Symp. Proc. **164**, 3 (1990)

Meier 1994	J. Meier, R. Flückiger, H. Keppner and A. Shah, Appl. Phys. Lett. 65 (7), 860 (1994)
Meier 1994a	J. Meier, S. Dubail, R. Flückiger, D. Fischer, H. Keppner and A. Shah, Proc. of 1st WCPEC, 409 (1994)
Meier 1995	J. Meier, S. Dubail, R. Flückiger, D. Fischer, H. Keppner and A. Shah, Tech. Digest of the 8th Sunshine Workshop on Thin Film Solar Cells, 61 (1995)
Meier 1995a	J. Meier, S. Dubail, D. Fischer, J.A. Anna Selvan, N. Pellaton Vaucher, R. Platz, Ch. Hof, R. Flückiger, U. Kroll, N. Wyrsch, P. Torres, H. Keppner and A. Shah, submitted to the 13th EC PVSEC, Nice (F), October 23-27 1995
Miyajima 1992	T. Miyajima, K. Sasaki and S. Furukawa, in Amorphous and Crystalline Silicon Carbide IV, edited by C.Y. Yang, M.M. Rahman and G.L. Harris (Springer-Verlag Berlin, Heidelberg, 1992), p. 281
Nakata 1993	M. Nakata, S. Wagner and T.M. Peterson, J. Non-Cryst. Sol. **164-166**, 179 (1993)
Nguyen 1993	H.V. Nguyen, Ph. D. thesis, The Pennsylvania State University, University Park, 1993
Oda 1988	S. Oda, J. Noda and M. Matsumura, Mat. Res. Soc. Symp. Proc. **118**, 117 (1988)
Oda 1995	S. Oda and M. Otobe, Mat. Res. Soc. Symp. Proc. 358, 721 (1995)
Overhof 1983	H. Overhof and W. Beyer, Phil. Mag. B 47 (4), 377 (1983)
Parsons 1994	G.N. Parsons, presented at the 1994 MRS Fall Meeting, Boston (MA), November 28 - December 2 1994
Perrin 1989	J. Perrin, Y. Takeda, N. Hirano, Y. Takeuchi and A. Matsuda, Surface Science **210**, 114 (1989)
Pipoz 1992	P. Pipoz, E. Sauvain, J. Hubin and A. Shah, Mat. Res. Soc. Symp. Proc. **258** , 777 (1992)
Prasad 1990	K. Prasad, F. Finger, H. Curtins, A. Shah and J. Baumann, Mat. Res. Soc. Symp. Proc. **164**, 27 (1990)
Prasad 1991	K. Prasad, Ph. D. thesis, Institute of Microtechnology, University of Neuchâtel, 1991
Prasad 1991a	K. Prasad, U. Kroll, F. Finger, A. Shah, J.-L. Dorier, A. Howling, J. Baumann and M. Schubert, Mat. Res. Soc. Symp. Proc. 219, 469 (1991)
Richter 1981	H. Richter and L. Ley, J. Appl. Phys. 52 (12), 7281 (1981)
Rubino 1993	A. Rubino, M.L. Addonizio, G. Conte, G. Nobile, E. Terzini and A. Madan, Mat. Res. Soc. Symp. Proc. 297, 509 (1993)
Sauvain 1993	E. Sauvain, A. Mettler, N. Wyrsch and A. Shah, Solid State Comm. 85 (3), 219 (1993)
Sauvain 1994	E. Sauvain, P. Pipoz, A. Shah and J. Hubin, J. Appl. Phys. 75 (3), 1722 (1994)
Scherrer 1918	P. Scherrer, Nachr. Göttinger Gesell. 98, (1918); Zsigmondy's Kolloidchemie, 3rd Ed., 394
Seto 1975	J.Y.W. Seto, J. Appl. Phys. 46 (12), 5247 (1975)
Shen 1993	D.S. Shen and P.K. Bhat, Solar Energy Materials and Solar Cells 30, 139 (1993)
Shimizu 1989	I. Shimizu, J. Non-Cryst. Sol. **114**, 145 (1989)

Shirai 1994	H. Shirai, B. Drévillon and I. Shimizu, Jpn. J. Appl. Phys. **33**, 5590 (1994)
Spear 1975	W.E. Spear and P.G. LeComber, Sol. St. Comm. **17**, 1193 (1975)
Spear 1981	W.E. Spear, G. Willeke, P.G. LeComber and A.G. Fitzgerald, J. de Phys. **42**, C4-257 (1981)
Staebler 1977	D.L. Staebler and C.R. Wronski, Appl. Phys. Lett. **31** (4), 292 (1977)
Street 1985	R.A. Street, J. Non-Cryst. Sol. **77&78**, 1 (1985)
Stutzmann 1984	M. Stutzmann, W.B. Jackson and C.C. Tsai, AIP Conference Proceedings **120**, 213 (1984)
Summonte 1993	C. Summonte, Mat. Res. Soc. Symp. Proc. **297**, 395 (1993)
Tang 1990	X.-M. Tang, J. Weber and Y. Baer, Solid State Comm. 74 (3), 171 (1990)
Torres 1994	P. Torres, H. Keppner, R. Flückiger, J. Meier and A. Shah, Proc. of 12th EC PVSEC, 705 (1994)
Torres 1995	P. Torres, R. Flückiger, J. Meier, H. Keppner, F. Finger and A. Shah, submitted to the 13th EC PVSEC, Nice (F), October 23-27 1995
Tsai 1988	C.C. Tsai, in Amorphous Silicon and Related Materials, edited by H. Fritzsche (World Scientific Publ. Co., 1988)
Usui 1979	S. Usui and M. Kikuchi, J. Non-Cryst. Sol. **34**, 1 (1979)
Veprek 1968	S. Veprek and V. Marecek, Sol. St. Elec. **11**, 683 (1968)
Veprek 1988	S. Veprek, M. Heintze, F.-A. Sarott, M. Jurcik-Rajman and P. Willmott, Mat. Res. Soc. Symp. Proc. **118**, 3 (1988)
Veprek 1991	S. Veprek, F.-A. Sarott and M. Rückschloss, J. Non-Cryst. Sol. **137&138**, 733 (1991)
Veprek 1995	S. Veprek, Th. Wirschem, M. Rückschloss, H. Tamura and J. Oswald, Mat. Res. Soc. Symp. Proc. **358**, 99 (1995)
Wang 1990	C. Wang and G. Lucovsky, Proc. of 21st IEEE PVSC, 1614 (1990)
Wang 1991	F. Wang, H.N. Liu, Y.L. He, A. Schweiger and R. Schwarz, J. Non-Cryst. Sol. **137&138**, 511 (1991)
Warren 1959	B.E. Warren, in Progress in Metal Physics, Vol. 8 (Pergamon Press, London, 1959), p. 147
Willeke 1992	G. Willeke, in Amorphous and Microcrystalline Semiconductor Devices: Materials and Device Physics, edited by J. Kanicki (Artech House, Norwood, 1992)
Williams 1991	M.J. Williams, C. Wang and G. Lucovsky, Proc. of Intern. Meeting on the Stability of a-Si:H, Golden, 1991
Yang 1994	J. Yang, A. Banerjee, T. Glatfelter, K. Hoffman, X. Xu and S. Guha, Proc. of 1st WCPEC, 380 (1994)
Zedlitz 1992	R. Zedlitz, M. Heintze and G.H. Bauer, Mat. Res. Soc. Symp. Proc. **258**, 147 (1992)

ACKNOWLEDGEMENTS

I would like to acknowledge:

Professor A. Shah, who spontaneously accepted me in his dynamic research group as a co-worker and also allowed me to realise this thesis work. It was for me a real great honour to work in his research group in an almost free way during all the past years. It was furthermore a great pleasure to be able to establish and develop my point of view through helpful discussions with Professor A. Shah, who besides being directly my head and thesis director, looked to me in a certain way, as a second father.

Dr. Ch. de Reyff and Dr. S. Nowak, for the financial support from the Swiss Federal Energy Department of the amorphous silicon solar cell project, in which the present work was integrated.

Dr. Johannes Meier, who carefully followed this entire work, day after day, and came quickly to my side to defend together the necessity of pursuing and extending the research on μc-Si:H material. I will never forget his deep philosophical advises and the nice time passed with this esteemed friend.

Dr. Kshem Prasad, who kindly helped me to make my introduction to the field of microcrystalline silicon.

Dr. Ulrich Kroll, whose multiple advises on fundamental physics and technology were most useful to me. I appreciated also very much his sincere friendship.

Michael Goetz and Christian Hof, for their great help and time spent on the degradation experiments.

Yvan Ziegler, who freely helped me with the temperature calibration of the film electrical properties measurement apparatus.

Dr. Herbert Keppner, who brought always quick solutions to my problems, whenever I really thought there would be no way out.

Reto Tscharner, who was always present for giving helpful advises in mechanics and electronics.

Dr. Nicolas Wyrsch, who helped me to run the computer software, by solving the numerous bugs.

Dr. Patrice Pipoz, Dr. Jacques Hubin and Natalie Beck, who helped me with tricky theoretical problems.

Sébastien Dubail, who delicately cleaned the countless substrates and electrode plates I used and kept in an unending enthusiasm the laboratory clean and functional.

Peter Torres, who will be probably the only one to have read entirely and meticulously this manuscript, for having carefully checked and corrected the writing. I specifically appreciated his sincere friendship and the unforgettable nice time spent together.

The secretaries Ingrid Mantle, Joëlle Banjac and Mrs. Y. Jucker, the accountant Mrs. S. Jacot, and the administrator J.-M. Wavre, who always freely and kindly helped me with administrative business.

All other colleagues of the research group and institute, who contributed on scientific or personal levels. I appreciated very much the family atmosphere created by the whole staff. I do hope this goes on in the future and would like to thank them all for their valuable contribution.

My sincere feelings to the following people, without their valuable contribution, this work would have been incomplete:

- Dr. Olivier Greim, for the ERDA measurements at Neuchâtel (CH)
- Dr. Hien V. Nguyen and Prof. R.W. Collins, for the SE measurements at University Park, PA (USA)
- Dr. Jörg Pohl, for the X-ray diffraction measurements at Konstanz (D)
- Dr. M. Brunel, for the grazing angle X-ray diffraction measurements at Grenoble (F)
- Dr. Reinhard Carius, Dr. Peter Hapke and Dr. M. Tzolov, for the Raman spectroscopy measurements at Jülich (D)
- Dr. M. Morris, for the planar view TEM photographs at Neuchâtel (CH)
- Dr. A. Catana, for the planar view TEM and TED photographs at Lausanne (CH)
- Dr. M. Luysberg, for the cross-sectional view TEM photographs at Jülich (D)
- Dr. V. Shklover, for the cross-sectional view TEM photographs at Zürich (CH)
- Dr. Friedhelm Finger and co-workers, for the scientific collaboration with the research group of Jülich (D)
- Prof. F. Demichelis, Dr. Fabrizio Pirri, Dr. Giorgio Crovini and co-workers from the research group of Torino (I), for the scientific collaboration.

My 4 months training in the group of Prof. C.R. Wronski has been beneficial on many levels. My best thanks to Prof. C.R. Wronski, Prof. R.W. Collins and Dr. Charles Fortmann who allowed me to pursue my research work at their laboratory at the Pennsylvania State University, University Park, PA (USA), and to their students and staff members who made my stay more comfortable.

My best acknowledgements to Prof. F. Demichelis, Prof. R. Dändliker, Dr. G. Willeke, Dr. J.-M. Moret, and Dr. C.F. Pirri for having freely accepted to act as expert and for their time devoted in reading and correcting this manuscript.

Finally, my fondest appreciation to my wife Muriel for her unending patience and understanding and all my apology to my son Julien for whom I did not devote the time I wanted and that he deserves.

All my best thanks and apology for who may feel I have left him out.

Roger Sylvain Flückiger